

RADAR RAINFALL OBSERVATIONS AT SUB-KILOMETRE AND
SUB-MINUTE SCALES

Dissertation

with the aim of achieving a doctoral degree
at the Faculty of Mathematics, Informatics and Natural Sciences
Department of Earth System Sciences
at Universität Hamburg

submitted by

FINN BURGEMEISTER

Hamburg, 2024

Department of Earth System Sciences

DATE OF ORAL DEFENSE:

22.11.2024

REVIEWERS:

Prof. Dr. Felix Ament
Dr. Marco Clemens

MEMBERS OF THE EXAMINATION COMMISSION:

Prof. Dr. Felix Ament
Dr. Marco Clemens
Prof. Dr. Anette Eschenbach
Dr. Benjamin Poschlod
Prof. Dr. Raphaela Vogel

CHAIR OF THE SUBJECT DOCTORAL COMMITTEE
EARTH SYSTEM SCIENCES:

Prof. Dr. Hermann Held

DEAN OF FACULTY MIN:

Prof. Dr.-Ing. Norbert Ritter

This document was typeset using `classicthesis` developed by André Miede and Ivo Pletikosić available at <https://bitbucket.org/amiede/classicthesis/>.

ABSTRACT

Knowledge of the true rainfall variability at sub-kilometre and sub-hourly scales is required for several meteorological and hydrological applications, especially in urban areas due to the large proportion of impervious surfaces and the stormwater infrastructure. However, variability at these scales is a blind spot for both operational rain gauge networks and operational radar networks. In the urban area of Hamburg, rainfall measurements of a local area X-band weather radar (LAWR) operating at high temporal (30 s), range (60 m), and azimuthal sampling (1°) resolutions within a 20 km scan radius address this observational gap. This dissertation provides new insights into (urban) rainfall variability based on the reanalysis of multi-year high-resolution weather radar observations.

In a first study, the reanalysis of the raw radar data is described in detail, the radar performance for the years 2013 to 2021 is outlined, and open issues and limitations of the data set are discussed. Several sources of radar-based errors were adjusted gradually affecting the radar reflectivity and rainfall measurements, e.g. noise, alignment, non-meteorological echoes, radar calibration, and attenuation. The deployment of additional vertically pointing micro rain radars (MRRs) yields drop size distributions at the radar beam height. These MRR measurements serve as a reference, effectively reduce errors concerning the radar calibration and attenuation correction and monitor the radar data quality. The LAWR radar reflectivities and rainfall rates are in very good agreement with independent MRR measurements. The reanalysed, quality-tested radar reflectivities and rainfall rates were made available as an open-access data set. This multi-year data set enables studies requiring rainfall data at hectometre spatial and sub-minute temporal resolution.

In a second study, the added value of a refined spatio-temporal resolution for weather radar observations at sub-hourly temporal and sub-kilometre spatial scales using the reanalysed radar data set is discussed. In fact, the smaller radar volumes of the LAWR result in a closer agreement in terms of radar reflectivity with local radar observations by MRRs compared to C-band radar systems, which are operational at coarser spatial (250 m) and temporal (5 min) resolutions than the LAWR. However, this advantage does not translate in a better match to rainfall accumulations recorded by rain gauges, as differences in the Z-R relation and sample volume sizes between radar and rain gauge dominate the uncertainty for both the LAWR and operational radar systems. Nevertheless, spatial rainfall structures captured by LAWR and rain gauge measurements are similar at sub-hourly timescales. Conventional available rainfall data sets, like the C-band radar measurement and radar-rainfall climatology RADKLIM, fail to capture the sub-hourly rainfall variability. As expected, RADKLIM underestimates rainfall variability due to the kilometre spatial scale. But interestingly, the operational C-band radar observations tend to overestimate spatial variability at sub-hourly temporal scale. This effect is caused by their intermittent scan strategy, taking just a snapshot every five minutes. The LAWR measurements benefit from its scan strategy, resulting to all measurements taken every 2.5 s. As a consequence, the LAWR is clearly superior in describing spatial rainfall structure. The refined spatio-temporal resolution and scan strategy

is also beneficial for measuring rainfall peaks and measuring steeper gradients. Consequently, the LAWR is capable to capture the microscale rainfall variability better than conventional radars.

In summary, this dissertation provides an open-access data set of reanalysed radar reflectivities and rainfall rates at sub-kilometre spatial and minute temporal scales, that can be used for studies on the spatial and temporal scales of precipitation and hydrological research, e.g. input data for high-resolution modelling, in an urban area. The dissertation demonstrates that a LAWR operating at hectometre spatial and 30 s temporal resolutions fills a gap in rainfall observations compared to conventional rainfall measurements.

ZUSAMMENFASSUNG

Die Kenntnis der Niederschlagsvariabilität hinsichtlich der Akkumulation innerhalb einer Stunde sowie in Auflösungen unter einem Kilometer ist für diverse meteorologische und hydrologische Anwendungen erforderlich. Dies gilt insbesondere für Städte aufgrund des hohen Anteils an versiegelten Oberflächen und der Regenwasserinfrastruktur. Die Variabilität auf diesen Skalen wird jedoch von operativen, in-situ-Netzwerken und Radarmessungen nicht erfasst. Um diese Beobachtungslücke zu schließen, wird im Stadtgebiet von Hamburg Niederschlag mit einem lokalen X-Band-Wetterradar (LAWR) gemessen, das sich durch eine hohen zeitliche (30 s), räumliche (60 m) und azimutale (1°) Auflösung innerhalb eines Radius von 20 km auszeichnet. Die vorliegende Dissertation verfolgt das Ziel, neue Erkenntnisse über die Variabilität von Niederschlag auf der Grundlage der Reanalyse von mehrjährigen hochauflösenden Wetterradarmessungen zu gewinnen.

Im Rahmen einer ersten Studie erfolgt eine detaillierte Beschreibung der Reanalyse der LAWR-Rohdaten, eine Untersuchung der Datenqualität für die Jahre 2013 bis 2021 sowie eine Diskussion von Einschränkungen des Datensatzes. In den Messdaten wurden mehrere radarbasierte Fehler schrittweise korrigiert, zum Beispiel Rauschen, Fehlausrichtung, nicht-meteorologische Echos, fehlende Kalibrierung und Dämpfung. Zusätzlich messende vertikal ausgerichtete Mikro-Regen-Radare (MRR) liefern Messungen der Tropengrößenverteilungen und dienen als Referenzmessung in der Messhöhe des LAWRs. Die MRR-Messungen ermöglichen eine Kalibration des LAWRs, eine Anpassung der Dämpfungskorrektur sowie eine Überwachung der Qualität der Radardaten. Die LAWR-Messungen stimmen sehr gut mit MRR-Messungen, die nicht für die Kalibration verwendet wurden, überein. Die korrigierten, qualitätsgeprüften Radarreflektivitäten und Niederschlagsraten wurde als Datensatz öffentlich zur Verfügung gestellt.

Im Rahmen einer zweiten Studie wird der Mehrwert einer verfeinerten räumlich-zeitlichen Auflösung für Wetterradarmessungen für zeitliche Skalen unter einer Stunde und räumliche Skalen unter einem Kilometer diskutiert. In der Tat stimmen die Radarreflektivitäten des LAWRs mit denen des MRRs besser überein im Vergleich zum operationellen C-Band-Radar, das eine gröbere räumliche (250 m) und zeitliche (5 min) Auflösung als das LAWR verwendet, aufgrund der kleineren Messvolumina des LAWRs. Dieser Vorteil führt jedoch nicht zu einer besseren Übereinstimmung mit den Niederschlagsmengen von Regenmessern, da die Unterschiede der *Z-R*-Beziehung sowie die Größe der Messvolumina zwischen Radar und Regenmesser die Unsicherheit für das LAWR als auch für das operationelle Radar dominieren. Räumlichen Niederschlagsstrukturen werden vom LAWR und dem Netzwerk von Regemessern für Niederschlagsakkumulationen unter einer Stunde ähnlich gemessen. Auf dieser zeitlichen Skala wird die Niederschlagsvariabilität von herkömmlichen Niederschlagsdatensätzen, wie den C-Band-Radaren oder der radargestützten Niederschlagsklimatologie RADKLIM, nicht richtig erfasst. Wie erwartet, unterschätzt RADKLIM die Niederschlagsvariabilität aufgrund der räumlichen Skala von einem Kilometer und der Anpassung an ein Netzwerk von Regenmessern, das größere Distanzen als das Netzwerk in dieser Studie hat.

Interessanterweise neigen die operationellen C-Band-Radarmessungen dazu, die räumliche Variabilität für Niederschlagsakkumulationen unter einer Stunde zu überschätzen. Der Effekt ist auf die Messstrategie zurückzuführen, bei der alle fünf Minuten eine instantane Messung an einem Ort erfolgt. Die LAWR-Messungen profitieren von der Messstrategie, bei der alle 2,5 s die Messung wiederholt wird. Folglich ist das LAWR bei der Messung der räumlichen Niederschlagsstruktur deutlich überlegen. Die verfeinerte räumlich-zeitliche Auflösung und Messstrategie ist zudem für die Erfassung von Niederschlagsmaxima und stärkeren räumlichen Gradienten von Vorteil. Das LAWR ermöglicht somit eine präzisere Erfassung der mikroskaligen Niederschlagsvariabilität als herkömmliche Radare.

Diese Dissertation präsentiert einen neuen, frei zugänglichen Datensatz, der korrigierte Radarreflektivitäten und Regenraten mit einer räumlichen Auflösung von 100 m und einer zeitlichen Auflösung von 30 s umfasst. Der Datensatz eignet sich für Studien zur Verbesserung der radarbasierten Niederschlagsmessung oder zur (städtischen) Niederschlagsvariabilität. Die Dissertation zeigt, dass ein LAWR, welches mit einer räumlichen Auflösung von 100 m und einer zeitlichen Auflösung von 30 s misst, im Vergleich zu konventionellen Niederschlagsmessungen eine Beobachtungslücke schließt.

PUBLICATIONS

The following two first-author publications were prepared as part of this dissertation. The publications are included in the appendix:

Appendix A

F. Burgemeister, M. Clemens, and F. Ament (2024c). “Reanalysis of multi-year high-resolution X-band weather radar observations in Hamburg.” In: *Earth System Science Data* 16.5, pp. 2317–2332. DOI: [10.5194/essd-16-2317-2024](https://doi.org/10.5194/essd-16-2317-2024)

Appendix B

F. Burgemeister, M. Clemens, and F. Ament (2024a). “Added value of spatio-temporal resolution for weather radar observations at urban scales.” In: *preparation for the submission to the Journal of Hydrometeorology*

Three data set publications were prepared for this dissertation:

F. Burgemeister, M. Clemens, and F. Ament (2022b). *Rainfall rates estimated from X-Band radar observations during FESSTVaL 2021*. Universität Hamburg [data set]. DOI: [10.25592/uhhfdm.10090](https://doi.org/10.25592/uhhfdm.10090)

F. Burgemeister, M. Clemens, and F. Ament (2022a). *Multi-year X-band weather radar observations in Hamburg (LAWR HHG) (Version 1)*. World Data Center for Climate (WDCC) at DKRZ [data set]. DOI: [10.26050/WDCC/LAWR_UHH_HHG](https://doi.org/10.26050/WDCC/LAWR_UHH_HHG)

F. Burgemeister, M. Clemens, and F. Ament (2024b). *Multi-year X-band weather radar observations in Hamburg (LAWR HHG) (Version 2)*. World Data Center for Climate (WDCC) at DKRZ [data set]. DOI: [10.26050/WDCC/LAWR_UHH_HHG_v2](https://doi.org/10.26050/WDCC/LAWR_UHH_HHG_v2)

One Python package to load, process and plot weather radar data was further developed and published:

F. Burgemeister, T. Finn, M. Schaper, and Y. Büchau (2023). *pylawr: A Python Package For Processing Local Area Weather Radars*. Zenodo [code]. Version vo.4.o. DOI: [10.5281/zenodo.8182628](https://doi.org/10.5281/zenodo.8182628)

As a PhD student, I have contributed to two other peer-reviewed publications:

C. Hohenegger, F. Ament, F. Beyrich, and 50 co-authors (incl. **F. Burgemeister**) (2023). "FESSTVaL: The Field Experiment on Submesoscale Spatio-Temporal Variability in Lindenberg." In: *Bulletin of the American Meteorological Society* 104.10, E1875–E1892. DOI: [10.1175/BAMS-D-21-0330.1](https://doi.org/10.1175/BAMS-D-21-0330.1)

A. U. Schmitt, **F. Burgemeister**, H. Dorff, T. Finn, A. Hansen, B. Kirsch, I. Lange, J. Radtke, and F. Ament (2023). "Assessing the weather conditions for urban cyclists by spatially dense measurements with an agent-based approach." In: *Meteorological Applications* 30.6, e2164. DOI: <https://doi.org/10.1002/met.2164>

CONTENTS

I Unifying Essay

1	Introduction	3
2	Synergistic rainfall measurements	7
2.1	Rainfall measurements in Hamburg	7
2.1.1	X-band radar (LAWR)	7
2.1.2	C-band radar and RADKLIM	8
2.1.3	Micro rain radar (MRR)	9
2.1.4	Rain gauges	10
2.2	Enhanced rainfall measurements	10
3	Reanalysis of multi-year high-resolution weather radar observations	13
3.1	Data reanalysis	14
3.2	Data quality	19
3.3	Key findings	22
4	Added value of spatio-temporal resolution	23
4.1	Comparison to a local reference	23
4.2	Spatial variability	25
4.3	Rainfall peaks	27
4.4	Sub-kilometre structure	29
4.5	Key findings	32
5	Uncertainty of high-resolution measurements	33
6	Summary and conclusions	37

II Appendix

A	Reanalysis of high-resolution weather radar observations	43
A.1	Introduction	45
A.2	Radar observations in Hamburg	46
A.2.1	X-band weather radar	47
A.2.2	Micro rain radar	47
A.3	Data reanalysis	48
A.3.1	Remove noise	48
A.3.2	Determine radar alignment	49
A.3.3	Detect clutter	49
A.3.4	Calibrate	52
A.3.5	Correct attenuation	54
A.3.6	Estimate rainfall rates	57
A.3.7	Data sets and availability	57
A.4	Data quality	58
A.5	Code and data availability	63
A.6	Conclusions	63
B	Added value of spatio-temporal resolution	67
B.1	Introduction	69
B.2	Rainfall observations	71

B.2.1	X-band radar (LAWR)	72
B.2.2	C-band radar and RADKLIM	72
B.2.3	Micro rain radar (MRR)	73
B.2.4	Rain gauges	73
B.3	Results and discussion	74
B.3.1	Radar reflectivity distributions	74
B.3.2	Rainfall distributions	78
B.3.3	Spatial correlations	82
B.3.4	Peak attenuation	86
B.3.5	Gradients	89
B.4	Conclusions	93
	Bibliography	97

Part I

UNIFYING ESSAY

INTRODUCTION

The rainfall process is characterized by high variability in space and time (Krajewski et al., 2003). Capturing the true rainfall variability at sub-kilometre and sub-hourly scales with measurements remains a challenge because of spatio-temporal resolution, spatio-temporal sampling, and measurement uncertainty. However, the knowledge of small-scale rainfall variability is needed for several meteorological and hydrological applications, particularly in urban environments due to the large proportion of impervious surfaces and the stormwater infrastructure (Einfalt et al., 2004; Sokol et al., 2021; Thorndahl et al., 2017). In general, hydrometeorological and fundamental studies of rainfall properties can benefit from long-term measurements at small spatio-temporal scales, as described in the following.

Our knowledge on rainfall variability bases mainly on measurements by radars and rain gauges. Both systems differ significantly in terms of sampling and resolution. Rain gauge networks provide reliable local precipitation measurements, but due to their limited operational network densities, they are unable to represent the spatial rainfall variability (e.g. Berne et al., 2004; Lengfeld et al., 2019; Ochoa-Rodriguez et al., 2019; Villarini et al., 2008). The spatial scale of rainfall is smaller than the inter distance of most operational rain gauge networks exposed with correlation distances of radar observations (Lengfeld et al., 2019; Marra and Morin, 2018a). Conventional weather radar systems, mostly operating at S- and C-band frequencies, are able to provide radar rainfall measurements over large domains with a temporal resolution of several minutes and spatial resolution of a few hundred metres. Long-term radar-based precipitation climatologies based on these conventional radars are available for Germany with a 5 min temporal and 1 km spatial resolution (Winterrath et al., 2018b), and for Europe with an hourly temporal and 2 km spatial resolution (Overeem et al., 2023). However, there is a gap in long-term radar rainfall data sets at the sub-kilometre spatial scale and temporal scales below 5 min.

Several studies have proven that the unmeasured rainfall variability in radar observations at sub-kilometre spatial scale is large. Jensen and Pedersen (2005) studied the variability in accumulated rainfall within a single radar pixel of $500 \times 500 \text{ m}^2$ using 9 rain gauges and found an astonishing variation up to 100 % between neighbouring rain gauges. Jaffrain and Berne (2012) investigated the spatial structure of drop size distributions with a network of 16 optical disdrometers within an area of approximately $1 \times 1 \text{ km}^2$. They found an error between 18.4 % and 24.5 % for rainfall upscaled from a point to areal measurement at spatial scales of $100 \times 100 \text{ m}^2$ and $1 \times 1 \text{ km}^2$. Gires et al. (2014) address the scale gap between rain gauges with a sampling radius of 10 cm and a radar with a sampling range of 1 km with disdrometer and rain gauge networks within an 1 km^2 area. They perform a downscaling with Universal Multifractals highlighting small-scale rainfall variability. Peleg et al. (2018) simulated the spatial variability of extreme rainfall intensities below 1 km^2 scale with a stochastic rainfall generator. They found that for extreme rainfall intensities, the point measurement is on average 10 % larger than the radar estimate.

Terink et al. (2018) conclude that at least 12 rain gauges per km² are required to capture the same spatial rainfall variability as radar rainfall estimates at 120 m range and 16 s temporal resolution. Rainfall is also characterized by high temporal variability, as Marra and Morin (2018a) found temporal autocorrelations between 1.8 and 6.4 min based on radar rainfall measurement at 1 min temporal resolution. This temporal scale is not fully covered by conventional weather radars operating with a 5 min sampling scale. There is a discontinuity in conventional observations to capture rainfall variability at sub-kilometre spatial scales and temporal scales below 5 min.

This small scale rainfall variability is relevant in application. In urban hydrology, missing spatial rainfall variability causes problems that cannot be solved by any model or finer resolution temporal data (Bárdossy and Anwar, 2023). Urban hydrological applications demand high-quality radar rainfall data with at least a temporal resolution of 1 min and spatial resolution of 100 m for small urban catchment sizes (Berne and Krajewski, 2013; Einfalt et al., 2004; Gires et al., 2013; Ochoa-Rodriguez et al., 2015; Thorndahl et al., 2017). Further studies call for the highest possible spatio-temporal resolution of rainfall measurements (e.g. Alves de Souza et al., 2018; Cao et al., 2023; Costabile et al., 2023). For example, Ferner et al. (2022) require the highest possible resolution of rainfall data as forcing for a microscale obstacle-resolving meteorological model. A higher temporal resolution would also reduce temporal sampling errors (Fabry et al., 1994; Shucksmith et al., 2011). Conventional radars perform a volumetric scan, resulting in an intermittent scanning strategy. Advection correction procedures can reduce temporal sampling errors in rainfall accumulations (e.g. Jasper-Tönnies and Jessen, 2014; Nielsen et al., 2014; Seo and Krajewski, 2015). However, there are applications where advection correction can not solve temporal sampling errors. For instance, for the study of the initial phase of convective precipitation, a scan performed every 5 min is too coarse (Kim et al., 2019). There is a need in hydrometeorological applications for rainfall data sets at the sub-kilometre spatial scale and temporal scales below 5 min.

These demands are potentially covered with measurements by research X-band radars. Research X-band radars monitor rainfall at temporal resolutions down to 16 s (van de Beek et al., 2010) and radial resolutions down to 3 m (Mishra et al., 2016), but most of them operate at or below 100 m spatial and 1 min temporal resolutions (e.g. Allegretti et al., 2012; Hosseini et al., 2020; Lengfeld et al., 2014; Schleiss et al., 2020; van de Beek et al., 2010; Ventura and Russchenberg, 2009; Wang and Chandrasekar, 2010; Yoon et al., 2017). Several X-band radars are deployed to refine rainfall estimates in areas of special interest, like urban areas (e.g. Berenguer et al., 2012; Lo Conti et al., 2015; Maesaka et al., 2011; van de Beek et al., 2010; Wang and Chandrasekar, 2010; Yoon et al., 2017). Although most of the latest X-band radars have dual-polarimetric capabilities (e.g. Anagnostou et al., 2018; Cao et al., 2023; Hosseini et al., 2023; Neely III et al., 2021; Pejcic et al., 2022; Schleiss et al., 2020), where dual-polarimetric quantities improve rainfall estimates, even low-cost, single-polarized X-band radars provide valuable information on the spatio-temporal variability of precipitation (Allegretti et al., 2012; Lo Conti et al., 2015; Marra and Morin, 2018a; van de Beek et al., 2010). However, single-polarized X-band radars require extensive post-processing and the deployment of independent additional sensors, like micro rain radars, disdrometers, or rain gauges, to reduce errors and uncertainty of rainfall estimates (Thorndahl et al., 2017; Villarini and Krajewski,

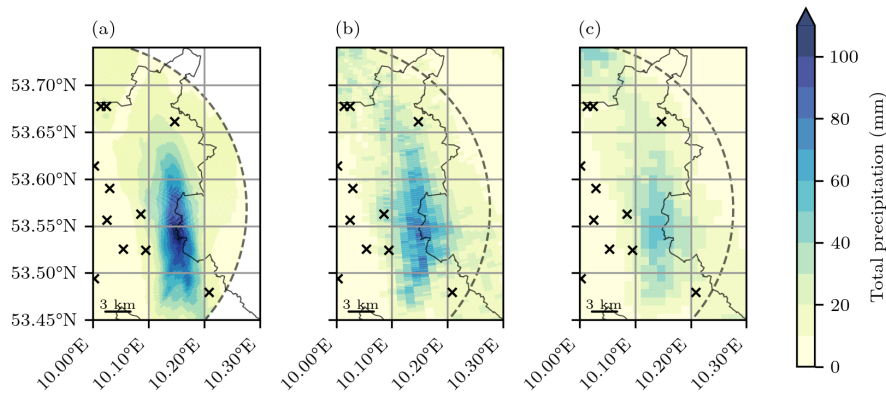


Figure 1.1: Total precipitation observed by (a) a local area weather radar (LAWR), (b) a C-band radar, and (c) the radar-rainfall climatology RADKLIM on a day with a flooding event (10.05.2018). The black crosses mark the locations of available rain gauges with 1 min temporal resolution. The maximal total precipitation is (a) 110 mm for the LAWR, (b) 85 mm for the C-band radar, and (c) 60 mm for RADKLIM. The south-east rain gauge measured the maximal total precipitation of the rain gauge network with 57 mm.

2010). Despite several studies operating high-resolution X-band radars, not all data is available and easy to use as recommended by Saltikoff et al. (2019) and Grimmond et al. (2020). There is a gap of well-documented, high-quality, open-access radar rainfall data sets at or below 100 m spatial and 1 min temporal resolutions.

One operational X-band radar can address this gap. A single-polarized X-band weather radar monitors precipitation within a 20 km scan radius around Hamburg's city center since 2013, operated in synergy with two micro rain radars (MRRs) and rain gauges. This local area weather radar (LAWR) operates at one elevation angle with a high temporal (30 s), range (60 m), and azimuthal sampling (1°) resolution, refining coarser observations of the German nationwide C-band radars at 250 m spatial and 5 min temporal resolution. Former studies on short time periods (several months and a case study) show that the LAWR provides detailed information on the structure of precipitation. Lengfeld et al. (2014) deployed a network of four LAWRs and micro rain radars in a rural area of northern Germany. They describe correction algorithms for single and networked LAWRs and discuss the performance of measurements of 5 months. Lengfeld et al. (2016) and Lengfeld et al. (2018) introduce a method to correct reflectivity measurements for attenuation using less attenuated radars, and they compare attenuation correction methods for single-polarized X-band radars using this LAWR network. The LAWR network was dismantled in 2017. However, the LAWR located in Hamburg is still in operation, extending a unique data set. Hoffmann et al. (2018) shows that the LAWR was able to capture the circular pattern and variability in rainfall rates during a tornado event with an approximate duration of 13 min and a path length of about 1.3 km. For refined rainfall estimates, a LAWR was deployed for studies on cold pool events during the Field Experiment on Sub-mesoscale Spatio-Temporal Variability in Lindenberg (FESSTVaL) from June to August 2021 (Burgemeister et al., 2022b; Hohenegger et al., 2023). The previous studies provide knowledge and algorithms to reanalyse a consistent long-term data set based on LAWR measurements.

The aforementioned challenges in capturing the true rainfall variability can be demonstrated by an exemplary heavy rainfall event that occurred in the urban area of Hamburg. Observations of the LAWR, the nationwide C-band radar network, and different rain gauge networks and the climatology RADKLIM yield disparate representations of this rainfall event (Figure 1.1). The rain gauge network misses the area affected by heavy rainfall, while the conventional weather radar observations (Fig. 1.1b) and the rainfall climatology RADKLIM (Fig. 1.1c) appear to underestimate the rainfall accumulations in magnitude. Although the rainfall data sets concur in the rainfall pattern, the LAWR measured significantly higher rainfall accumulations (Fig. 1.1a) in comparison to the other rainfall data sets. Two additional rain gauges of the municipal water and wastewater utility Hamburg Wasser, which provided daily data and are not available for other dates, corroborate the extreme nature of the event (A. Kuchenbecker, personal communication, August 8, 2022). One rain gauge provided a daily rainfall accumulation of 122 mm at 10.19° E and 53.50° N for this event, which lends confidence to the LAWR rainfall estimates. In general, several rainfall events revealed strong differences in rainfall variability between the rainfall data sets at different spatio-temporal resolution, highlighting the present uncertainty of rainfall observations.

This dissertation aims to provide new insights into (urban) rainfall variability based on the reanalysis of multi-year high-resolution weather radar observations at hectometre and 30 s resolutions. In order to achieve this objective, I will address the following research questions:

1. How can we create a consistent rainfall data set from the multi-year LAWR measurements?
2. What is the uncertainty of the LAWR rainfall measurements?
3. What is the added value of high-resolution rainfall measurements at sub-kilometre and sub-hourly scales?

In Chapter 2 of this thesis, I describe the synergy of rainfall observations and the unique availability of rainfall data sets in Hamburg. Additionally, I outline the existing measurement setup and present the recent extension of this measurement network. Chapter 3 explains the reanalysis of the multi-year LAWR measurements in Hamburg, which resulted in an open-access data set of radar reflectivities and rainfall rates (Study A). I outline the radar performance for the years 2013 to 2021, and discuss open issues and limitations of the data set. In Chapter 4, I examine the rainfall properties of the reanalysed radar data from the LAWR in comparison with an operational C-band radar, a dense rain gauge network, and the radar-rainfall climatology RADKLIM. This analysis leads to a comprehensive discussion of the added value of a refined spatio-temporal resolution for weather radar observations at sub-hourly temporal and sub-kilometre spatial scales (Study B). Chapter 5 presents first thoughts and preliminary results on an experiment on the uncertainty of the LAWR measurements, followed by the summary and conclusions of this dissertation in Chapter 6.

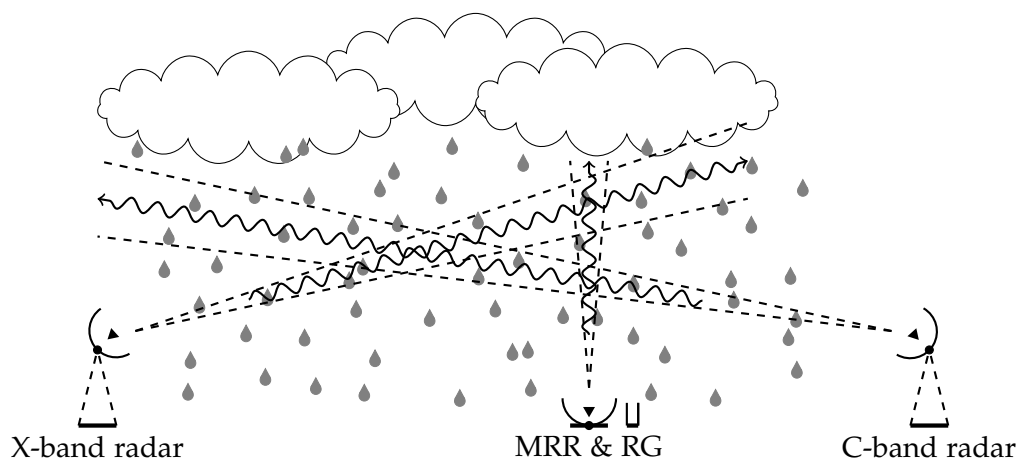


Figure 2.1: Sketch of the synergistic rainfall measurements in Hamburg combining observations of X-band radars, C-band radars, micro rain radars (MRRs), and rain gauges (RGs). The lines indicate the radar beams at different heights.

2

SYNERGISTIC RAINFALL MEASUREMENTS

In order to capture the true variability of rainfall, it is necessary to deploy a network of different measurement techniques (Fig. 2.1), as each method has inherent limitations and uncertainties. The focus of this dissertation is on the single-polarized X-band weather radar, as it provides rainfall measurements at hectometre spatial and sub-minute temporal scales over several years in Hamburg. In this chapter, I give a brief overview of the rainfall observations and data sets in Hamburg with their specifications (Sect. 2.1). Furthermore, I elucidate the extension of the measurement network and changes in measurement strategy in which I was involved and which were not previously documented (Sect. 2.2).

2.1 RAINFALL MEASUREMENTS IN HAMBURG

The study area around Hamburg, Germany (Fig. 2.2) is densely covered by rainfall observations with two local area X-band radars (Sect. 2.1.1), the nation-wide C-band radar network (Sect. 2.1.2), five micro rain radars (MRRs, Sect. 2.1.3), and networks of rain gauges (Sect. 2.1.4).

2.1.1 X-band radar (LAWR)

The Universität Hamburg operates two single-polarized X-band weather radars (Fig. 2.2), to investigate rainfall variability at hectometre spatial and sub-minute temporal scales. The LAWR HHG is measuring in the city centre of Hamburg since 2013. The LAWR ALT is located 21.7 km apart from the LAWR HHG in the west of Hamburg, measuring since 2021. These local area weather radars (LAWRs) are modified ship navigation radars of type GEM scanner SU70-25E operating at a

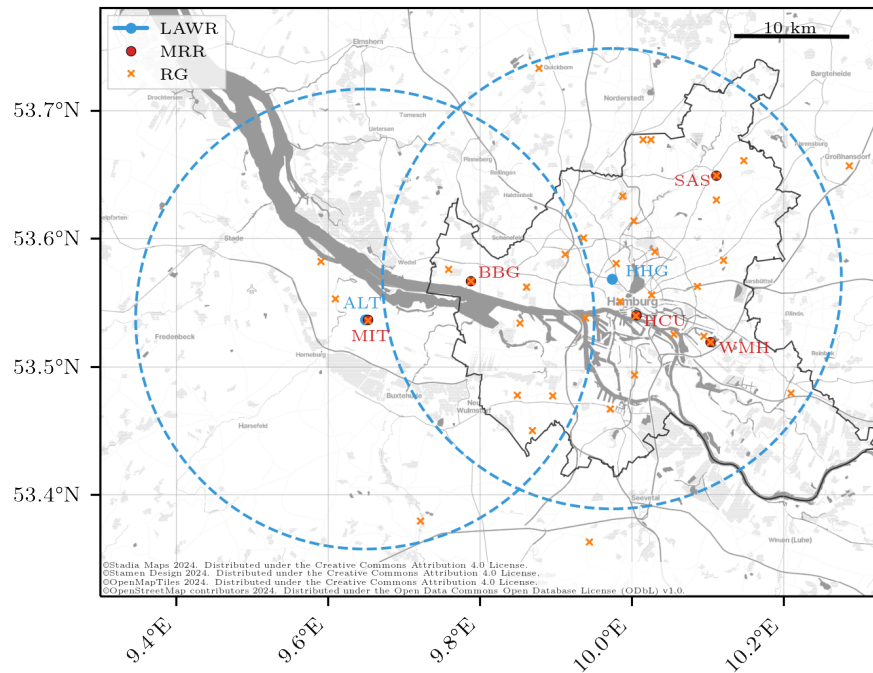


Figure 2.2: Rainfall observations in Hamburg. The local area weather radars (LAWRs, blue points) are located on the rooftop of the Geomatikum building in Hamburg (HHG) and on an 8 m mast on an apple farm in the Altes Land (ALT) region near to Hamburg. The blue dashed lines show their coverage with the 20 km scan radius. The locations of five micro rain radars (MRRs, red points) are by name Blankenese Bauersberg (BBG), HafenCity Universität (HCU), Mittelnkirchen (MIT), Sasel (SAS), and Wettermast Hamburg (WMH). Locations of rain gauges are indicated by orange crosses.

frequency of 9.41 GHz (Lengfeld et al., 2014). In general, a weather radar transmits microwaves, which are partially backscattered by hydrometeors, e.g. cloud droplets, raindrops, snowflakes, and hailstones. As a result of this backscattered signal (Doviak et al., 1993), the LAW R provides radar reflectivity measurements, at one fixed elevation angle ($\approx 3.5^\circ$) with 30 s temporal, 60 m range, and 1° azimuthal sampling resolution within a scan radius of 20 km. The radar reflectivity represents a 30 s average of approximately 67 pulses per 1° collected during 12 sweeps. The high spatio-temporal resolution and the continuous measurement sampling distinguish the LAW R from conventional radars. The measurements are affected by a number of sources of error, including noise, alignment, non-meteorological echoes, radar calibration, and attenuation. These factors limit the quantitative use of the resulting measurement data. Therefore, the LAW R radar data were reanalysed, resulting in corrected radar reflectivities and estimated rainfall rates, as described in detail in Chapter 3.

2.1.2 C-band radar and RADKLIM

The German weather service (DWDs) operates a network of C-band weather radars for nation-wide, volumetric rainfall observations every five minutes. All C-band radars have dual-polarization and Doppler capabilities. For details on the C-band

radar technical setup, data quality, and calibration, refer to Frech et al. (2017). The DWD's scan strategy includes an orography-following precipitation scan for hydrological applications and volume scans at 9 elevation angles every five minutes (Frech et al., 2023). This dissertation uses the precipitation scan from the nearest C-band radar to Hamburg, located near Boostedt about 50 km north of Hamburg. The distances between this C-band radar and the LAWRs are 48.7 km (HHG), 58.1 km (ALT), respectively. The Boosted C-band radar's precipitation scan provides radar reflectivity measurements within a 150 km radius, covering the entire study area. The scan operates at a constant elevation angle of 0.8° with a 5 min temporal, 250 m range, and 1° sampling resolution. The measurements represent a 83 ms average of approximate 50 pulses per 1° azimuth collected during 1 sweep within the 5 min measurement interval. The radar reflectivities were corrected for attenuation using the method of Jacobi and Heistermann (2016), implemented by Heistermann et al. (2013). The rainfall rates R were derived from attenuation-corrected horizontal reflectivities Z using a standard power-law relationship between these quantities, the Marshall-Palmer Z - R relationship (Marshall et al., 1955).

Based on the C-band radar network and the rain gauge network, the DWD provides the radar-based precipitation climatology RADKLIM (Winterrath et al., 2018a). The observations of the C-band radar network were adjusted with rain gauge measurement, corrected for errors, and quality-checked. Rainfall rates are available at 5 min and hourly temporal resolution. For details on the climatology, refer to Winterrath et al. (2017). In this dissertation, ground-based rainfall rates of the YW product (Winterrath et al., 2018a), with a 5 min temporal and a 1 km^2 spatial resolution, are used.

2.1.3 *Micro rain radar (MRR)*

The MRR is a vertically pointing frequency-modulated-continuous wave (FM-CW) Doppler radar manufactured by METEK Meteorologische Messtechnik GmbH (Peters et al., 2002). The MRR retrieves drop size distributions (DSDs) from measured Doppler spectra using the terminal fall velocity given by Atlas et al. (1973). Rainfall rates and radar reflectivities are calculated from DSDs (Doviak et al., 1993). The transmit frequency is at 24.23 GHz (K-band). Further details on the MRR are provided in Study A. The deployed MRRs provide DSD profiles for 31 range gates (MRR-2 model) or 128 range gates (MRR-PRO model), with a range resolution of 35 m and a temporal resolution of 10 s. The MRR profiles intersect with the radar beams of the LAWRs and the C-band radar. The rainfall rates and radar reflectivities were adjusted with a rain gauge at the same location (Study A). Additionally, the adjacent rain gauges monitor the MRR's performance.

The MRRs are deployed at five measurement sites in the study area (Fig. B.2). The MRR Blankenese Bauersberg (BBG) is deployed at a waterworks of the municipal water and wastewater utility Hamburg Wasser in the west of Hamburg since 2017. The MRR HafenCity University (HCU) is measuring on the rooftop of the HafenCity University since 2021. The MRR Mittelnkirchen (MIT) is deployed on an apple farm close to the LAWR ALT since 2020. The MRR Sasel (SAS) was installed by the Meteorological Institute on an official measuring field of the DWD in 2022. The MRR Wettermast Hamburg (WMH) is located at the scientific measuring site of the

Meteorological Institute of the Universität Hamburg in the south-eastern part of the city since 2008. The MRRs and the LAWR HHG are between 3.8 km (HCU) and 12.7 km (SAS) apart. The MRR MIT is outside the LAWR HHG scan radius. The MRRs and the LAWR ALT are 0.3 km (MIT) and 9.8 km (BBG) apart, respectively. The other MRRs are outside the LAWR ALT scan radius. The distances between the MRRs and the C-band radar Boostedt are between 39.6 km (SAS) and 58.0 km (MIT).

2.1.4 Rain gauges

60 rain gauges (Fig. 2.2) from different rain gauge networks were available over the years 2013 to 2023. For the study of rainfall variability (Chapt. 4), 33 rain gauges were used that were available for the year 2019. The University of Hamburg operates a network of weather stations throughout Hamburg, covering, inter alia, 8 tipping bucket rain gauges (Campbell Young 52203) and 2 weighing rain gauges (OTT Pluvio). Two weighing rain gauges and two tipping bucket rain gauges are located close to the MRRs as ground reference. Hamburg Wasser, the municipal water and wastewater utility, operates the largest rain gauge network and provided measurements of 18 weighing rain gauges (OTT Pluvio) for the year 2019. The DWD operates five weighing rain gauges (Lambrecht rain[e]H3) in and around Hamburg. The combined rain gauge network has a maximal pair distance of 46 km and median pair distance of 15 km. Although this rain gauge network is denser than widely-used rain gauge networks, 4 rain gauge pairs are placed side-by-side, and only 3 rain gauge pairs have a larger distance below 1 km, capturing the rainfall variability at a sub-kilometre scale. All rain gauges were checked for the data quality, by investigating the cumulative rainfall accumulation and the probability of detecting with different rainfall thresholds (not shown).

2.2 ENHANCED RAINFALL MEASUREMENTS

Within the scope of this dissertation project, the networked rainfall observations were expanded and improved:

- The LAWR ALT addresses the spatial limitation of rainfall observations at hectometre spatial and sub-minute temporal scales. Since 2021, the LAWR ALT expands the spatial coverage of rainfall measurements in the west of Hamburg (Fig. 2.2). The additional coverage allows for an earlier observation of rain cells approaching the urban area of Hamburg, as the wind direction in the study area has a pronounced southwest to west maximum (Schlünzen et al., 2010). This provides a solution to spatial limitations in nowcasting of rain cells and general studies on rainfall in the area of Hamburg. Since the LAWR ALT and LAWR HHG overlap in their coverage, the LAWR ALT provides duplicated rainfall information in the western districts of Hamburg. These duplicate measurements can reduce errors of rainfall estimates in these areas, by filling measurement gaps, detecting clutter (e.g. Lengfeld et al., 2014), or overcoming attenuation effects (e.g. Lim et al., 2011). Moreover, the LAWR ALT measurements can benefit from its radar site in a rural area, characterized by low apple trees and farms. The measurements in rural areas

are less affected by non-meteorological echoes (clutter) than in urban areas because of fewer objects, e.g. high buildings. The reduced occurrence of clutter signals allows measurements at a lower beam elevation angle and consequently measurements closer to the ground compared to the LAWR HHG measuring in the city center. Measurements closer to the ground reduces effects of the vertical rainfall variability, e.g. due to evaporation, wind drift, or the transition between snow and rain (melting layer) (Villarini and Krajewski, 2010). A discussion on clutter and the radar alignment is provided in Study A. For the LAWR ALT, I contributed to the site selection test measurements and was responsible for maintaining the operational measurements, data management and data processing.

- Three additional MRRs address the gaps in the representation of rainfall profiles at different sites. The MRR-2s have been recently set up at the HCU, MIT and SAS sites, establishing a dense MRR network in the study area (Fig. 2.2). All MRRs give insights about microphysical rainfall properties by measuring drop size distributions and their vertical variability. The MRRs enable the improvement of LAWR rainfall estimates by providing a relationship between the rainfall rate and the radar reflectivity, which is unknown by the LAWR. This relationship can be highly variable, even within the same storm (Villarini and Krajewski, 2010), and additional MRR measurements may capture this variability. Furthermore, the MRRs can provide the exact height of the melting layer at their location (Brast and Markmann, 2020), a height, where the LAWR radar reflectivity can be overestimated by a factor of 2-5, up to a factor of 10 (Villarini and Krajewski, 2010).

The new MRR sites were chosen due to individual reasons and availability. The MRR HCU provides measurement in the city center of Hamburg and is the closest MRR to the LAWR HHG. The LAWR measurements are less likely affected by attenuation at this distance, thus the MRR HCU can evaluate the calibration and performance of the LAWR HHG best. The MRR SAS closes a gap in rainfall observations in the north-eastern districts of Hamburg. The MRR MIT is located within the first range gates of the LAWR ALT and could improve or replace the near-field measurements, which are often affected by clutter, as shown in Study A. For all new MRR sites, I contributed to the site selection, site planning, to maintain the operational measurements, and check measurement data.

- A new MRR-PRO addresses the gap in rainfall profiles at altitudes between 105 m and 4480 m. The MRR BBG was upgraded by replacing the MRR-2 model by its successor model, MRR-PRO, in 2022. The specific site BBG was chosen because both the measurements of LAWR HHG and LAWR ALT cover this location. The MRR-PRO model comes along with an increased sampling frequency and enhanced sensitivity in radar reflectivity. This allows a higher number of range gates. Consequently, the MRR BBG is configured with 128 range gates and a range resolution of 35 m. By measuring at higher altitudes, this configuration solves the issues, where the LAWR radar beam overshoots the MRR measurement volumes discussed in Study A. The MRR BBG provides measurements matching the radar beam of the C-band radar

precipitation scan. Furthermore, the observations of higher altitudes allows studies of the melting layer and mixed-phase precipitation at more seasons. For the MRR-PRO, I contributed to maintain the operational measurements and check measurement data.

- The decreased range resolution at four MRR sites addresses the gap in rainfall profiles at higher altitudes. The range resolution of the MRR HCU, MIT, SAS, and WMH (MRR-2 model) was decreased from 35 m to 70 m on 01 January 2024. The MRRs provide profiles of drop size distributions between 210 m and 2170 m. This configuration solve the same issues of partially mismatching the measurement heights, similarly to the MRR-PRO model at the BBG site.

The improvements to the measurement network were partly informed by the findings of the studies [A](#) and [B](#). Due to the pandemic, some measurement setups could only go into operation after a delay, so that the potential of the new measurements could not be fully explored in this dissertation. Nevertheless, the presented synergistic rainfall observations can be regarded as a foundation for future urban precipitation studies in Hamburg.

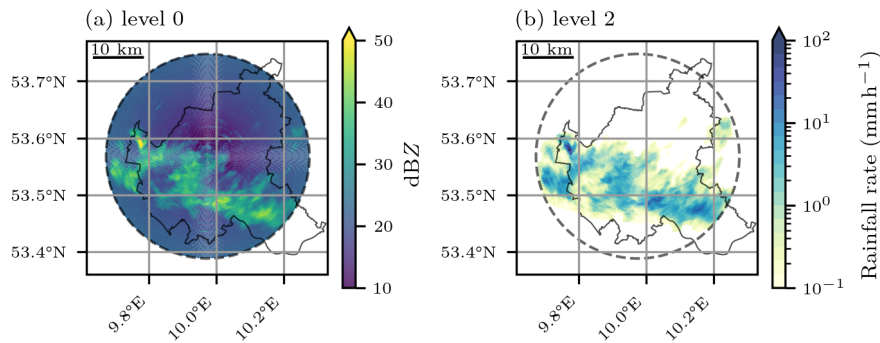


Figure 3.1: LAWR observations of an exemplary rainfall event at different stages of data reanalysis on 31.07.2023 at 18:13 UTC. (a) The level 0 radar reflectivity is superimposed by several errors, including a range-dependent noise signal, and is prior to the data reanalysis (Fig. 3.2). (b) The level 2 rainfall rate shows no evident errors and represents the final stage of the data reanalysis.

3

REANALYSIS OF MULTI-YEAR HIGH-RESOLUTION X-BAND WEATHER RADAR OBSERVATIONS

*Old measurements are precious: once lost, they cannot be replaced.
But without carefully saved information of how the data were measured,
we also create a risk of false conclusions.*

— (Saltikoff et al., 2019)

The LAWR HHG has been in operation for over a decade, generating a multi-year radar data set with higher spatio-temporal resolution than conventional radars today. However, the rainfall estimates are affected by several radar-based errors (Fig. 3.1) and prone to inconsistencies and breaks over the years, e.g. introduced by advancement in the processing algorithms or delayed calibration after hardware changes. As a result, processing a consistent rainfall data set has been a challenge, which has limited the usability of the LAWR data in studies in recent years.

Users of a long-term data set of homogeneously reanalysed rainfall estimates from LAWR observations will need to know the details on data processing, availability, and accuracy. Study A makes the multi-year LAWR HHG radar reflectivities and rainfall rates usable for further studies by providing a well-documented high-quality, open-access radar data set (Burgemeister et al., 2024b). The data set was published for the years 2013 to 2021. The reanalysis procedures of Study A also enabled the creation of an additional LAWR rainfall data set (Burgemeister et al., 2022b), which contributed to the study on cold pool events during the Field Experiment on Sub-mesoscale Spatio-Temporal Variability in Lindenberg (FESSTVaL) from June to August 2021 (Hohenegger et al., 2023). The documented data reanalysis can be employed to extend the time series of the presented data sets and to any measurements from the LAWR ALT or other single-polarized weather radars.

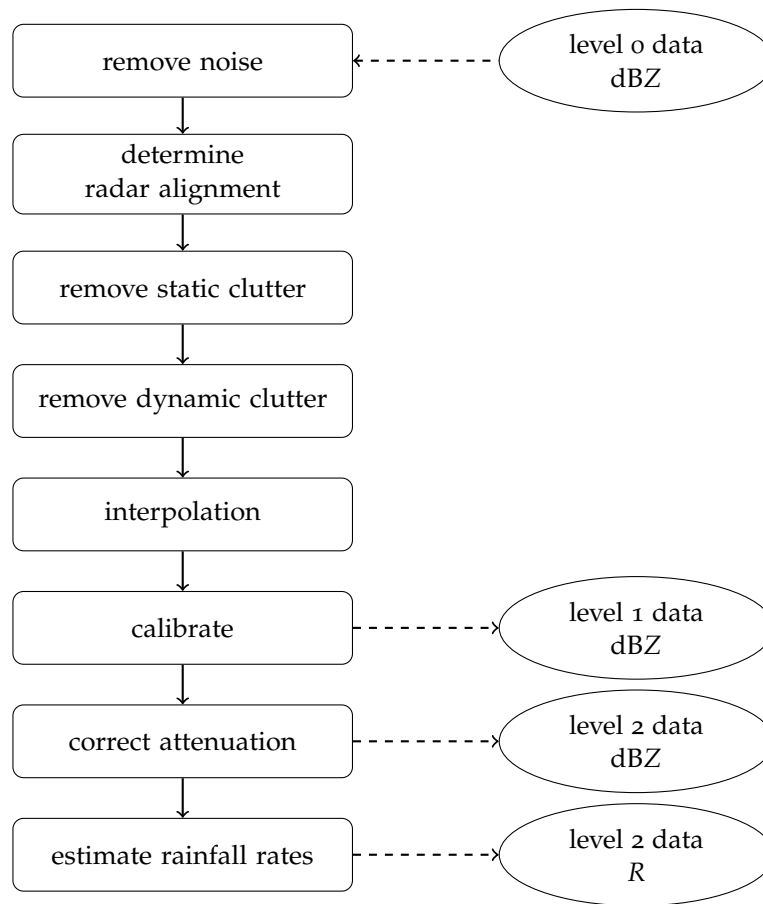


Figure 3.2: Flow chart of the data reanalysis with in- and output data levels. The level 0 data set includes the radar reflectivity dBZ and the standard deviation of the radar reflectivity factor of the averaged single pulses in hourly netCDF files. The level 1 data set includes the calibrated radar reflectivity dBZ in daily netCDF files. The level 2 data sets contain the attenuation-corrected radar reflectivity dBZ and rainfall rate R in daily netCDF files.

This chapter details the reanalysis of the multi-year measurements, with a particular focus on the main procedures (Sect. 3.1). Section 3.2 provides an overview of the radar performance over multiple years, along with a discussion of open issues and limitations.

3.1 DATA REANALYSIS

Several sources of radar-based errors affect the radar reflectivity and rainfall measurements of the LAWR, e.g. noise, alignment, non-meteorological echoes, radar calibration, and attenuation (Fig. 3.1a). The reanalysis radar data set is based on a set of consistent, state-of-the-art data processing procedures (Fig. 3.2) dealing with these errors, which are detailed in Study A and outlined in the following.

Remove noise

The level 0 radar reflectivities are superimposed by microwave noise that comes from the atmosphere and the radar itself. The radar cannot measure this background

noise directly; however, an accurate estimation of the noise is mandatory to detect weak weather signals. Therefore, as a first step in data processing (Fig. 3.2), the background noise removal is dynamically fitted for every 30 s time step. In contrast to the received signal, which is proportional to the squared distance to the radar, the background noise is range-independent. The noise estimate is based on the 10th percentile of the received signal multiplied with the inverse of the squared distance. If more than 10% of the radar bins are affected by rain, the prior noise estimate is used. Furthermore, to stabilize the algorithm regarding radar artefacts, the 10 recent noise levels are averaged. The noise level is subtracted from the radar field, yielding a noise-free radar reflectivity. Specific details on the noise removal can be found in Lengfeld et al. (2014). The noise-free radar reflectivity enables subsequent steps of data processing.

Determine radar alignment

The radar alignment of LAWR was adjusted manually at installation and after maintenance, leading to unknown uncertainties in antenna pointing. Without knowledge about the radar alignment, the location of the measurements is unknown, thus comparisons with other measurement devices are not possible. Fortunately, since the beginning of operational measurements of the LAWR, spikes in radar reflectivity are observed in the direction of the sun during sunrise and sunset (Fig. 3.3). These solar signals facilitate the subsequent determination of the antenna azimuth and the beam elevation angle (Huuskonen and Holleman, 2007), using the known position of the sun, without interrupting the operational measurements (Reda and Andreas, 2008; Stafford et al., 2021). The solar signal in radar reflectivity is the strongest spike in the direction of the sun position and is determined empirically in the radar reflectivity after noise removal during rain-free events. The continuous maximal reflectivity (Fig. 3.3) is detected at 3658 sunrises and sunsets for 23 min on average. The mean calculated sun elevation angle of one sunrise or sunset is the radar beam elevation angle. Changes in radar alignment due to maintenance are clearly visible. The data reanalysis revealed six different beam elevation angles, ranging between 3.3° and 6.1° , and seven different offsets of the azimuth angle up to 5.6° . The high variation of the beam elevation angles and offsets in the azimuth angle highlights the importance of this step in data reanalysis implemented with Study A (Fig. 3.2).

Remove static and dynamic clutter

The noise-corrected and well-aligned radar reflectivities still contain static and dynamic non-meteorological echoes (clutter) characterized by high values and erroneous spatio-temporal gradients. Static clutter is caused by static objects, e.g. trees and buildings. Dynamic clutter is caused by dynamic objects, e.g. planes, birds, and other emitters at X-band frequencies. All these clutter values cannot be easily detected within the LAWR measurements due to the lack of polarimetric or Doppler quantities. The clutter detection requires the application of several gradient-based and time-dependent correction algorithms. As a first step of clutter correction, static clutter is removed by subtracting a static clutter field, where radar reflectivities and clutter are assumed to be additive. The static clutter field is estimated from a temporal median of rain-free radar measurements. The correction of static clutter

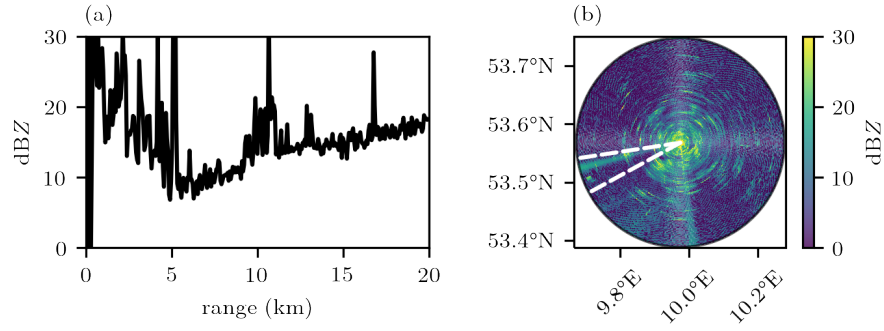


Figure 3.3: Radar reflectivity after noise removal at sunset, 02.03.2020 16:20 UTC. (a) Radar reflectivity at the 255.5° azimuth angle representing the solar signal. (b) Radar reflectivity with continuous signal over range which is visible during the sun set. The white lines indicate a 20° window around the true sun position in the radar azimuth angle.

using the static clutter field subtracts clutter leaving the measurement, so there is no need for interpolation. This additive static clutter field has not been used before for long time series and is described in detail in Study A. Further dynamic clutter signals are removed by several gradient-based correction algorithms, where five different filter algorithms are applied: the texture of the logarithmic reflectivity (TDBZ) filter (Hubbert et al., 2009), the SPIN filter (Hubbert et al., 2009), a spike filter (Lengfeld et al., 2014), a ring filter (Lengfeld et al., 2014), and a speckle filter. The dynamic clutter removal is initially described by Lengfeld et al. (2014), but the application of the algorithms was refined in Study A. Identified and removed clutter signals yield missing values in the reflectivity field. These missing values are interpolated with ordinary Kriging (Cressie, 1993).

Calibrate

The observational synergy between the LAWR and MRR facilitates the calibration and evaluation of the radar measurements, as the LAWR is a low-budget system that has not been accurately calibrated in the laboratory and signal drift can occur over time. The MRR provides the radar reflectivity factor derived from the drop size distributions, which is used to directly calibrate the LAWR radar reflectivity factor. Calibration and evaluation using MRR measurements have three main advantages. The same variable and the same measurement height are compared over sufficiently large sample volumes. A calibration with a disdrometer would increase errors because of the height difference and different sampling volume sizes. The calibration with a rain gauge would introduce an error based on uncertainties associated with the relationship between the radar reflectivity and rainfall rate.

The calibration methodology is initially described by Lengfeld et al. (2014) and the calibration coefficient c_{LAWR} is defined as

$$c_{\text{LAWR}} = 10^{0.1 \cdot (\text{dBZ}_{\text{LAWR}} - \text{dBZ}_{\text{MRR}})} \quad (3.1)$$

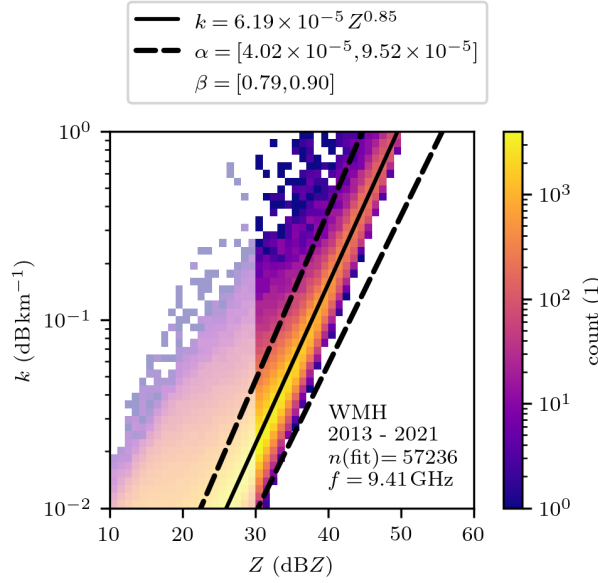


Figure 3.4: Relation between the specific attenuation k and the radar reflectivity dBZ estimated from micro rain radar measurements at 105 m height and 10 s temporal resolution. Only measurements at temperatures above 0°C are used to exclude ice phase. The radar variables are computed at the X-band frequency from measured drop size distributions with T-matrix calculations (Waterman, 1965) implemented by Leinonen (2014) using raindrop axis ratios from Brandes et al. (2002), a canting angle distribution with zero mean and 10° width, and the complex refractive index of water from Liebe et al. (1991) at a temperature of 15°C . The power-law fit for the k - Z relation is based on measurements above 30 dBZ (non shaded area) and is shown with a black solid line, including uncertainties indicated as dashed black line.

with the radar reflectivity of MRR WMH dBZ_{MRR} averaged to altitudes and temporal resolution matching to the LAWR radar reflectivity dBZ_{LAWR} . The calibrated radar reflectivity factor Z'_{LAWR} is then derived from

$$Z'_{\text{LAWR}} = \frac{Z_{\text{LAWR}}}{c_{\text{LAWR}}}, \quad (3.2)$$

with the measured radar reflectivity Z .

Study A revealed 13 calibration periods with a calibration parameter c_{LAWR} between approximately 0.03 (strong overestimation) and 4.4 (strong underestimation). In comparison to a perfect calibration characterised by a value of 1.0, the calibration parameter varies a lot, due to maintenance including technical changes or drifts in signal intensity. The wide range of calibration parameters underscores the necessity for calibrating the radar reflectivity for the general use and interpretation of the measurements. The calibration ensures the comparability of the long-term measurements taken at different times and enables subsequent processing steps. Further details and results are given in Study A. The calibrated radar reflectivities are provided as level 1 data set (Burgemeister et al., 2024b) (Fig. 3.2).

Correct attenuation

The scattering and absorption of the emitted and reflected electromagnetic wave propagating in precipitation is called attenuation. The power loss of the backscattered signal due to attenuation leads to strongly underestimated reflectivities and thus rainfall rates, specifically at X-band frequencies. The radar reflectivity factor Z' at range r suffers from attenuation integrated over the path,

$$Z'(r) = Z(r) - 2 \int_0^r k(s) ds, \quad (3.3)$$

where $Z(r)$ is the unattenuated radar reflectivity factor at range r , and $k(s)$ is the specific attenuation of each range bin. The second term in Eq. (3.3) is known as the two-way path-integrated attenuation (PIA). In Study A the attenuation is corrected with the modified Kraemer (MK) approach (Jacobi and Heistermann, 2016) as suggested by Overeem et al. (2021) for single-polarized radars. The attenuation is corrected with a forward gate-by-gate attenuation correction (Hitschfeld and Bordan, 1954) based on an iterative scheme to improve empirical parameters of a relationship between the attenuation and radar reflectivity (Krämer and Verworn, 2008) including additional constraints of the attenuation PIA and radar reflectivity Z (Jacobi and Heistermann, 2016). The attenuation k used in Eq. (3.3) is estimated from Z (in $\text{mm}^6 \text{m}^{-3}$) using the power-law relation

$$k = \alpha Z^\beta, \quad (3.4)$$

with empirical parameters α and β . These empirical parameters are determined iteratively during the attenuation correction procedure between specific limits depending on the radar frequency. The MK approach is detailed in the literature (Jacobi and Heistermann, 2016; Overeem et al., 2021) and the specific settings of the implementation are documented in Study A.

The specific attenuation k at X-band frequency is derived from the multi-year MRR drop size distributions (Fig. 3.4). With the approach by Overeem et al. (2021) the uncertainties of Eq. (3.4) and the limits of the empirical parameters are estimated. The limits of α and β are $\alpha_{\min, \max} = [4.02 \cdot 10^{-5}, 9.52 \cdot 10^{-5}]$ and $\beta_{\min, \max} = [0.79, 0.90]$. For details, how to estimate the uncertainties, refer to Study A. This valid range of α and β is in agreement with estimates of other k - Z relations at X-band frequencies (e.g. Berne and Uijlenhoet, 2006; Delrieu et al., 1999; Delrieu et al., 2022; Diederich et al., 2015; van de Beek et al., 2010).

Study A makes the limits at X-band frequencies available, which are not defined in existing literature, as Jacobi and Heistermann (2016) and Overeem et al. (2021) applied the MK approach only at C-band frequencies. Other studies that seek to implement the MK approach at X-band frequencies may benefit from the provided specific settings, given that not every study has access to drop size distribution measurements to adapt the algorithm parameters. The attenuation-corrected radar reflectivities are provided as level 2 data set (Burgemeister et al., 2024b) (Fig. 3.2).

Estimate rainfall rates

Rainfall rates R are estimated from the attenuation-corrected reflectivities Z using a standard power-law relationship between these quantities, the Marshall-Palmer Z - R relationship (Marshall et al., 1955):

$$Z = a R^b, \quad (3.5)$$

where the multiplicative factor $a = 200$ and the exponent $b = 1.6$ are empirical constants. Although, keeping in mind that Z and R depend on the drop size distribution, which varies geographically, with rainfall rate, and over time (e.g. Berne and Krajewski, 2013; Doviak et al., 1993; Villarini and Krajewski, 2010), consequently the empirical constants can be highly variable. Nevertheless, the Marshall-Palmer Z - R relation is an appropriate representation of average rainfall conditions in this climate, as investigated with multi-year MRR drop size distributions in Hamburg (not shown) and by Holleman (2006) and Kirsch et al. (2019). The estimated rainfall rate R (Eq. 3.5, in mm h^{-1}) is provided as a level 2 data set (Burgemeister et al., 2024b) and constitutes the final data product of the data reanalysis (Fig. 3.2).

3.2 DATA QUALITY

The data reanalysis of the multi-year LAWR measurements has led to an improvement in the data quality of the radar reflectivity and, consequently, the rainfall rate estimate, demonstrated in Study A. However, it should be noted that the data reanalysis and discussion on data quality is constrained to the liquid phase, based on a temperature threshold, which avoids effects from a decreased data quality as caused by a melting layer. This section provides quantitative evidence for the performance of the multi-year X-band radar observations, underlined by qualitative examples.

The reanalysed LAWR measurements are quantitatively evaluated using MRR measurements at matching heights and a matching temporal resolution of 30 s, which comes with the same advantage as for the calibration. The same variable and the same measurement height are compared over sufficiently large sample volumes. The LAWR attenuation-corrected radar reflectivity (level 2 data set) is in very good agreement with the MRR WMH reference, as evidenced by a low bias of 0.52 dB, a moderate root-mean-square error (RMSE) of 3.93 dB and a high Pearson correlation coefficient of $r = 0.88$. The independent reflectivity measurements of the MRR BBG confirm the data quality: bias of -0.30 dB, RMSE of 3.85 dB, and $r = 0.88$. Therefore, the LAWR reflectivity is not biased in total.

The LAWR rainfall rates (level 2 data set) exhibit good agreement with the MRR WMH reference, demonstrated with a low bias of 0.42 mm h^{-1} , a moderate RMSE of 4.69 mm h^{-1} , and a correlation coefficient for the logarithmic rainfall rate of $r = 0.74$. Since the reflectivities of LAWR and the MRRs are in good agreement, the comparison of the rainfall rates mainly investigates the performance of the Marshall-Palmer Z - R relation. The average underestimation of rainfall rates is consistent with the findings of Kirsch et al. (2019), who show that the Marshall-Palmer Z - R relation underestimates rainfall accumulation derived from drop size distributions by 6.3% to 17.4%. The error increases in cases of strong convective precipitation because

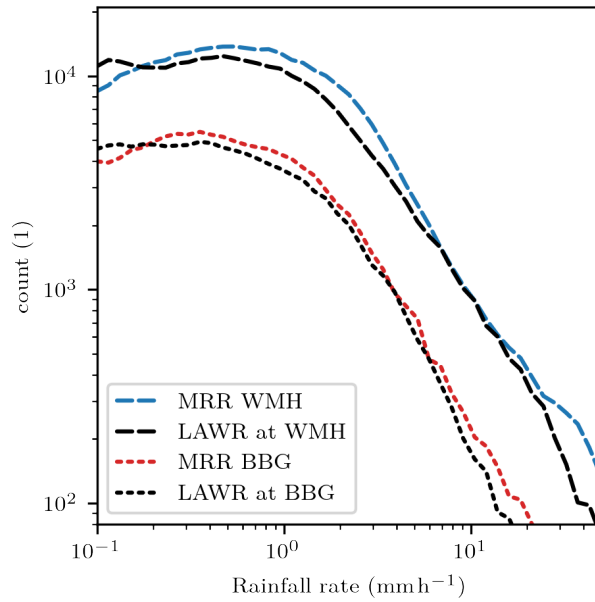


Figure 3.5: Frequency distribution of rainfall rates estimated from LAWR using a Z-R-relation and MRR WMH and MRR BBG based on drop size distributions averaged at beam height at a temporal resolution of 30 s.

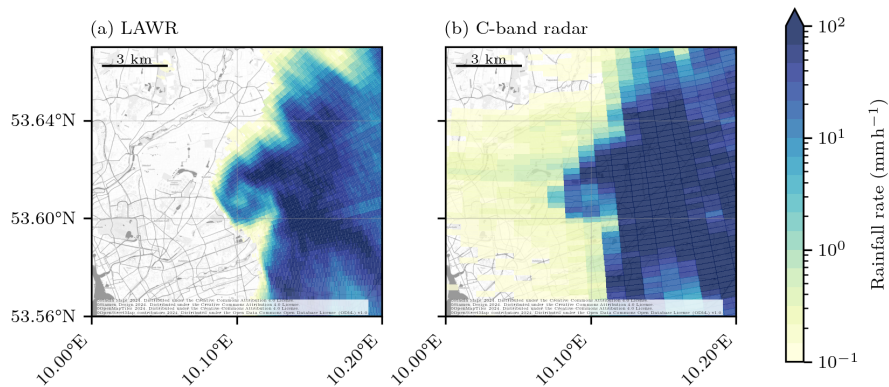


Figure 3.6: Rainfall pattern during a tornado event on 07.06.2016 at 16:25:30 UTC, observed by (a) the LAWR and (b) the C-band radar. The rainfall rate is shown for a north-eastern section of the measurement domain in Hamburg.

raindrop size distributions begin to diverge from Marshall-Palmer distributions for these cases (Schleiss et al., 2020).

Although, the rainfall rate estimates can deviate for individual time steps, LAWR measurements reproduce the frequency distribution of rainfall rates as observed by two MRRs very well (Fig. 3.5). In particular, the LAWR is able to identify rainy time intervals. Consequently, the LAWR measurements yield reliable rainfall rate estimates at beam height and sub-minute temporal scale. A qualitative example of a rainfall event illustrates this point additionally (Fig. 3.6a). The LAWR resolved a characteristic circular hook echo in the 30 s average rainfall rate, demonstrating a rotating rainfall circulation around a tornado, first discussed by Hoffmann et al. (2018). The hook echo is clearly visible for 8 min, in 16 measurement time steps, ac-

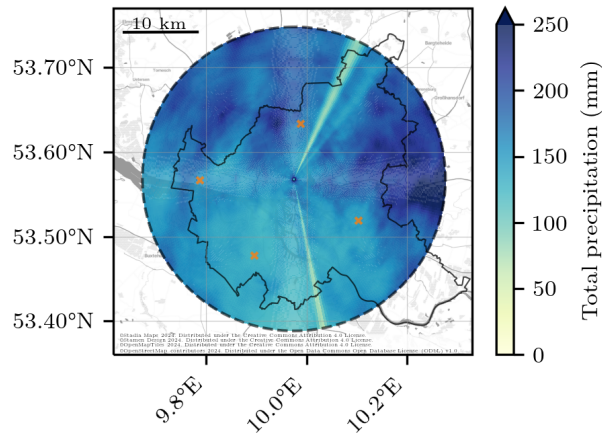


Figure 3.7: Three-month total precipitation measured by the LAWR during June, July, and August 2019. The radar estimates at four rain gauge locations (orange crosses) are 174.7 mm (north), 146.7 mm (east), 132.1 mm (south), and 157.1 mm (west).

cordingly. The German nationwide C-band radars, measuring with 5 min temporal and 250 m range resolutions, show the general rainfall pattern, but the hook echo is only at one measurement time step (Fig. 3.6b). As a consequence, this event gives a first hint that the LAWR, with its refined spatio-temporal resolution compared to coarser resolved C-band radars, is capable of resolving rainfall patterns with a short duration and relevant gradients at hectometre spatial scales. Consequently, the LAWR measurements provide continuous spatio-temporal rainfall patterns.

This still holds for longer time scales. Fine-scale structures in rainfall patterns are smoothed by temporal accumulation; nevertheless, spatial differences are still visible in a three-month rainfall accumulation (Fig. 3.7). The rainfall accumulations reveal long-term measurement errors, inter alia remaining clutter close to the radar and three spikes. First, range gates close to the radar are still affected by clutter after the application of correction algorithms, resulting in a small circle of high rainfall accumulations. Approximately 500 m around the radar location, the first 8 of 333 range gates show the overestimated total precipitation. Second, three spikes are characterized by an underestimation of total precipitation affecting multiple azimuth angles over the whole range. Without these errors, the 3-month total precipitation is in general not affected by clutter, noise, or attenuation (Fig. 3.7). However, note that rainfall patterns at ground can deviate in comparison to measured rainfall pattern at beam height because of vertical rainfall variability (Villarini and Krajewski, 2010). Four rain gauges measured 194.8 mm (north), 127.6 mm (east), 134.0 mm (south), and 172.9 mm (west) during the 3 months (Fig. 3.7). The absolute biases between the radar rainfall accumulations and rain gauge measurements are low, ranging from 1.9 mm to 20.1 mm. In general, the rain gauge observations are in agreement with the estimated radar rainfall accumulations during this measurement period.

Study A points out that the reanalysed radar reflectivities and rainfall rates can be used for meteorological and hydrological studies, considering the following limitations:

- The LAWR data set is limited to estimates during the precipitation's liquid phase.

- The attenuation correction can become unstable; thus, radar reflectivities can be overestimated. In rare cases, radar reflectivities are not corrected for cases with a numerically unstable attenuation correction.
- Differences between the LAWR measurements at beam height and ground observations are a result of vertical variability of rainfall due to wind advection and evaporation of rainfall. Variations between measurement devices can be caused by differences in measurement principles and mismatches in the measured volumes.
- Single measurements can be overestimated because of remaining clutter and noise. The measurements in the first range gates can be superimposed by clutter.
- The beam of the LAWR HHG is blocked in three directions, resulting in three distinct spikes in the measurements.

3.3 KEY FINDINGS

In brief, Study [A](#) answers the first two research questions and yields the following key results:

- Quality-tested radar reflectivities and rainfall rate estimates with 30 s temporal and hectometre spatial resolutions covering the years 2013 to 2021 are provided as an open-access data set (Burgemeister et al., [2024b](#)).
- The reanalysed multi-year LAWR measurements give insight into the spatio-temporal structure of rainfall at 30 s temporal scale and hectometre spatial scale in an urban area.
- A local-area X-band weather radar (LAWR) can provide reliable rainfall estimates, despite the lack of polarization and Doppler information, as evidenced by good agreement between LAWR and MRR measurements.

ADDED VALUE OF SPATIO-TEMPORAL RESOLUTION FOR WEATHER RADAR OBSERVATIONS AT URBAN SCALES

The recent available reanalysed LAWR observations of Study A enable further studies on the spatial and temporal scales of precipitation between the scales captured by rain gauges and conventional weather radars. The LAWR offers the highest area-wide spatio-temporal resolution (60 m and 30 s) of measurements compared to the network of available rain gauges (point measurement, 1 min), the nearest operational C-band radar (250 m and 5 min), and the radar-rainfall climatology RADKLIM (1 km and 5 min). However, the higher spatio-temporal resolution does not need to translate to measurements close to the unknown truth. Several rainfall events reveal strong differences in the spatial variability of rainfall observed by different measurement devices, as already demonstrated in Chapter 1 with disparate representations of a rainfall event observed by the different measurements (Figure 1.1). Study B explores the added value of spatio-temporal resolution for weather radar observations at sub-hourly and sub-kilometre scales by addressing three research questions:

- Is the local rainfall rate of the LAWR superior to other rainfall estimates?
- Is the LAWR better in capturing spatial rainfall variability?
- Are there structures within the LAWR measurements not obtained by other measurement devices?

In the following, I outline the main results of Study B, which answer the research questions with a comparative study focussing on five months of measurements in 2019.

4.1 COMPARISON TO A LOCAL REFERENCE

The local rainfall observations are represented by MRRs and rain gauges as a reference. The LAWR and C-band radar both provide rainfall rates retrieved from their radar reflectivities, but differ in spatio-temporal resolution and scanning strategy. The LAWR measurements have a radial resolution of 60 m and represent a true 30 s average of its measurement interval. In contrast, the C-band measurements have a radial resolution of 250 m and measure just 83 ms per azimuth of a represented 5 min measurement interval.

The MRR reference reveals, that at a 30 s temporal resolution, both the LAWR and C-band rainfall rates perform equally well (Fig 4.1a and b). This is also evidenced by conventional statistical metrics, such as the bias and RMSE (Table 4.1). Both radars are able to distinguish between rainfall and no rainfall, which is also defined as rainfall intermittency. This is demonstrated by the critical success index (CSI, Table 4.1), a statistical metric suggested for evaluating the performance of radar rainfall measurements by Germann et al. (2006), which is also described in Study

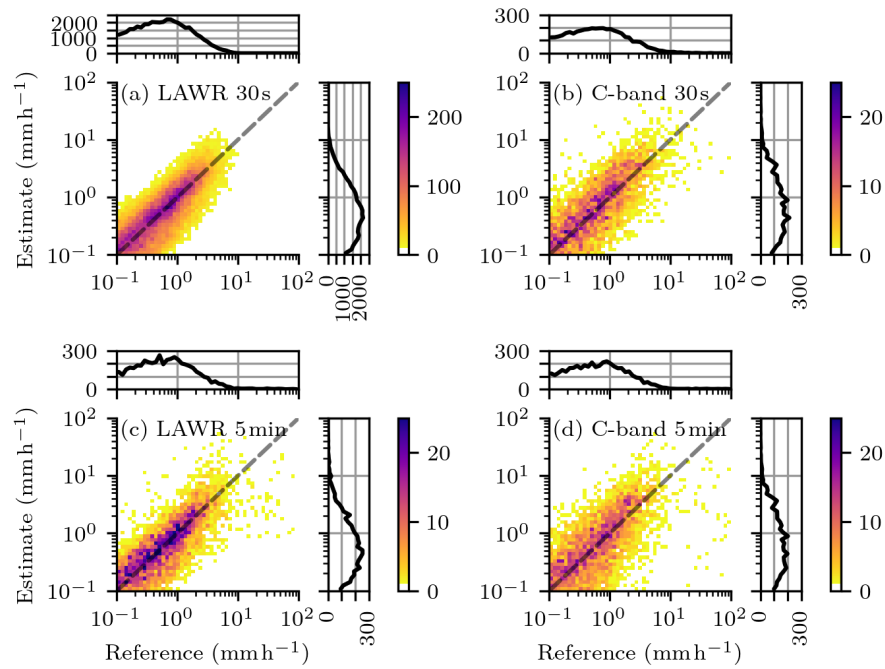


Figure 4.1: Joint distribution of radar rainfall rates estimated from LAWR and C-band radar observations versus two MRRs as reference. The measurements are compared at overlapping heights for the period May to September 2019. The MRR rainfall rates were averaged to (a, b) 30 s and (c, d) 5 min. The LAWR rainfall rates are shown at (a) 30 s temporal resolution and (c) were averaged to 5 min. The C-band rainfall rates in (b, d) are the instantaneous measurements from the 5 min measurement interval.

B. At a temporal resolution of 5 min, the LAWR rainfall rates are superior to those of the C-band radar (Fig 4.1c and d). Furthermore, at a 5 min temporal resolution, the LAWR is more effective at detecting the intermittent nature of rainfall than the C-band radar. The better performance of the LAWR is expected because the LAWR rainfall rate is based on a continuous 5 min observation, whereas the C-band rainfall rate is an instantaneous observational sample based on one 83 ms measurement average.

This better performance does not translate in a better match to rainfall accumulations recorded by rain gauges, as differences in the Z-R relation and sample volume sizes between radar and rain gauge dominate the uncertainty for both the LAWR and C-band radar. As a reference, the rain gauge network shows that rainfall estimates from LAWR and C-band radar measurements perform equally well at ground level, analysed with rainfall accumulations between 15 min and 1 d, detailed in Study B. The LAWR and C-band radar measurements underestimate rainfall accumulations from rain gauges slightly, evidenced by a bias ranging from -0.11 mm for a 15 min duration to -0.40 mm for a daily duration.

In conclusion, Study B demonstrates that the LAWR rainfall estimates outperform the C-band radar rainfall estimate at a 5 min temporal resolution shown with MRR measurements at beam height. For point rainfall observations at the ground, the LAWR and the C-band radar demonstrate comparable performance in capturing rainfall accumulations across all durations. In order to investigate the performance

Table 4.1: Evaluation metrics of rainfall rate distributions comparing the LAWR and C-band radar with the MRRs, respectively. n is the number of observations above 0.1 mm h^{-1} for both rainfall rates. The standard statistical metrics are the bias and the root-mean-square error (RMSE). Based on hits, misses, false alarms, and correct negatives, the critical success index (CSI), the false alarm ratio (FAR), and the probability of detection (POD) is calculated.

	30 s		5 min	
	(a) LAWR	(b) C-band	(c) LAWR	(d) C-band
n	45242	4183	4848	4224
bias / mm h^{-1}	0.10	0.19	-0.04	0.00
RMSE / mm h^{-1}	3.46	2.94	3.61	4.69
CSI	0.75	0.75	0.81	0.71
FAR	0.20	0.21	0.12	0.21
POD	0.92	0.94	0.91	0.87

of rainfall estimation, as intended with the first research question of this section, it appears that the MRR is a more suitable reference than the rain gauge network.

4.2 SPATIAL VARIABILITY

The spatial rainfall structure is determined for the different rainfall data sets using the spatial correlation. The Pearson's product-moment correlation is used to estimate the spatial correlation, as commonly done in many studies (e.g. Ciach and Krajewski, 2006; De Vos et al., 2017; Krajewski et al., 2003; Leth et al., 2021; Peleg et al., 2013; Tokay et al., 2014; Villarini et al., 2008). The correlograms are calculated based on pairs of rain gauges and pairs of a randomly drawn sample of 100 grid points using a bin size of 100 m and different timescales, ranging from 1 min to daily rainfall accumulations. The correlation decays as the separation distance between two locations increases due to spatio-temporal rainfall variability. The spatial correlation can be parameterised with an isotropic, three-parameter exponential function:

$$r(d) = r_0 \exp \left[- \left(\frac{d}{d_0} \right)^{s_0} \right] \quad (4.1)$$

where d is the separation distance between two locations, r_0 is the nugget parameter, d_0 is the decorrelation distance and e-folding distance, and s_0 is the shape parameter (e.g. Ciach and Krajewski, 2006; Foelsche et al., 2019; Habib et al., 2001; Krajewski et al., 2003; Peleg et al., 2013; Villarini et al., 2008).

The nugget parameter r_0 represents the zero-distance correlation and thus describes the uncertainty of measurements at the same location. The analysis of the rainfall data sets yields a nugget parameter of one. Accordingly, only a two-parameter exponential function without the nugget parameter is used, as done by other studies (Leth et al., 2021; Mascaro, 2017; Thomassen et al., 2022). The shape parameter s_0 , characterising the shape of the exponential function, is below 1 for every rainfall data set, and does not contribute any further insights within the

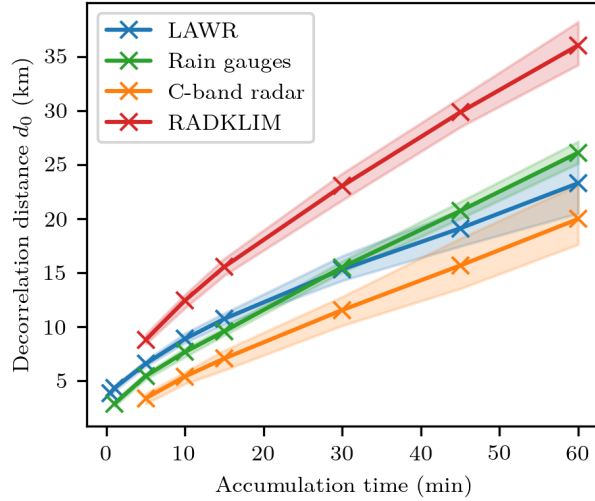


Figure 4.2: Decorrelation distance for different timescales (30 s, 1 min, 5 min, 15 min, 30 min, 45 min, and 1 h; crosses) for the months May to September 2019. The colors indicate the rainfall data sets: LAWR (blue), rain gauges (green), C-band radar (orange), RADKLIM (red). The solid lines mark the median and the shaded area is the 5- to 95-percentile range of a bootstrap sample.

scope of this investigation. Therefore, this dissertation focuses on the decorrelation distance d_0 , describing the decay of the spatial correlation, which provides insight into the spatial variability of rainfall.

The decorrelation distance increases with timescale, from a few kilometers for rainfall accumulation of a few minutes to several tens of kilometres for hourly rainfall accumulations (Fig. 4.2). The rainfall data sets capture a different rainfall variability, with distances between 3.84 km and 23.28 km for the LAWR, 2.89 km and 26.10 km for the rain gauges, 3.44 km and 19.97 km for the C-band radar, and 8.79 km and 36.03 km for RADKLIM. The uncertainty of the decorrelation distance is analysed by calculating the correlograms for different samples of the same rainfall data sets. For the rain gauge network, bootstrapping is applied using the same sample size. For the gridded rainfall data sets, 100 randomly drawn samples of 100 grid points were created. The 5- to 95-percentile range of distances, as measure of uncertainty, increases with timescale. The 5- to 95-percentile range, in relation to the median, tends to be narrow and constant for timescales up to an hour.

The spatial rainfall structure of the LAWR and rain gauge measurements match best for sub-hourly timescales, since differences of the decorrelation distances are between 278 m and 1.58 km (Fig. 4.2). The differences between the distances can be explained by different measurement principles, because point and areal measurements are compared. Surprisingly, the C-band radar underestimates decorrelation distances for timescales up to an hour. The 5 min C-band radar measurements have a decorrelation distance of 3.44 km, which is lower than the 5 min rain gauge distance of 5.48 km. This underestimation contradicts the assumption that a decreased spatio-temporal resolution comes along with a decrease in decorrelation distances, but is a consequence of the C-band radar scan strategy. The C-band radar scans 83 ms per azimuth and needs 30 s for the measurement scan, therefore the C-band radar measures at an expected timescale of 5 min, a mixture of spatial variabilities

below a timescale of 30 s. The RADKLIM rainfall underestimates the spatial rainfall variability compared to the other observations. This underestimation comes along with the lowest spatial resolution compared to the other rainfall data sets and is a consequence of spatial averaging and the rain gauge adjustment to a rain gauge network with larger separation distances, than used in this study. Kreklow et al. (2020) and Pöschmann et al. (2021) outline the underestimation of high intensity rainfall due to spatial averaging. Peleg et al. (2018) show that extreme rainfall intensities within a radar pixel are on average at least 10 % larger than values estimated from weather radars at a spatial resolution of 1 km. Rainfall accumulations of longer timescales than an hour are discussed in Study B, but the decorrelation distances become increasingly uncertain and therefore less meaningful due to the limited spatial scope of the rainfall data sets, which encompass separation distances of up to 40–55 km.

In conclusion, Study B finds that conventional available rainfall data sets fail to capture the sub-hourly rainfall variability. The spatial rainfall structures captured by LAWR and rain gauge measurements are similar at sub-hourly timescales. The C-band radar overestimates the spatial rainfall variability at sub-hourly timescales due to its intermittent scanning strategy every five minutes. The radar-rainfall climatology RADKLIM underestimates spatial rainfall variability due to its coarser spatial resolution. The matching variability of the LAWR and dense rain gauge measurements create confidence in the LAWR rainfall data set. Therefore, the LAWR measurements provide an added value at the sub-hourly scale compared to C-band radar measurements and RADKLIM.

4.3 RAINFALL PEAKS

The link between spatio-temporal rainfall variability and flood response is complex (Zhou et al., 2021). One driver for the hydrological response are rainfall peaks (e.g. Bruni et al., 2015; Cao et al., 2023). Wang et al. (2023a) conclude that the accuracy of rainfall estimates significantly impact modelled peak flows in cases of heavy rainfall. Bárdossy and Anwar (2023) highlight that interpolation and low rainfall data density can lead to peak flow underestimation in rainfall-runoff modelling. Rain gauge networks sample less likely from the upper tail of the rainfall distribution due to their limited spatial coverage. Contrastingly, weather radars fill the gap in spatial coverage, they however represent volume samples and averages. The differences in spatio-temporal resolution and scan strategy affect the spatio-temporal variability of the observed rainfall distributions. Therefore, the effect of spatio-temporal coarsening on rainfall peaks is investigated.

Following Cristiano et al. (2018, 2019), the peak attenuation ratio $P(R)$ for rainfall is calculated,

$$P(R) = -\frac{R_{\max,\text{ref}} - R_{\max,\Delta s\Delta t}}{R_{\max,\text{ref}}}, \quad (4.2)$$

where $R_{\max,\text{ref}}$ is the peak rainfall rate at the highest spatio-temporal resolution and $R_{\max,\Delta s\Delta t}$ is the peak rainfall rate at radial resolution Δs and temporal resolution Δt . The peak attenuation ratio quantifies the rainfall peak underestimation as a consequence of spatio-temporal coarsening.

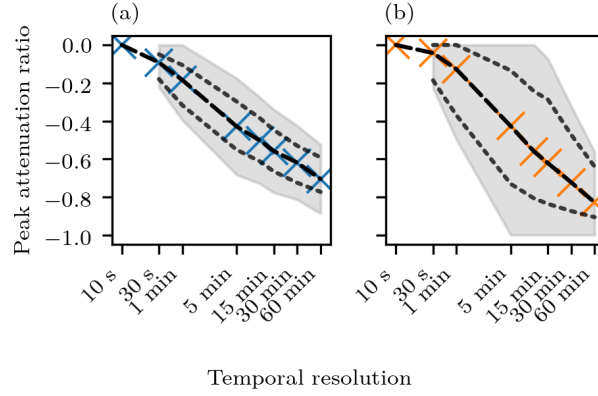


Figure 4.3: Peak attenuation ratio (Eq. 4.2) associated with the rainfall rate at different temporal resolutions based on MRR measurements available at 10 s temporal resolution. Variables were averaged (a) or the first sample of the interval was used (b). The crosses show the median, the dotted lines show the interquartile range, and the grey area is the range of the whiskers.

Firstly, Study B indicates that temporal coarsening has a strong impact on rainfall peaks (Fig. 4.3). Rainfall peaks are reduced by 9% in median for 30 s averages and up to 70% in median for hourly averages in comparison to the 10 s rainfall rates (Fig. 4.3a). Using only the first 10 s measurement to represent the measuring period reduces rainfall peaks by 4% in median for the 30 s timescale and up to 83% in median for the hourly timescale compared to the 10 s rainfall rates (Fig. 4.3b). At the 5 min timescale, both scan strategies underestimate the rainfall peaks by 43%. However, temporal sampling instead of averaging causes a larger variability, as shown by the quantiles of the peak attenuation ratio in Figure 4.3. For timescales longer than 5 min, temporal averaging outperforms temporal sampling in terms of capturing rainfall peaks in the median. At all timescales, temporal coarsening by sampling can result in the total loss of rainfall peaks by missing them, whereas averaging smooths and hence preserves information about rainfall peaks.

Secondly, Study B indicates that temporal averaging exerts a greater impact on rainfall peaks than spatial averaging (Fig. 4.4), which is in line with previous studies by (Cristiano et al., 2018, 2019). Rainfall peaks are reduced up to 91% in median at 1980 m and 60 min spatio-temporal resolution compared to the reference resolution of 60 m and 30 s. On the one hand, spatial averaging reduces rainfall peaks by 4% at a spatial resolution of 120 m (Fig. 4.4b) up to 41% at a spatial resolution of 1980 m (Fig. 4.4f) for a temporal resolution of 30 s. On the other hand, temporal averaging results reduces rainfall peaks by 9% at a temporal resolution of 1 min up to 83% at a temporal resolution of 60 min (Fig. 4.4a) for a spatial resolution of 60 m. The reduction in rainfall peaks is twice as great when the temporal scale is doubled (30 s to 1 min, Fig. 4.4a) in comparison to the spatial resolution (60 m to 120 m, Figures 4.4a and b).

In conclusion, Study B shows the importance of spatio-temporal resolution and scan strategy in accurately measuring rainfall peaks. Furthermore, Study B highlights that the LAWR is able to capture rainfall peaks better than the C-band radar due to the used scan strategy (Fig. 4.3) and spatio-temporal resolution (Fig. 4.4). Consequently, the LAWR can provide an added value in measuring

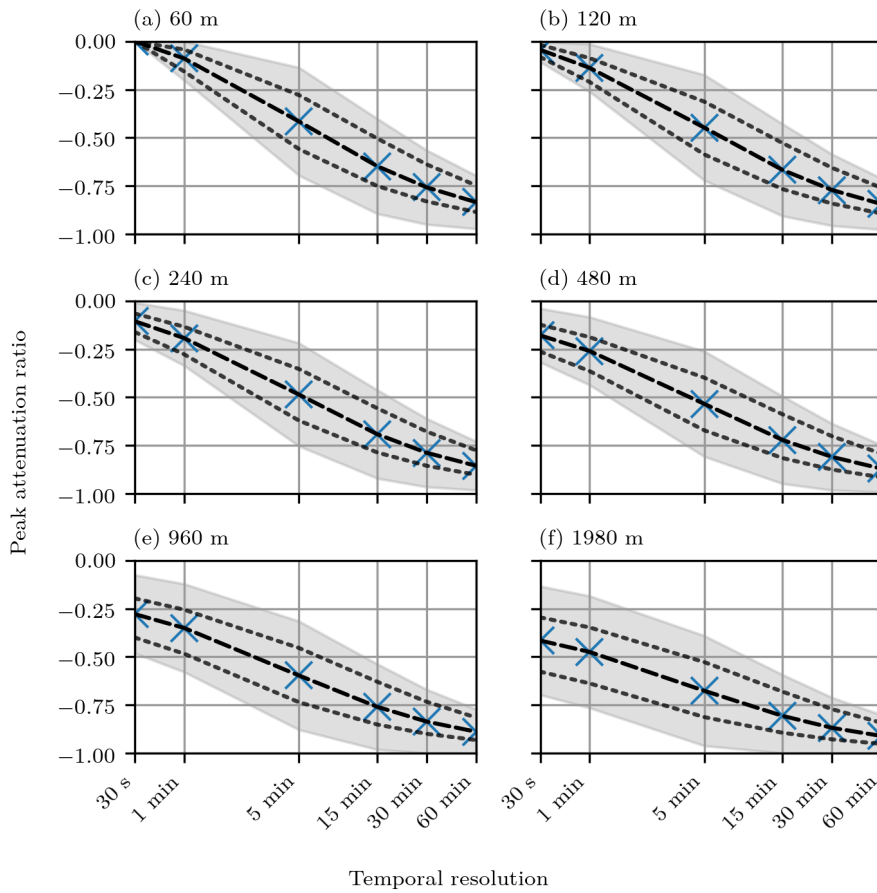


Figure 4.4: Peak attenuation ratio (Eq. B.6) associated with the rainfall rate at different temporal resolutions based on LAWR measurements available at 60 m range and 30 s temporal resolution. Rainfall rates were coarsened for spatial scales of (a) 60 m, (b) 120 m, (c) 240 m, (d) 480 m, (e) 960 m, (f) 1980 m and for temporal scales from 30 s to 60 min.

rainfall peaks compared to C-band radar measurements, that can be relevant for the hydrological response, e.g. caused by a localized rainfall event in an urban area.

4.4 SUB-KILOMETRE STRUCTURE

Since differences in spatio-temporal resolution and scan strategy affect peaks and spatial structure of the measured rainfall distribution, Study B investigates observations of sub-kilometre spatial radar rainfall variability in more detail. To analyse the continuity and new structures of radar rainfall variability at the microscale, gradients of radar reflectivity are computed. Study B discusses the statistics of radar reflectivity gradients of the LAWR derived at higher (60 m) spatial resolution compared to the C-band radar at 250 m spatial resolution. To derive gradients, the differences in radar reflectivities at different lag distances are computed first (Fig. 4.5).

The radar reflectivity difference distributions are unbiased for both radars and all lag distances (Table B.4), represented by the distributional mean. Resulting from spatial variability, the variances increase with lag distance. Derived from the

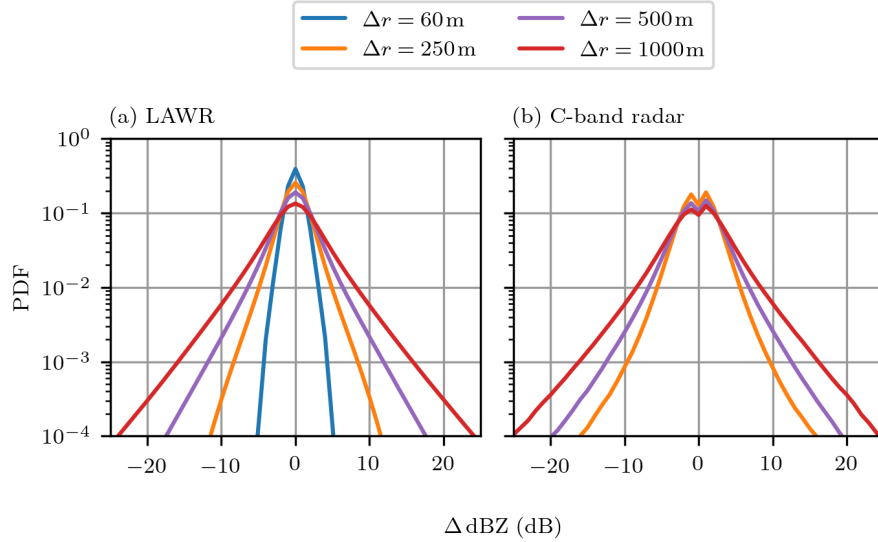


Figure 4.5: PDF of (a) LAWR and (b) C-band radar reflectivity differences for radar reflectivities larger than 10 dBZ in beam direction using lag distances Δr of 60 m, 250 m, 500 m, and 1000 m.

Table 4.2: Distribution moments of (a) LAWR and (b) C-band radar reflectivity differences using lag distances Δr of 60 m, 250 m, 500 m, and 1000 m.

Δr	LAWR				C-band		
	60 m	240 m	480 m	1020 m	250 m	500 m	1000 m
mean (dB)	-0.00	-0.01	-0.02	-0.05	-0.01	-0.01	-0.01
variance (dB ²)	1.16	3.94	8.81	18.84	5.94	10.43	19.08
skewness	0.00	0.02	0.03	0.02	-0.02	-0.02	-0.04
kurtosis	4.17	5.88	7.16	6.90	13.31	8.07	7.45

second moment, the variance is used by many studies to describe the spatial rainfall variability estimated from radar observations (e.g. Berne et al., 2004; Emmanuel et al., 2012; Germann and Joss, 2001; Ochoa-Rodriguez et al., 2015). Contrastingly, higher statistical moments, like the skewness and kurtosis, are not commonly discussed in other studies, but may give insights in errors and extremes, as discussed in Study B. The distributions are unskewed. The absence of biases and skewness indicate that the attenuation correction is successful on average. Derived from the fourth moment, the kurtosis is mainly influenced by the distribution tails (Westfall, 2014). The kurtosis indicates that the C-band radar measures more radar reflectivity gradients at the distribution tails than the LAWR, despite the coarser spatial resolution.

The higher spatial variability of the C-band radar measurements compared to the LAWR measurements has already been discussed in Section 4.2 and is also represented by the variances at different lag distances (Fig. 4.6). At a 250 m lag distance, the LAWR variance is reduced by 34% in comparison to the C-band radar variance (Fig. 4.6a). At zero lag distance, the variance is defined as nugget variance and expected to be zero (Cressie, 1993). However, the variogram of the

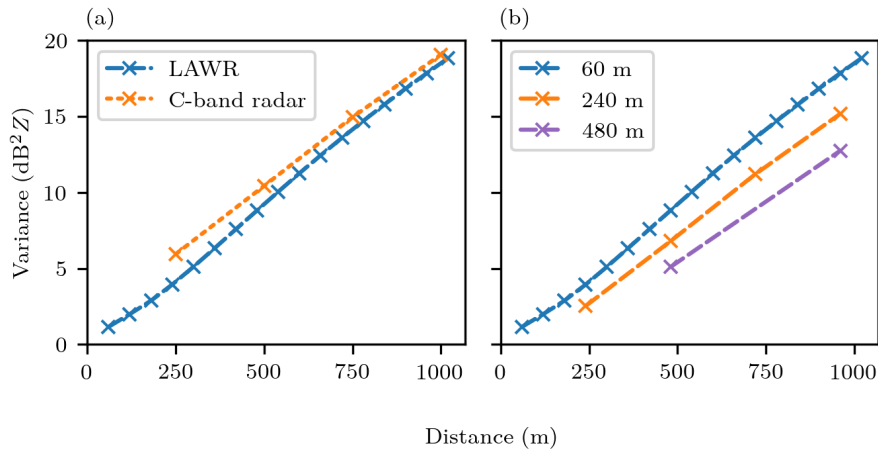


Figure 4.6: Variogram of radar reflectivities above 10 dBZ. (a) LAWYR radar reflectivities at 60 m spatial resolution (blue) are compared with C-band radar reflectivities at 250 m spatial resolution (orange). (b) LAWYR radar reflectivities at 60 m spatial resolution (blue) are compared with averages at 240 m (orange) and 480 m (purple) spatial resolution.

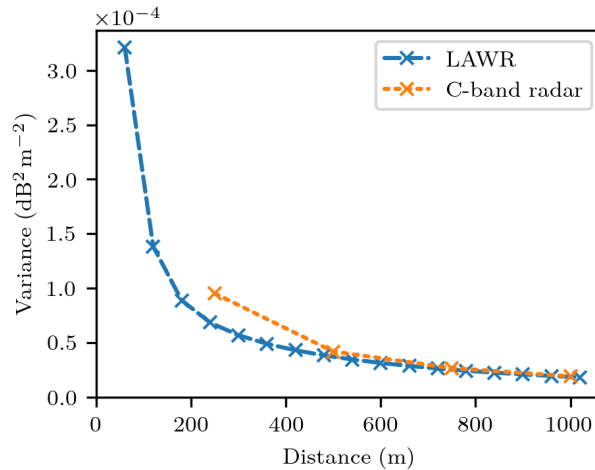


Figure 4.7: Variance of radar reflectivity gradients for LAWYR and C-band radar reflectivities above 10 dBZ.

radar reflectivities indicates a higher nugget variance than zero (Fig. 4.6a). The non-zero nugget variance is a discontinuity caused by microscale variability and measurement errors (Germann and Joss, 2001), which well explains that the C-band radar measurements with a 250 m radial resolution seem to have a higher discontinuity than the LAWYR observations with a 60 m resolution. Thus, Study B evidences that the LAWYR is capable to measure microscale rainfall variability better than the C-band radar due to its higher spatial resolution and scan strategy.

At higher spatial resolutions, the LAWYR is capable of measuring steeper radar reflectivity gradients than the C-band radar (Fig. 4.7). The variance of radar reflectivity gradients decreases with increasing lag distances. Because the variance of gradients is not constant, the radar reflectivities differ from a white noise field. At a 250 m lag distance, the LAWYR and C-band radar are directly comparable. Despite

the C-band radar having a coarser spatial resolution than the LAWR, the C-band radar measures steeper gradients than the LAWR, due to differences in scan strategy and hence temporal resolutions. However, the LAWR radar reflectivity gradients exhibit higher variance at 60 m and 120 m lag distances than the C-band radar reflectivity gradients at 250 m lag distance. The variance of C-band radar reflectivity gradients with the native 250 m spatial resolution is reduced by 30 % compared to LAWR with a native 60 m spatial resolution. Because of these steeper gradients, measurements of the LAWR can capture distinctly finer rainfall structures.

A lower spatial resolution results in a reduction of the measured spatial variability, as expressed by a lower variance of gradients (Fig. 4.6b). The variance of radar reflectivity gradients for a lag distance of 240 m is reduced by 35 % at a radial resolution of 240 m compared to the native radial resolution of 60 m. A comparable reduction in variance is observed in the comparison of the C-band radar at a radial resolution of 250 m to the LAWR at a radial resolution of 60 m, as discussed with Figure 4.7. The spatial averages of LAWR radar reflectivities demonstrate the importance of spatial resolution to capture the spatial variability of rainfall.

In conclusion, Study B shows that a radar with higher spatio-temporal resolution is capable of measuring steeper gradients and captures microscale rainfall variability more accurately than conventional radars at coarser resolutions. The LAWR measurements can provide an added value at the sub-kilometre scales compared to C-band radar measurements and RADKLIM.

4.5 KEY FINDINGS

In brief, Study B yields the following key results:

- For 5 min time scales, the LAWR measurements outperform observations of the C-band radar due to the continuous scan strategy and temporal resolution. This better performance does not translate in a better match to rainfall accumulations recorded by rain gauges, as differences in the Z - R relation and sample volume sizes between radar and rain gauge dominate the uncertainty of radar rainfall estimates.
- A high spatio-temporal resolution and continuous scan strategy results in more accurate measurements of rainfall peaks.
- The most accurate measurements of spatial rainfall variability at sub-hourly timescales are those made by a dense network of rain gauges or a radar with high spatio-temporal resolution and a continuous scan strategy, like the LAWR.
- The variance of the radar reflectivity gradients highlights that a radar with higher spatio-temporal resolution, like the LAWR, is capable of measuring steeper gradients and captures microscale rainfall variability more accurately than conventional radars.

Study A and Study B demonstrate the data quality and the added value of the reanalysed LAWR measurements. The multi-year data set reanalysis of the LAWR measurements are a result of the best estimate of parameters of the correction algorithms for long-term applications. Despite the considerable effort invested, the provided radar reflectivities and rainfall rates remain susceptible to errors up to a certain degree. The uncertainty of the reanalysed radar data is the superposition of the several error sources, which are discussed in Study A - these include among other things noise, alignment, non-meteorological echoes, radar calibration, and attenuation. The uncertainty of radar rainfall estimates has been investigated by several studies (e.g. Germann et al., 2009; Green et al., 2024b; Krajewski and Georgakakos, 1985; Villarini et al., 2014). For example, Germann et al. (2006) propose the generation of an ensemble of radar rainfall fields through the addition of a correlated stochastic perturbation. In this dissertation, I aim to propose an alternative simplified approach to estimating the uncertainty associated with LAWR measurements as an outlook. In this approach, multiple realizations of radar fields are generated by perturbing the parameters of the correction algorithms introduced with the presented radar reanalysis in Study A, which is inspired by an ensemble. For instance, multiple realizations of radar reflectivities can be processed with the data reanalysis by disturbing the noise level, the calibration coefficient or parameters of other applied processing procedures. This chapter presents first thoughts and preliminary results on an experiment on the uncertainty of the LAWR measurements.

In a first experiment towards the uncertainty of LAWR radar reflectivities, only the noise level is disturbed within the processing chain of the radar reanalysis, as it is the first step of the processing (Chapt. 3). The experiment is conducted for a randomly selected summer rainfall event characterised by a high noise level variability, on 31.07.2023 between 19 UTC and 23:30 UTC (Fig. 5.1). The two LAWRs and five MRRs of the measurement network (Chapt. 2) were processed following Study A. The MRRs serve as a reference and the LAWR ALT as a benchmark. The reanalysed LAWR HHG radar reflectivities, without disturbed noise levels, vary between non-rainy values below 10 dBZ and moderate to heavy rain of 42 dBZ (Fig. 5.1). The LAWR HHG radar reflectivities are in good agreement with the MRRs, as evidenced with low biases below 2.1 dB and RMSEs between 2.53 dB and 3.62 dB (Table 5.1). The radar reflectivities are highly correlated with Pearson correlation coefficients ranging from 0.82 to 0.94. During this rainfall event, the noise level estimate is temporally highly variable (Fig. 5.1a), yielding a dynamically changing sensitivity of the radar reflectivity depending on the range (Fig. 5.2), which is the lowest detectable radar reflectivity at a specific range. Given that noise is primarily generated by the radar itself (Chapt. 3), the found noise level variability appears unrealistic. Therefore, multiple temporally constant noise levels are selected for the noise level disturbance. Eleven noise levels are randomly selected within the range of the initially found noise level (Fig. 5.1a), generating multiple realizations

Table 5.1: Validation metrics of radar reflectivities comparing the LAWR HHG and the four MRRs, respectively, showing the Pearson correlation coefficient estimator (r), the mean bias, the root-mean-square error (RMSE), and the sample size (n). Z_0 refers to the reanalysed LAWR HHG radar reflectivity without disturbed noise level. Z_* refers to the LAWR HHG radar reflectivity processed with the lowest noise level of all radar reflectivity realizations.

	BBG		HCU		SAS		WMH	
	Z_0	Z_*	Z_0	Z_*	Z_0	Z_*	Z_0	Z_*
n	362	421	436	436	420	454	427	440
r	0.88	0.91	0.90	0.90	0.82	0.87	0.94	0.96
bias (dB)	-2.08	-1.02	1.07	1.18	-1.01	0.23	-1.10	-0.29
RMSE (dB)	3.62	2.74	2.53	2.55	3.03	2.31	2.67	2.10

of LAWR HHG radar reflectivities (Fig. 5.1b-e), hereafter referred to as ensemble of LAWR reflectivities.

The ensemble of LAWR HHG reflectivities demonstrate the range of possible reanalysed reflectivities (Fig. 5.1b-e). The ensemble indicates a high uncertainty at periods with a large deviation between the ensemble radar reflectivities. For example, at 20:10 UTC the initial LAWR HHG radar reflectivity measures a radar reflectivity indicating no rain unlike the MRR SAS measuring light rain (Fig. 5.1d). As the noise level increases, the sensitivity of the LAWR HHG radar reflectivity declines (Fig. 5.2). However, ensemble members of the LAWR HHG reflectivities with a low noise level indicate rain with the same intensity as the MRR. Notwithstanding, the initial LAWR HHG reflectivity appears as a good solution during most periods.

The ensemble of LAWR HHG reflectivities reveal that the noise level variability is overestimated. The ensemble member with the lowest noise level performs best. The biases are below 1.1 dB and demonstrate improvement at three of the four MRR locations, and the bias remains equal at the MRR HCU location (Table 5.1). The RMSEs exhibit a decrease at all MRR locations, with values between 2.1 dB and 2.7 dB. The correlations demonstrate improvement at all MRR locations, with values ranging between 0.87 and 0.95. For ensemble members with higher noise levels, the scores deteriorate noticeably.

The results demonstrate the constraints of the noise removal algorithm, which can be revisited in future studies. The impact of the noise removal variability on the multi-year reanalysed rainfall data set is beyond the scope of this work and could be the subject of future investigations. This sensitivity study can be applied for each processing procedure, with the aim to improve the parameters, or for multiple steps simultaneously, with the objective to estimate the uncertainty of the reanalysed measurements. In conclusion, this dissertation demonstrates an approach to generate multiple representations of radar reflectivity by modifying the parameters of the correction algorithms. The preliminary findings from the experiment on the uncertainty of the LAWR measurements indicate the possibility of improving the multi-year radar reanalysis. In addition, this chapter presents the first measurements from the improved measurement network (Chapter 2), including the added MRRs and the second LAWR.

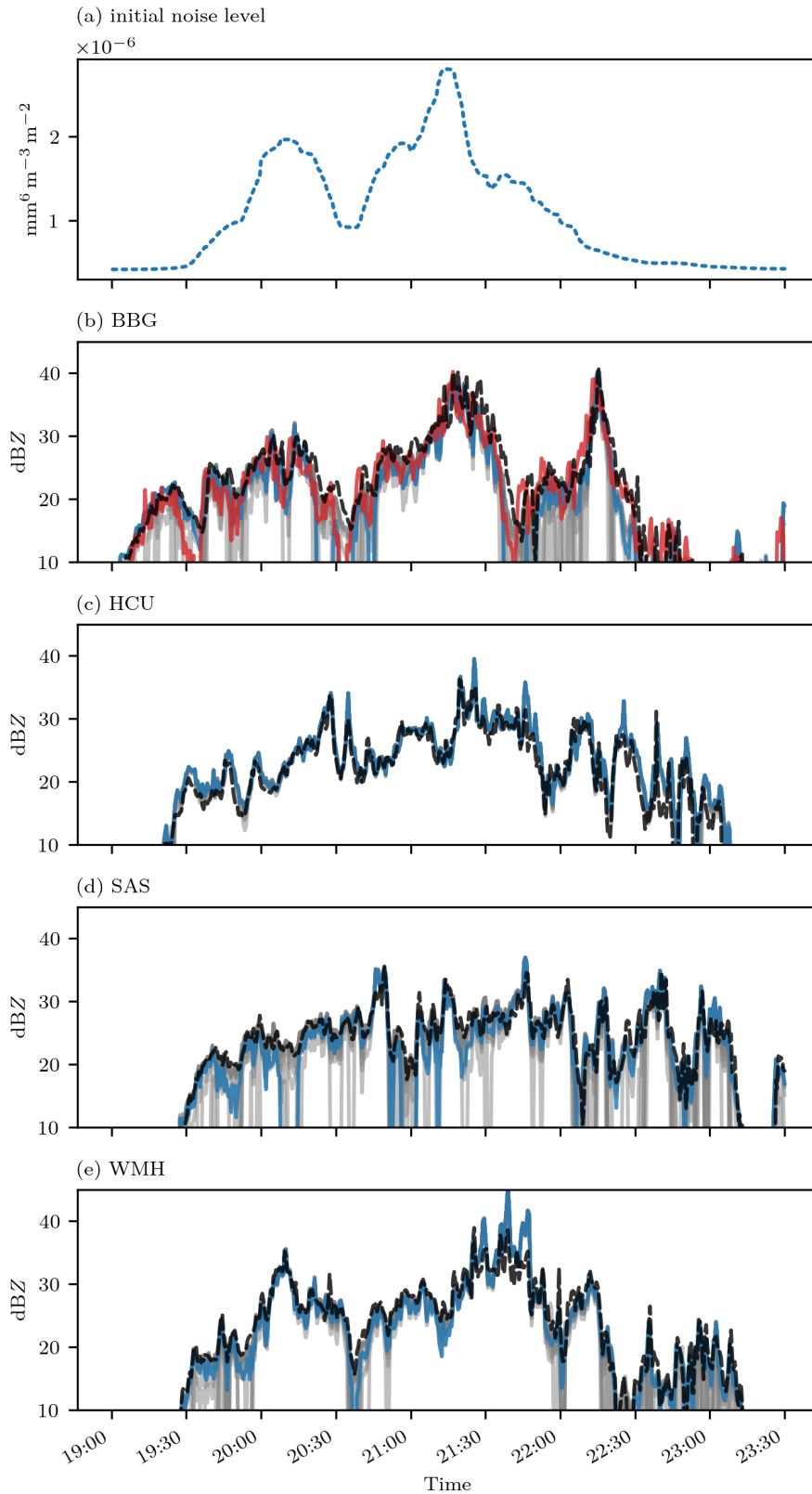


Figure 5.1: Radar observations of an exemplary rainfall event on 31.07.2023. (a) The noise level of LAW R HHG is temporally variable (Study A). (b-e) The radar reflectivities from LAW Rs and MRRs are shown at common volumes and a temporal resolution of 30 s. The dashed black lines in (b-e) show MRR radar reflectivities. The blue lines in (b-e) show LAW R HHG reflectivities. The grey lines in (b-e) show an 11 different realizations of LAW R HHG reflectivities based on constant noise levels in the range of the dynamically fitted noise level (a). The red line (b) shows LAW R ALT reflectivities.

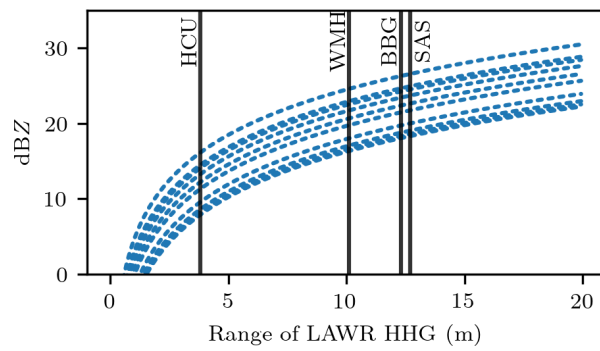


Figure 5.2: Sensitivity of LAWR HHG radar reflectivities at specific ranges for the different constant noise levels introduced in Figure 5.1. The vertical black lines indicate the ranges, at which the MRRs are located.

SUMMARY AND CONCLUSIONS

This thesis investigates radar rainfall observations at sub-kilometre and sub-minute scales. These are relevant scales for meteorological and hydrological applications in urban environments, yet they are not adequately observed because of the spatio-temporal resolutions of conventional radars. In Study A, I detail the data reanalysis of multi-year measurements of a local area X-band weather radar (LAWR), which resulted in an open-access data set of radar reflectivities and rainfall rates at hectometre spatial and 30 s temporal resolutions (Burgemeister et al., 2024b). This data set facilitates Study B, in which I investigate the added value of a refined spatio-temporal resolution for weather radar observations at sub-hourly temporal and sub-kilometre spatial scales compared to conventional measurements.

The networked rainfall observations in Hamburg are the measurement data basis for the raised research question proposed in Chapter 1 and are described in Chapter 2. As part of this dissertation project, I contributed to the expansion and enhancement of the measurement network, with the objective to close gaps and inaccuracies in the observations for futures studies. Chapters 3 and 4 describe the key methods and findings of Study A and Study B, respectively. Both chapters demonstrate the data quality and the added value of the reanalysed LAWR measurements. However, the reanalysed LAWR measurements are a result of a number of corrections that have been tuned to my best knowledge. These deterministic results include a variable uncertainty, which I investigate in an outlook in Chapter 5. Chapters 3, 4, and 5 answer the specific research questions proposed in Chapter 1:

1. *How can we create a consistent rainfall data set from the multi-year LAWR measurements?*

Precipitation data sets that are generated by operational data processing are prone to inconsistencies and breaks, e.g. introduced by advancement in the processing algorithms or delayed calibration after hardware changes. This dissertation describes the reanalysis of the radar data set, which is based on a set of consistent, state-of-the-art data processing procedures. A number of potential sources of error in radar data were identified and addressed in a step-by-step manner, with the aim of improving the precision of precipitation estimates. These included issues related to noise, alignment, non-meteorological echoes, radar calibration, and attenuation. In particular, the multi-year operation of the LAWR introduce challenges for creating a homogeneous data set. Any maintenance resulted in a slightly incorrect alignment of the LAWR. This unknown LAWR alignment is accurately determined using the solar signal appearing in radar reflectivities during sunrise and sunset, which facilitates comparisons with other measurement devices. The replacement and ageing of the LAWR hardware over the years resulted in unknown deviations from a well-calibrated measurement signal. Subsequent calibration of the LAWR is mandatory because of strongly biased measurement periods due to the maintenance, evidenced by MRR observations. The

MRRs provide measurements at the LAWR beam height and enabled the calibration. After calibration, the attenuation correction method, the modified Kraemer (MK) approach, is applied. The MRR drop size distributions facilitate the adjustment of the relationship between the radar reflectivity and specific attenuation to apply the MK approach at X-band frequencies. This dissertation facilitates the use of the MK approach at X-band frequencies and shows that this method is a reliable attenuation correction for single-polarized X-band radars, demonstrated with a long-term data set. The LAWR rainfall rates were estimated from attenuation-corrected reflectivities using the Marshall-Palmer Z-R relationship.

As a result, this dissertation provides radar reflectivities and rainfall rate estimates with 30 s temporal and hectometre spatial resolutions covering the years 2013 to 2021 (Burgemeister et al., 2024a), addressing the gap of well-documented, high-quality, open-access radar rainfall data sets at sub-kilometre and sub-minute scales.

2. *What is the uncertainty of the LAWR rainfall measurements?*

The reanalysis of the LAWR measurements reduces the uncertainty of the rainfall estimates effectively, especially after successful calibration and attenuation correction. However, the uncertainty of the LAWR rainfall estimation can only be estimated by comparison with other measurement devices. The reanalysed, multi-year LAWR radar reflectivities and rainfall rates are in very good agreement with MRR measurements, which is also demonstrated with a MRR as a reference that has been not used for calibration.

The LAWR spatio-temporal resolution and scan strategy can reduce the uncertainty of rainfall measurements in comparison with conventional radars. The LAWR operates with a radial resolution of 60 m and a temporal resolution of 30 s. The radar reflectivity represents a 30 s average of approximately 67 pulses per 1° collected during 12 sweeps, therefore it is a true average within the measurement interval. In contrast, the C-band radar operates with a radial resolution of 250 m and a temporal resolution of 5 min. The radar reflectivity represents a 83 ms average of approximate 50 pulses per 1° azimuth collected during 1 sweep within 30 s every 5 min, therefore it is an instantaneous sample. Notwithstanding these differences, the LAWR and C-band radar can be compared spatially well, as the measurements are highly correlated up to 0.93, where the measuring heights and sampling volumes are at closest. The MRR observations show that both the LAWR and C-band radar reflectivities and rainfall rates perform equally well at 30 s temporal resolution. For 5 min time scales, the LAWR measurements outperform observations of the C-band radar due to a continuous scan strategy and temporal resolution. This better performance does not translate in a better match to rainfall accumulations recorded by rain gauges, as differences in the Z-R relation and sample volume sizes between radar and rain gauge dominate the uncertainty for both the LAWR and C-band radar.

Furthermore, the reanalysis of LAWR measurements includes a temporally and spatially variable uncertainty. Each correction algorithm has its own associated uncertainty, and consequently, the reanalysis of the data propagates

errors. I provide an outlook on the uncertainty of radar measurements by perturbing the parameters of the correction algorithms introduced during the data reanalysis, which is inspired by an ensemble of measurements. In an initial experiment addressing the uncertainty of LAWR radar reflectivities, the parameter of the first correction algorithm, noise removal, is perturbed, making this approach similar to a sensitivity study of noise removal. The multiple realizations of LAWR HHG reflectivities reveals that the variability in noise levels is overestimated. The variant with the lowest noise level performs best, indicating potential improvements for this algorithm.

This dissertation proves the long-term performance of a local-area X-band weather radar (LAWR) despite the lack of polarization and Doppler information. The initial findings from the experiment on the uncertainty of LAWR measurements are presented, suggesting potential avenues for enhancing the multi-year radar reanalysis. This error source-based uncertainty investigation may lead to improved handling of uncertainties.

3. *What is the added value of high-resolution rainfall measurements at sub-kilometre and sub-hourly scales?*

This dissertation demonstrates that a LAWR operating at hectometre spatial and 30 s temporal resolution fills a gap in rainfall observations capturing variability at short-duration, sub-kilometre scales compared to conventional radar measurements or rainfall data sets.

This dissertation highlights the importance of spatio-temporal resolution and scan strategy in accurately measuring rainfall peaks, which can be relevant for the hydrological response, e.g. caused by a localized rainfall event in an urban area. The LAWR is capable to capture rainfall peaks better than the C-band radar due to the used scan strategy and spatio-temporal resolution. The temporal resolution exerts a greater impact on rainfall peaks than the spatial resolution, as shown with measurements at different spatio-temporal resolutions.

This dissertation finds that conventional available rainfall data sets, like the C-band radar measurement and radar-rainfall climatology RADKLIM, fail to capture the sub-hourly rainfall variability. The spatial rainfall structures captured by LAWR and rain gauge measurements are similar at sub-hourly timescales. The found matching variability of the LAWR and dense rain gauge measurements create additional confidence in the quality of the LAWR rainfall data set. Contrastingly, the C-band radar is overestimating spatial rainfall variability at sub-hourly timescales, despite the lower spatio-temporal resolution but due to its intermittent scan strategy every five minutes. RADKLIM is found to underestimate spatial rainfall variability due to its interpolation on a coarser spatial resolution and adjustment to a coarser rain gauge network than used in this study. Consequently, The LAWR measurements provide an added value at the sub-hourly scale compared to C-band radar measurements and RADKLIM.

This dissertation shows that a radar with higher spatio-temporal resolution is capable of measuring steeper gradients, which is relevant to capture the microscale rainfall variability. For instance, gradients of radar reflectivity

are high in case of local heavy rainfall events. The bias, variance, skewness, and kurtosis of radar reflectivity gradients can serve as an indicator of both measurement errors and rainfall variability. The variance of the C-band radar reflectivity gradients at 250 m spatial resolution is reduced by 30 % compared to the LAWR radar reflectivity gradients at 60 m spatial resolution. The variance of the radar reflectivity gradients highlights that the LAWR is capable of measuring steeper gradients and captures microscale rainfall variability more accurately than conventional radars. Therefore, the LAWR measurements can provide an added value at the sub-kilometre scale compared to C-band radar measurements and RADKLIM.

Present operational measurements and their reanalyses do not, and will not, fully capture the rainfall variability at short-duration and sub-kilometre scales. A LAWR can fill this observational gap; however, its added value depends on data quality, availability, and usability. Parts of this dissertation project depended on collaboration with different institutions, and some operational measurement data were not publicly available, highlighting the need for open-access measurement data. The multi-year open-access radar rainfall data set introduced with this dissertation provides a foundation for further meteorological and hydrological research, particularly to understand rainfall processes at these scales in urban areas. This data set has already proven its utility in several meteorological studies (e.g. Ferner et al., 2022; Kirsch et al., 2024, 2022; Schmitt et al., 2023). The spatial limitation of the LAWR will be overcome in future rainfall studies by the introduced extension and improvement of the measurement network.

Part II

APPENDIX

The following two publications were prepared over the course of the doctoral studies.



REANALYSIS OF MULTI-YEAR HIGH-RESOLUTION X-BAND WEATHER RADAR OBSERVATIONS IN HAMBURG

This work in this appendix has been published as:

F. Burgemeister, M. Clemens, and F. Ament (2024c). “Reanalysis of multi-year high-resolution X-band weather radar observations in Hamburg.” In: *Earth System Science Data* 16.5, pp. 2317–2332. DOI: [10.5194/essd-16-2317-2024](https://doi.org/10.5194/essd-16-2317-2024)

AUTHOR CONTRIBUTIONS

All authors conceptualized the project and reviewed the draft. FB planned and processed the data sets, performed the evaluation, and wrote and revised the draft. FB and MC maintained the X-band radar. FB and FA edited the draft. MC and FA conceptualized and implemented the measurement network.

Reanalysis of multi-year high-resolution X-band weather radar observations in Hamburg

Finn Burgemeister¹, Marco Clemens¹, Felix Ament¹

¹Meteorological Institute, Center for Earth System Research and Sustainability (CEN), Universität Hamburg

ABSTRACT

This paper presents an open-access data set of reanalysed radar reflectivities and rainfall rates at sub-kilometre spatial and minute temporal scales. Variability at these scales is a blind spot for both operational rain gauge networks and operational radar networks. In the urban area of Hamburg, precipitation measurements of a single-polarized X-band weather radar operating at a high temporal (30 s), range (60 m), and azimuthal sampling (1°) resolutions are made available for a period of more than 8 years.

We describe in detail the reanalysis of the raw radar data, outline the radar performance for the years 2013 to 2021, and discuss open issues and limitations of the data set. Several sources of radar-based errors were adjusted gradually affecting the radar reflectivity and rainfall measurements, e.g. noise, alignment, non-meteorological echoes, radar calibration, and attenuation. The deployment of additional vertically pointing micro rain radars yields drop size distributions at the radar beam height, which effectively reduces errors concerning the radar calibration and attenuation correction and monitors the radar data quality. A statistical evaluation revealed that X-band radar reflectivities and rainfall rates are in very good agreement with the micro rain radar measurements. Moreover, the analyses of rainfall patterns shown for an event and accumulated rainfall of several months prove the quality of the data set.

The provided radar reflectivities facilitate studies on attenuation correction and the derivation of further weather radar products, like an improved rainfall rate. The rainfall rates themselves can be used for studies on the spatial and temporal scales of precipitation and hydrological research, e.g. input data for high-resolution modelling, in an urban area. The radar reflectivities and rainfall rates are available at https://doi.org/10.26050/WDCC/LAWR_UHH_HHG_v2 (Burgemeister et al., 2024b).

A.1 INTRODUCTION

Knowledge of small-scale rainfall variability is needed for several meteorological and hydrological applications, particularly in urban environments due to their water-related sensitivity. For instance, urban hydrological applications demand high-quality radar rainfall data with at least a temporal resolution of 1 min and spatial resolution of 100 m (Berne and Krajewski, 2013; Einfalt et al., 2004; Gires et al., 2013; Ochoa-Rodriguez et al., 2015; Thorndahl et al., 2017). In general, hydrometeorological and fundamental studies on rainfall properties may benefit from long-term measurements at small spatio-temporal scales.

Rain gauge networks provide reliable local precipitation measurements, but due to their limited operational network densities, they are unable to represent rainfall variability for large domains at small temporal scales (e.g. Berne et al., 2004; Lengfeld et al., 2019; Maier et al., 2020; Villarini et al., 2008). Conventional weather radar systems, mostly operating at S- and C-band frequencies, are able to provide radar rainfall measurements over large domains with a temporal resolution of several minutes and spatial resolution of a few hundred metres. Long-term radar-based precipitation climatologies based on these conventional radars are available for Germany with a 5 min temporal resolution and 1 km spatial resolution (Winterrath et al., 2018b), and for Europe with an hourly temporal resolution and 2 km spatial resolution (Overeem et al., 2023). Consequently, there is a gap in long-term radar rainfall data sets at the sub-kilometre spatial scale and temporal scales below 5 min. X-band radars are able to refine rainfall estimates at temporal resolutions down to 16 s (van de Beek et al., 2010) and radial resolutions down to 3 m (Mishra et al., 2016), but most of them operate at or below 100 m spatial resolutions and 1 min temporal resolutions in areas of special interest, like urban areas (e.g. Allegretti et al., 2012; Berenguer et al., 2012; Hosseini et al., 2020; Lengfeld et al., 2014; Lo Conti et al., 2015; Maesaka et al., 2011; Schleiss et al., 2020; van de Beek et al., 2010; Ventura and Russchenberg, 2009; Wang and Chandrasekar, 2010; Yoon et al., 2017). However, long-term reanalyses of these radar observations are not available. Therefore, the aim of this paper is to present the data reanalysis of X-band radar observations at the sub-minute and hectometre scale in the urban area of Hamburg for multiple years, which resulted in an open-access data set of radar reflectivities and rainfall estimates (Burgemeister et al., 2024b).

The operational, single-polarized X-band weather radar monitors precipitation within a 20 km scan radius around Hamburg's city centre since 2013, operated in synergy with two micro rain radars (MRRs) and rain gauges. The local area weather radar (LAWR) operates at one elevation angle with a high temporal (30 s), range (60 m), and azimuthal sampling (1°) resolutions, refining coarser observations of the German nationwide C-band radars at 250 m spatial and 5 min temporal resolution. Although most of the latest X-band radars have dual-polarimetric capabilities (e.g. Anagnostou et al., 2018; Cao et al., 2023; Hosseini et al., 2023; Neely III et al., 2021; Pejcic et al., 2022; Schleiss et al., 2020), where dual-polarimetric quantities improve rainfall estimates, even low-cost, single-polarized X-band radars provide valuable information on the spatio-temporal variability of precipitation (e.g. Lo Conti et al., 2015; Marra and Morin, 2018b; van de Beek et al., 2010). The single-polarized X-band radars require extensive post-processing and the deployment of independent additional sensors, like micro rain radars, disdrometers, or rain gauges

(Thorndahl et al., 2017; Villarini and Krajewski, 2010). Former studies on short time periods (several months and a case study) show that the LAWR provides detailed information on the structure of precipitation. Lengfeld et al. (2014) deployed a network of four LAWRs and micro rain radars in a rural area of northern Germany. They describe correction algorithms for single and networked LAWRs and discuss the performance of measurements of 5 months. Lengfeld et al. (2016) and Lengfeld et al. (2018) introduce a method to correct reflectivity measurements for attenuation using less attenuated radars, and they compare attenuation correction methods for single-polarized X-band radars using this LAWR network. The LAWR network was dismantled in 2017. However, the LAWR located in Hamburg is still in operation, extending a unique data set. Hoffmann et al. (2018) shows that the LAWR is able to capture the circular pattern in rainfall rates because of its higher resolutions in space and time. In a recent study, a LAWR was deployed to provide rainfall estimates for studies on cold pool events during the Field Experiment on Sub-mesoscale Spatio-Temporal Variability in Lindenberg (FESSTVaL) from June to August 2021 (Burgemeister et al., 2022b). The previous studies provide knowledge and algorithms to reanalyse a consistent long-term data set based on LAWR measurements.

Any user of the presented long-term data set of homogeneously reanalysed rainfall estimates from X-band radar observations will need to know the details on data processing, availability, and accuracy. In this paper, we describe the setup of the LAWR in synergy with two MRRs and rain gauges in Hamburg (Sect. A.2). We explain the reanalysis of the multi-year measurements, addressing the noise removal, correction of non-meteorological echoes, calibration, attenuation correction, and rainfall estimation (Sect. A.3). Finally, we check the performance of the multi-year measurements with MRR observations, present rainfall patterns, and discuss limitations of the data set (Sect. A.4).

A.2 RADAR OBSERVATIONS IN HAMBURG

In the urban area of Hamburg, synergistic precipitation observations of a local area weather radar (LAWR) operating at X-band frequency, a micro rain radar (MRR), and a rain gauge (RG) are available since 2013 (Fig. A.1). The measurements can refine the observations of the German nationwide C-band radars and supplement and cover additional rain gauges. The LAWR Hamburg Geomatikum (HHG) is located on the rooftop of the Meteorological Institute of the Universität Hamburg in the centre of Hamburg. The MRR Wettermast Hamburg (WMH) is located at the scientific measuring site of the Meteorological Institute of the Universität Hamburg in the south-eastern part of the city. The MRR Blankenese Bauersberg (BBG) is deployed at a waterworks of the municipal water and wastewater utility Hamburg Wasser in the west of Hamburg since December 2017. The MRR WMH and LAWR HHG are 10.1 km apart. The MRR BBG and LAWR HHG are 12.3 km apart. The closest C-band radar of the German Weather Service (DWD) covering the whole measuring area of the LAWR HHG was in Hamburg Fuhlsbüttel (airport) with a distance of 7.3 km until 2014 and is since then in Boostedt 48.7 km away.

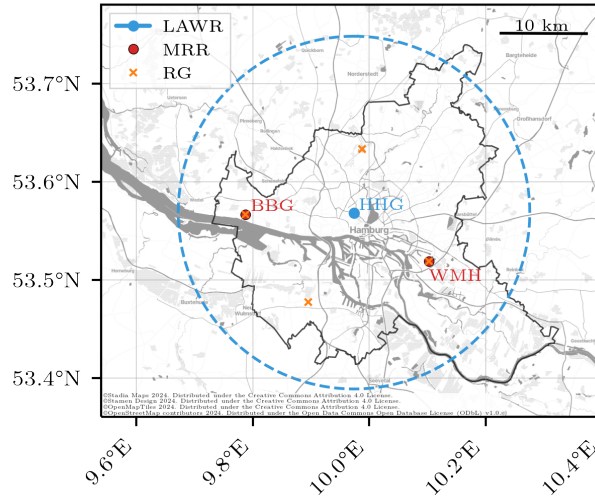


Figure A.1: Precipitation observations in Hamburg. The location of the local area weather radar (LAWR) / X-band radar (WRX) on the rooftop of the Geomatikum building in Hamburg (HHG) is indicated with a blue point. The dashed blue line shows the coverage with the 20 km scan radius. The locations of two micro rain radars (MRRs, red points) are, by name, Blankenes Bauersberg (BBG) and Wettermast Hamburg (WMH). Rain gauges (RGs, orange crosses) are located next to the MRRs and at sites of the German Weather Service (DWD).

A.2.1 X-band weather radar

The LAWR is a modified ship navigation radar of type GEM scanner SU70-25E. This single-polarized X-band radar operates at a frequency of 9.41 GHz. The LAWR provides horizontally radar reflectivity measurements at one fixed elevation angle with 30 s temporal, 60 m range, and 1° azimuthal sampling resolutions. The elevation angle was adjusted several times over the years for optimal operation during maintenance to reduce disturbances by non-meteorological echoes. The advantages of the LAWR are its low costs, high spatio-temporal resolution, and scanning strategy (Lengfeld et al., 2014). The LAWR costs less than 20 % of conventional X-band radars. The radar reflectivity represents an 30 s average of approximately 67 pulses per 1° collected during 12 sweeps, whereas conventional weather radars provides instantaneous measurements based on 1 sweep. The LAWR specifications are summarized in Table A.1, and we refer to Lengfeld et al. (2014) for technical details on the radar.

A.2.2 Micro rain radar

The MRR is a vertically pointing frequency-modulated continuous-wave (FM-CW) Doppler radar manufactured by METEK Meteorologische Messtechnik GmbH (Peters et al., 2002). The MRR retrieves drop size distributions (DSDs) from measured Doppler spectra using the terminal fall velocity given by Atlas et al. (1973). Rainfall rates and radar reflectivities are calculated from DSDs (Doviak et al., 1993). Noise and attenuation corrections are performed by the manufacturer's software (Metek, 2015). The DSD retrieval assumes stagnant air. Vertical wind and turbulence effects

Table A.1: Technical LAWR specifications (Lengfeld et al., 2014)

	Specification
Range resolution	60 m
Temporal resolution	30 s
Scan radius	20 km
Angular resolution	2.8°
Azimuthal sampling resolution	1°
Beam width	2.8°
Transmit power	25 kW
Frequency	9.41 GHz
Pulse width	0.4 s
Pulse repetition frequency	800 Hz
Rotation speed	24 rpm

are discussed in Peters et al. (2005) and are neglected in this study. The transmit frequency is at 24.23 GHz (K-band). Before November 2014, the MRR WMH measured with a transmit frequency of 24.0 GHz. Both MRRs measure DSD profiles for 31 range gates, with a range resolution of 35 m and a temporal resolution of 10 s. Adjacent rain gauges monitor the MRR's performance.

A.3 DATA REANALYSIS

Precipitation data sets that are generated by operational data processing are prone to inconsistencies and breaks, e.g. introduced by advancement in the processing algorithms or delayed calibration after hardware changes. As a decisive advantage, this reanalysis radar data set is based on a set of consistent, state-of-the-art data processing procedures. To ensure traceability, we document in this section the essential data processing procedures: removal of noise (Sect. A.3.1), correction of misalignment (Sect. A.3.2), detection of non-meteorological echoes (Sect. A.3.3), radar calibration (Sect. A.3.4), correction of attenuation (Sect. A.3.5), and the conversion to rainfall rates by a Z-R relation (Sect. A.3.6). The availability of corrected radar reflectivities and rainfall estimates will finally be summarized in the last section (Sect. A.3.7).

A.3.1 Remove noise

The raw radar reflectivities measured by the LAWR are superimposed by microwave noise that comes from the atmosphere and the radar itself. The radar cannot measure the background noise directly; however, an accurate estimation of the noise is mandatory to also detect weak weather signals. The background noise removal is dynamically fitted for every 30 s time step following Lengfeld et al. (2014). In contrast to the received signal, which is proportional to the squared distance (r^2) to the radar, the background noise is range-independent. Therefore, the radar

reflectivity factor Z is multiplied by r^{-2} and an initial guess of the noise level estimated from a rain-free field is subtracted from the radar field $Z \cdot r^{-2}$. The noise level is multiplied by a factor of 1.03 to remove all noise artefacts. If more than 10% of the radar bins remain rain-free, the 10th percentile of the original $Z \cdot r^{-2}$ becomes the new noise level estimate; otherwise, the noise level from the prior time step is kept. The estimated noise level is used as an initial guess for the next time step. The 10 recent noise level estimates are averaged to stabilize the algorithm regarding radar artefacts. Finally, the dynamic background noise is subtracted from the radar field, yielding the noise-free radar reflectivity factor after the multiplication by r^2 .

A.3.2 Determine radar alignment

The radar alignment of LAWR was adjusted manually at installation and after maintenance, leading to unknown uncertainties in antenna pointing. Since the beginning of operational measurements of the LAWR, spikes in radar reflectivity are observed in the direction of the sun during sunrise and sunset (Fig. A.2). These solar signals facilitate the subsequent determination of the antenna azimuth α and the beam elevation angle ε (Huuskonen and Holleman, 2007), using the known position of the sun (Reda and Andreas, 2008; Stafford et al., 2021).

The solar signal in radar reflectivity is the strongest spike in the direction of the sun position and is determined empirically in the radar reflectivity after noise removal during rain-free events. The continuous maximal reflectivity (Fig. A.2) is detected at 3658 sunrises and sunsets during 23 min on average. The mean calculated sun elevation angle of one sunrise or sunset is the radar beam elevation angle ε . The mean difference of the sun azimuth angle α_{sun} and the azimuth angle of the detected solar signal α_{detect} is the azimuth offset:

$$\Delta\alpha' = \overline{\alpha_{\text{detect}} - \alpha_{\text{sun}}}. \quad (\text{A.1})$$

The detection of one sunrise or sunset is constrained to a minimal duration of 15 min and maximal standard deviations of the beam elevation $\sigma_{\varepsilon'} < 1^\circ$ and the azimuth offset $\sigma_{\Delta\alpha'} < 1^\circ$. The determined ε' and $\Delta\alpha'$ are averaged between maintenance dates, resulting in the final beam elevation angle ε and azimuth offset $\Delta\alpha$ (Table A.2). Between 27.05.2013 and 11.08.2021 the radar alignment is characterized by six ε values, ranging between 3.3° and 6.1° , and seven $\Delta\alpha$ values with a maximum of 5.6° . The estimates of ε and $\Delta\alpha$ are stable within periods of at least two months up to several years, with a maximal standard deviation of $\pm 0.4^\circ$. The known radar alignment and thus location and height of the measurements allows for comparisons with other measurement devices and hence its calibration after clutter correction.

A.3.3 Detect clutter

The noise-corrected radar reflectivities contain static and dynamic non-meteorological echoes (clutter) characterized by high values and erroneous spatio-temporal gradients. Static clutter is caused by static objects, e.g. trees and buildings. Dynamic clutter is caused by dynamic objects, e.g. planes, birds, and other radars measuring at X-band frequencies. Consequently, measurements in urban areas are more affected by clutter than in rural areas. Additionally, ship navigation radars located

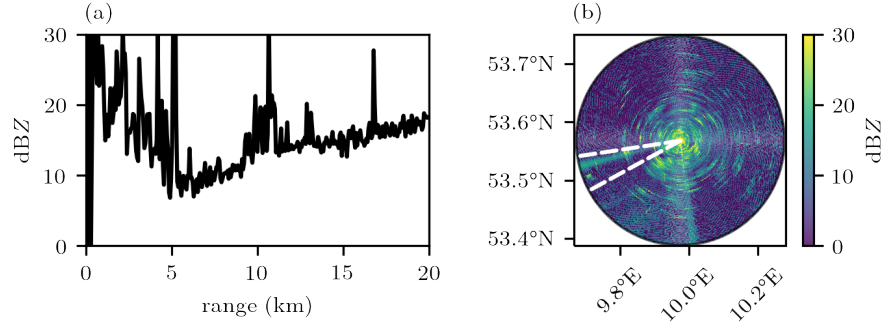


Figure A.2: Radar reflectivity after noise removal at sunset, 02.03.2020 16:20 UTC. (a) Radar reflectivity at the 255.5° azimuth angle representing the solar signal. (b) Radar reflectivity with continuous signal over range which is visible during the sun set. The white lines indicate a 20° window around the true sun position in the radar azimuth angle.

Table A.2: X-band radar (LAWR) HHG alignment, defined by the beam elevation angle ε and azimuth offset $\Delta\alpha$.

Modification date	ε ($^\circ$)	σ_ε ($^\circ$)	$\Delta\alpha$ ($^\circ$)	$\sigma_{\Delta\alpha}$ ($^\circ$)
27.05.2013 14 UTC	4.4	± 0.3	0.9	± 0.4
12.07.2014 00 UTC	6.1	± 0.1	2.5	± 0.1
23.09.2014 15 UTC	4.2	± 0.2	-	-
12.03.2015 14 UTC	-	-	3.2	± 0.1
09.06.2015 13 UTC	5.4	± 0.2	-	-
22.03.2017 15 UTC	-	-	4.1	± 0.2
20.04.2018 08 UTC	-	-	3.9	± 0.1
25.04.2020 16 UTC	3.3	± 0.1	5.0	± 0.1
03.07.2020 15 UTC	3.5	± 0.1	5.6	± 0.2

at the Hamburg harbour can cause interferences in the form of spikes or rings. All these clutter values cannot be easily detected within the LAWR measurements due to the lack of polarimetric or Doppler quantities. The clutter detection requires the application of several gradient-based and time-dependent correction algorithms.

As a first step of clutter correction, static clutter is removed by subtracting a static clutter field. Radar reflectivities and clutter are assumed to be additive. The static clutter field is estimated from the temporal median of the noise-corrected, rain-free radar reflectivity factor. A stable estimate of the static clutter field requires the measurement's stability, i.e. continuous relative calibration, alignment, and adjustment of the radar receiver, which is valid over multiple weeks, months, or years. Due to computing time, the static clutter field is updated on a roughly monthly basis for periods with similar clutter signals. To restrict the temporal median of the radar reflectivity factor to mainly rain-free cases, a rain threshold based on the rain fraction is introduced, represented by the fraction of radar reflectivities exceeding 5 dBZ for every time step. The radar reflectivity of 5 dBZ represents a rainfall rate R of 0.1 mm h^{-1} using a standard Z - R relationship. The

rain threshold was empirically set to the 75th percentile of the rain fraction, avoiding rain patterns affecting the static clutter field. Furthermore, this threshold of the rain fraction is also dependent on the measurement's stability. Changes in the rain fraction indicate technical maintenance of the radar, which is represented by a change point of the rain fraction based on a different calibration or technical errors of the radar receiver, which is represented by a drift of the rain fraction based on a slow reduction of radar sensitivity. The correction of static clutter using a stable estimate of a static clutter field subtracts clutter leaving the measurement, so there is no need of interpolation.

Dynamic clutter signals are removed by several gradient-based correction algorithms. Five different filter algorithms are applied: the texture of the logarithmic reflectivity (TDBZ) filter (Hubbert et al., 2009), the SPIN filter (Hubbert et al., 2009), a spike filter (Lengfeld et al., 2014), a ring filter (Lengfeld et al., 2014), and a speckle filter. Since isolated clutter signals, spikes and rings vary in length and width, two variants of the spike filter, two variants of the ring filter, and five variants of the speckle filter are applied, each with different parameters.

The TDBZ filter calculates the TDBZ field as the mean of the squared logarithmic reflectivity difference between adjacent range gates according to (Hubbert et al., 2009):

$$\text{TDBZ} = \left[\sum_i^N (\text{dBZ}_i - \text{dBZ}_{i-1})^2 \right] / N \quad (\text{A.2})$$

where dBZ is the reflectivity and N is the number of range gates used. The TDBZ filter labels a range gate as a clutter signal if the TDBZ field exceeds $\text{TDBZ} > 9$ dBZ within $N = 3$ consecutive range gates. The filter was modified to computations along range gates following Lengfeld et al. (2014).

The SPIN filter detects clutter based on a measure of how often the reflectivity gradient changes sign along the radial direction according to Hubbert et al. (2009). The reflectivity gradient and sign change is calculated between three consecutive range gates, e.g. dBZ_{i-1} , dBZ_i and dBZ_{i+1} :

$$\text{sign} \{ \text{dBZ}_i - \text{dBZ}_{i-1} \} = -\text{sign} \{ \text{dBZ}_{i+1} - \text{dBZ}_i \}, \quad (\text{A.3})$$

and

$$\frac{|\text{dBZ}_i - \text{dBZ}_{i-1}| + |\text{dBZ}_{i+1} - \text{dBZ}_i|}{2} > \text{spin_thres}, \quad (\text{A.4})$$

where spin_thres is a reflectivity threshold, which is set to 3 dBZ. The SPIN filter labels a range gate as a clutter signal if more than two range gates in a centred window of five range gates meet the conditions of the equations A.3 and A.4.

The spike filter identifies clutter in the form of spikes by calculating the reflectivity gradients for consecutive radar beams. The reflectivity gradient is calculated between the reflectivity dBZ_i and the reflectivities with a distance of W degrees in azimuth dBZ_{i-W} and dBZ_{i+W} :

$$[\text{dBZ}_i - \text{dBZ}_{i-W} > \text{spike_thres}] \wedge [\text{dBZ}_i - \text{dBZ}_{i+W} > \text{spike_thres}] \quad (\text{A.5})$$

where spike_thres is a reflectivity threshold, which is set to 3 dBZ. Two spike filters are applied: one spike filter is configured with the parameters $N = 3$ and $W = 1$,

and the second one is applied with $N = 11$ and $W = 2$. The spike filter labels a range gate as clutter signal if more than 50% in a window of N consecutive radar beams meet the condition of Eq. (A.5). The ring filter identifies clutter in the form of rings by calculating reflectivity gradients for consecutive range gates. Consequently, the ring filter is similar to the spike filter but computes the reflectivity gradients using Eq. (A.5) with a distance of W metres in range and a `ring_thres` of 3 dBZ. The ring filter labels a range gate as clutter signal if more than 50% in a surrounding window of N range gates meet the condition of Eq. (A.5). Two ring filters are applied: one ring filter is configured with the parameters $N = 11$ and $W = 1$, and the second one is configured with $N = 11$ and $W = 2$. The choice of the parameters for the four filters were determined empirically by processing different case studies (not shown).

The application of one TDBZ filter, one SPIN filter, two spike filters, and two ring filters removes dominant clutter patterns, but there remain isolated clutter signals. For this purpose, the speckle filter assumes that rain areas are connected and thus consist of more than a few isolated high reflectivities. This filter counts radar reflectivities of grid cells $\text{dBZ}_{i,j}$ greater than a rain threshold of 5 dBZ within a two-dimensional window of size $k \times l$:

$$\sum_{i=1}^k \sum_{j=1}^l f(\text{dBZ}_{i,j}) < \text{speckle_thres} \quad (\text{A.6})$$

where $f(\text{dBZ}_{i,j}) = 0$ for $\text{dBZ}_{i,j} \leq 5$ dBZ and $f(\text{dBZ}_{i,j}) = 1$ for $\text{dBZ}_{i,j} > 5$ dBZ. If the sum of Eq. (A.6) is smaller than the `speckle_thres`, the centre of the $k \times l$ window is identified as clutter. Five speckle filters are applied using different window sizes and thresholds: $k = \{3, 3, 5, 5, 7\}$, $l = \{3, 5, 5, 7, 7\}$, and `speckle_thres` = $\{3, 5, 10, 16, 26\}$.

To assess the effectiveness of these five filters, we have analysed exemplarily the clutter detection from May to September 2019: the TDBZ filter is the most effective filter by detecting 66.1% of all clutter pixels. Many clutter pixels are as well identified by the SPIN filter (25.7%) and one of the five speckles filters (14.0% to 31.5%). In contrast, the detection rate is low for the two spike filters (3.1% and 0.4%) and the two ring filters (1.0% and 1.4%).

Identified and removed clutter signals yield missing values in the reflectivity field. Missing values are interpolated with ordinary Kriging (Cressie, 1993). The temporal-constant spatial covariance is modelled by a Gaussian semivariance with a length scale of 5 km and stationary random noise, which represents the nugget. For computational efficiency, the Kriging method is spatially localized (Wesson and Pegram, 2004) by using the 20 nearest neighbours to the grid points that should be interpolated. However, it is important to keep in mind that some clutter signals remain within the measurements and may affect the interpolation of missing radar reflectivities.

A.3.4 Calibrate

The observational synergy of the LAWR, MRR, and RG facilitates calibration and adjustment of the radar measurements. The MRR provides the radar reflectivity factor Z_{MRR} and rainfall rate R_{MRR} derived from drop size distributions. With Z_{MRR} , the LAWR radar reflectivity factor Z_{LAWR} is calibrated directly. The calibration

and evaluation with MRR measurements has mainly three advantages. The same variable and the same measuring height are compared at sufficiently large sampling volume sizes. A calibration with a disdrometer would increase errors because of the height difference and different sampling volume sizes. The calibration with a RG would add an error based on uncertainties introduced by Z - R relationships. However, the MRR measurements are adjusted with a RG at the same location. The methodology is described by Lengfeld et al. (2014).

Before calibration, R_{MRR} and consequently Z_{MRR} are adjusted with RG measurements. The logarithmic calibration factor for the MRR C_{MRR} is derived from 3 h averages of R_{MRR} at 105 m height and RG rainfall rate R_{RG} :

$$C_{\text{MRR}} = \overline{\text{dBR}_{\text{MRR}}} - \overline{\text{dBR}_{\text{RG}}} \quad (\text{A.7})$$

with $\text{dBR} = 10 \cdot \log(R)$. Wind-induced losses of R_{RG} were corrected using the wind speed of a wind sensor (Rubel and Hantel, 1999). Rainfall rates at temperatures below 5 °C were not included to constrain the adjustment on the liquid phase. The MRR variables, e.g. Z_{MRR} and R_{MRR} , are adjusted at all 31 height levels with C_{MRR} in logarithmic or linear units, respectively. C_{MRR} is sufficiently stable for periods covering multiple months (Table A.3) and changes were a result of maintenance.

Table A.3: Micro rain radar (MRR) logarithmic calibration factor C_{MRR}

MRR	Period	C_{MRR}	$\sigma_{C_{\text{MRR}}}$
WMH	01.01.2013 - 09.11.2014	-3.06 dB	± 1.22 dB
	10.11.2014 - 20.06.2015	0.87 dB	± 1.06 dB
	21.06.2015 - 31.08.2021	-1.61 dB	± 1.34 dB
BBG	06.12.2017 - 31.08.2021	-1.37 dB	± 1.49 dB

The adjusted MRR WMH radar reflectivity is used to calibrate the LAWR radar reflectivity (Fig. A.3a), yielding a consistent calibration, because the MRR WMH and the LAWR are measuring simultaneously since May 2013. The distance between the MRR WMH and the LAWR is 10.07 km. At the MRR WMH location, the LAWR mean radar beam height is between 680 m and 1170 m over the years, due to changes in radar alignment (Sect. A.3.2), and the radar beam width is 490 m, covering a maximum of 14 range bins of the MRR (Fig. A.3b). For radar beam elevation angles above 4.2°, the radar beam exceeds the maximal MRR range gate partly, increasing the volume mismatch. The profile of Z_{MRR} is averaged within the LAWR radar beam using a Gaussian weighting function, with its maximum at the beam centre (Fig. A.3b). Z_{MRR} values at 10 s temporal resolution are averaged to the matching 30 s LAWR resolution. Following Lengfeld et al. (2014), the calibration coefficient c_{LAWR} is derived with

$$c_{\text{LAWR}} = 10^{0.1 \cdot (\text{dBZ}_{\text{LAWR}} - \text{dBZ}_{\text{MRR}})} \quad (\text{A.8})$$

with dBZ_{MRR} being the radar reflectivity of MRR WMH and dBZ_{LAWR} being the radar reflectivity of the LAWR. c_{LAWR} is calculated for radar reflectivities ≥ 10 dBZ and < 60 dBZ. The calibration is constrained on the liquid phase; hence, radar reflectivities affected by the melting layer and ice phase are not taken into account. Therefore, the 0 °C isotherm level is estimated using a constant wet adiabatic

lapse rate of 5.5 K km^{-1} and the 2 m temperature measured at the MRR WMH site. Radar reflectivities below the 0°C isotherm level are used for calibration only. The calibrated radar reflectivity factor Z'_{LAWR} is derived from

$$Z'_{\text{LAWR}} = \frac{Z_{\text{LAWR}}}{c_{\text{LAWR}}}, \quad (\text{A.9})$$

with the measured radar reflectivity Z . The calibration results in 13 calibration periods with c_{LAWR} between ≈ 0.03 and ≈ 4.4 (Table A.4), due to maintenance including technical changes or drifts in signal intensity. The calibrated radar reflectivity $\text{dBZ}'_{\text{LAWR}}$ is provided as level 1 data set (Burgemeister et al., 2024b).

Table A.4: Calibration parameters for the LAWR with the calibration coefficient c_{LAWR} (Eq. (A.8)), the mean bias, the root-mean-square error (RMSE), the sample size (n), and the Pearson correlation coefficient (r). Measurements are only available in these periods.

Period	c_{LAWR}	Bias (dB)	RMSE (dB)	n	r
27.05.2013 - 20.02.2014	0.062068	-12.07	12.47	7278	0.75
12.07.2014 - 23.09.2014	0.080461	-10.94	12.13	2061	0.50
23.09.2014 - 15.01.2015	0.026707	-15.73	16.16	728	0.43
17.01.2015 - 09.06.2015	3.865626	5.87	6.60	3362	0.84
09.06.2015 - 02.05.2016	2.053080	3.12	4.33	26017	0.87
02.05.2016 - 09.03.2017	1.761379	2.46	3.92	15710	0.87
22.03.2017 - 15.05.2017	0.342959	-4.52	5.78	1898	0.78
16.05.2017 - 05.07.2017	0.097155	-10.13	10.72	5658	0.72
05.07.2017 - 01.02.2018	0.971519	-0.13	3.12	25567	0.83
01.02.2018 - 18.04.2018	0.306367	-5.14	5.96	1603	0.86
20.04.2018 - 07.03.2020	2.837791	4.53	5.49	36207	0.86
25.04.2020 - 09.06.2020	4.409915	6.44	7.33	851	0.86
03.07.2020 - 11.08.2021	0.237148	-6.25	7.11	14379	0.79

A.3.5 Correct attenuation

Rain-induced attenuation at X-band frequencies leads to strongly underestimated radar reflectivities and thus rainfall rate estimates. The radar reflectivity factor Z' at range r suffers from attenuation integrated over the path,

$$Z'(r) = Z(r) - 2 \int_0^r k(s) ds, \quad (\text{A.10})$$

where $Z(r)$ is the unattenuated radar reflectivity factor at range r , and $k(s)$ is the specific attenuation of each range bin. The second term in Eq. (A.10) is known as the two-way path-integrated attenuation (PIA). Overeem et al. (2021) suggest the modified Kraemer (MK) approach (Jacobi and Heistermann, 2016) to correct the attenuation for single-polarized radars. The MK approach is a forward gate-by-gate attenuation correction (Hitschfeld and Bordan, 1954) based on an iterative

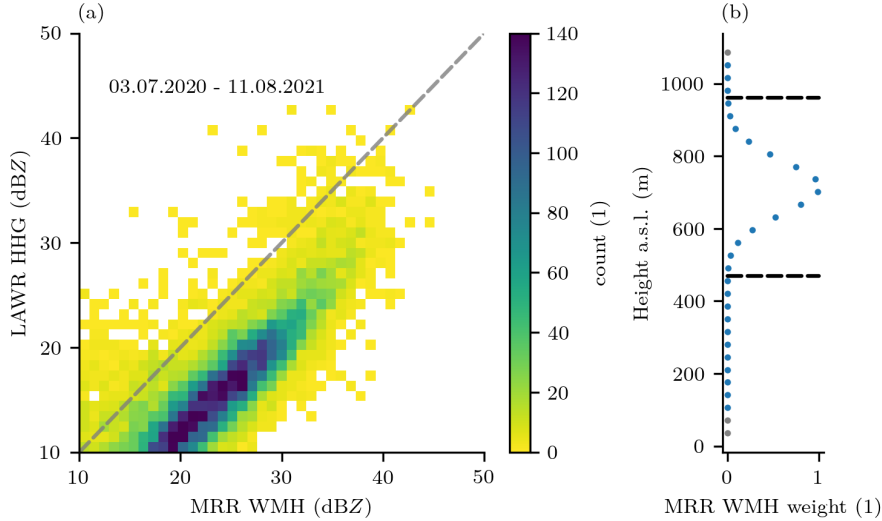


Figure A.3: Calibration of LAWR radar reflectivities using height averaged MRR radar reflectivities. (a) Comparison of uncalibrated LAWR radar reflectivities to calibrated radar reflectivities of the MRR WMH of the period 03.07.2020 to 11.08.2021 (Table A.4). (b) Weights (dots) to average the MRR WMH radar reflectivity profile within the LAWR beam (indicated by black dashed line) measuring at a beam elevation of 3.5° .

scheme to improve empirical parameters of a relationship between k and Z (Krämer and Verworn, 2008) including additional constraints of the PIA and Z (Jacobi and Heistermann, 2016). The attenuation k used in Eq. (A.10) is estimated from Z (in $\text{mm}^6 \text{m}^{-3}$) using the power-law relation

$$k = \alpha Z^\beta, \quad (\text{A.11})$$

with empirical parameters α and β . These empirical parameters are determined iteratively during the attenuation correction procedure. For details of this technique, we refer to the literature (Jacobi and Heistermann, 2016; Overeem et al., 2021) and document here only the specific settings of our implementation: the maximum allowed corrected reflectivity to assume a stable correction scheme is set to 59 dBZ. The PIA is constrained by 10 dB (Delrieu et al., 1999) to avoid numerical instabilities. The number of iterations for α is 100 and for β is 6. The limits of α and β are set to $\alpha_{\min, \max} = [4.02 \cdot 10^{-5}, 9.52 \cdot 10^{-5}]$ and $\beta_{\min, \max} = [0.79, 0.90]$ (Figure A.4). This valid range of α and β is in agreement with estimates of other k - Z relations at X-band frequencies (e.g. Berne and Uijlenhoet, 2006; Delrieu et al., 1999; Delrieu et al., 2022; Diederich et al., 2015; van de Beek et al., 2010).

However, these limits were not available from literature as Jacobi and Heistermann (2016) and Overeem et al. (2021) applied the MK approach only at C-band frequencies. We applied the approach by Overeem et al. (2021) at X-band frequencies. The k - Z relation is estimated from multi-year MRR measurements (Fig. A.4). The fit of the k - Z relation (Eq. (A.11)) results in $\hat{\alpha} = 6.91 \cdot 10^{-5}$ and $\hat{\beta} = 0.85$. The fit is applied only to $Z \geq 30$ dBZ to stabilize the solution for relevant values of k affecting the attenuation correction. Overeem et al. (2021) introduced the uncertainties of Eq. (A.11) based on the errors of k estimates, assuming that the uncertainties

in $\log(\alpha)$ and β are independent and contributing equally to the total uncertainty in $\log(k)$:

$$\varepsilon_{\log(\alpha)} = \frac{\log(k) - \log(\hat{\alpha}Z^{\hat{\beta}})}{2}, \quad (\text{A.12})$$

$$\varepsilon_{\beta} = \frac{\log(k) - \log(\hat{\alpha}Z^{\hat{\beta}})}{2\log(Z)}. \quad (\text{A.13})$$

The uncertainties result in the aforementioned limits of the empirical parameters $\alpha_{\min, \max} = \hat{\alpha} \exp(\pm 2\sigma_{\varepsilon_{\log(\alpha)}})$ and $\beta_{\min, \max} = \hat{\beta} \pm \sigma_{\varepsilon_{\beta}}$. The standard deviations are estimated from the difference between the 0.16 and 0.84 quantiles of ε (Overeem et al., 2021).

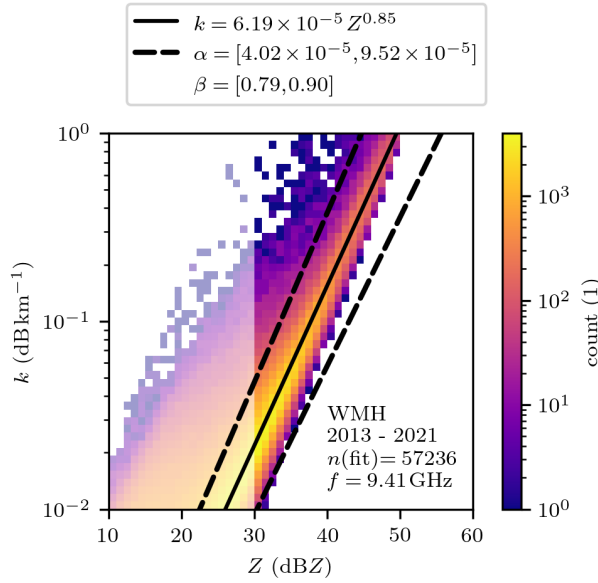


Figure A.4: Relation between the specific attenuation k and the radar reflectivity dBZ estimated from micro rain radar measurements at 105 m height and 10 s temporal resolution. Only measurements at temperatures above 0 °C are used to exclude ice phase. The radar variables are computed at the X-band frequency from measured drop size distributions with T-matrix calculations (Waterman, 1965) implemented by Leinonen (2014) using raindrop axis ratios from Brandes et al. (2002), a canting angle distribution with zero mean and 10° width, and the complex refractive index of water from Liebe et al. (1991) at a temperature of 15 °C. The power-law fit for the k - Z relation is based on measurements above 30 dBZ (non shaded area) and is shown with a black solid line, including uncertainties indicated as dashed black line.

Finally, the MK approach is applied to the radar reflectivity from the level 1 data set, resulting in attenuation-corrected radar reflectivity of the level 2 data set. Additionally, the level 2 data set includes the parameter `pia_stability` describing the stability of the attenuation correction for every time step. The parameter is 0 for a stable PIA estimate, 1 for a PIA > 10 dB, and 2 for a numerically unstable PIA. The attenuation is not corrected if the PIA estimate is numerically unstable. Since the attenuation correction is based on the reflectivity, a prior successful

calibration (Section A.3.4) is mandatory for a stable attenuation correction. The attenuation correction algorithm can be easily applied using the Python package wradlib (Heistermann et al., 2013).

A.3.6 Estimate rainfall rates

For use in meteorological or hydrological studies, quantitative precipitation estimates are of interest. The attenuation-corrected radar reflectivity factor Z (in $\text{mm}^6 \text{m}^{-3}$) is converted to a rainfall rate R (in mm h^{-1}) by applying a power-law Z - R relation,

$$Z = a R^b, \quad (\text{A.14})$$

where the multiplicative factor a and the exponent b are empirical constants. This study uses fixed parameters $a = 200$ and $b = 1.6$ proposed by Marshall et al. (1955), keeping in mind that Z and R depend on the drop size distribution, which varies geographically, with rainfall rate, and time (e.g. Berne and Krajewski, 2013; Doviak et al., 1993; Villarini and Krajewski, 2010). However, the Marshall-Palmer Z - R relation is an appropriate representation of average rainfall conditions in this climate, as investigated with multi-year MRR drop size distributions in Hamburg (not shown) and by Holleman (2006) and Kirsch et al. (2019). The coefficients of the Marshall-Palmer Z - R relation are commonly used for long-term studies in similar climates (e.g. Imhoff et al., 2021; Overeem et al., 2021). Polarimetric rain retrievals cannot be applied due to the lack of polarimetric measurements, but would perform better compared to single radar reflectivity methodologies (e.g. Delrieu et al., 2022; Schleiss et al., 2020). The estimated rainfall rate R (Eq. (A.14)) (in mm h^{-1}) is provided as a level 2 data set (Burgemeister et al., 2024b).

A.3.7 Data sets and availability

The LAWR is measuring raw radar reflectivities since 27.05.2013 with a yearly data availability of up to 98 % (Table A.5). Maintenance, radar errors or memory errors have reduced the data availability. The LAWR measurements are saved at the listed data levels following the data standard described by Lammert et al. (2018):

- The **raw radar data** are the direct radar output saved as hourly binary files.
- The **level 0 data** set includes the radar reflectivity dBZ and the standard deviation of the radar reflectivity factor of the averaged single pulses in hourly netCDF files.
- The **level 1 data** set includes the calibrated radar reflectivity dBZ (Sect. A.3) in daily netCDF files and is freely available (Burgemeister et al., 2024b), facilitating studies on attenuation correction and the derivation of further weather radar products, e.g. an improved rainfall rate. Furthermore, new interpolation methods can be tested because interpolated values are tagged with a clutter mask.
- The **level 2 data** sets contain the attenuation-corrected radar reflectivity dBZ and rainfall rate R in daily netCDF files. R is provided as open-access data

set (Burgemeister et al., 2024b), facilitating refined studies on the spatial and temporal scales of precipitation and further hydrological research, e.g. input data for high-resolution modelling, in an urban area.

All data sets are gridded on the polar observation grid. Additionally, the level 2 data set includes the georeferenced grid information with the latitude, longitude, and height.

Table A.5: LAWR data availability between the years 2013 and 2021

Year	Percentage of availability (%)
2013	57
2014	61
2015	97
2016	98
2017	93
2018	96
2019	98
2020	79
2021	61

A.4 DATA QUALITY

Several sources of radar-based errors were adjusted gradually (Sect. A.3), aiming to improve the data quality of the radar reflectivity and, consequently, the rainfall rate estimate. This section outlines the performance of the multi-year X-band radar observations and discusses open issues and limitations of the reanalysed data set.

Quantitatively, the reanalysed LAWR measurements are evaluated using MRR measurements at matching heights, following the same procedure as in Sect. A.3.4 for the calibration. Therefore, the MRR radar reflectivity factor and rainfall rate are averaged at height levels within the LAWR radar beam using a Gaussian weighting function. The MRR's 10 s temporal resolution is averaged to the matching LAWR's 30 s resolution. The comparison of measurements is constrained to the liquid phase, using the 2 m temperature and a constant wet adiabatic lapse rate, which reduces effects from a bright band.

The LAWR attenuation-corrected radar reflectivity dBZ (level 2 data set) is on average 0.52 dB higher than the MRR WMH reference (Fig. A.5). The root-mean-square error (RMSE) equals to 3.93 dB and the reflectivities are highly correlated with a Pearson correlation coefficient $r = 0.88$. The positive bias is a result of the performed calibration without attenuation correction, because calibrated reflectivities are a prerequisite for stable attenuation correction (Sect. A.3.5). Accordingly, all scores improve, if only cases with moderate attenuation, below the $\text{PIA} \leq 10$ dB threshold, are considered: bias of 0.26 dB, a RMSE of 3.52 dB, and $r = 0.89$. Just 8.5 % of the applied attenuation estimates are unstable with $10 \text{ dB} < \text{PIA} < 27.12 \text{ dB}$. These unstable attenuation estimates appear as a slight visible overestimation of the LAWR measurements at high reflectivities ($\gtrsim 30$ dBZ) (Fig. A.5), but these measurements

are still usable with $r = 0.79$. In the case of a numerically unstable attenuation estimate, radar reflectivities are not corrected (79 times; 0.03%). Note that only 19.7% of the LAWR measurements (Fig. A.5) are interpolated. The scores depicted in Fig. A.5 do not change if these measurements are discarded. The independent reflectivity measurements of the MRR BBG (not shown) confirm the data quality: bias of -0.30 dB, RMSE of 3.85 dB, and $r = 0.88$. Hence, the LAWR reflectivity is not biased in total.

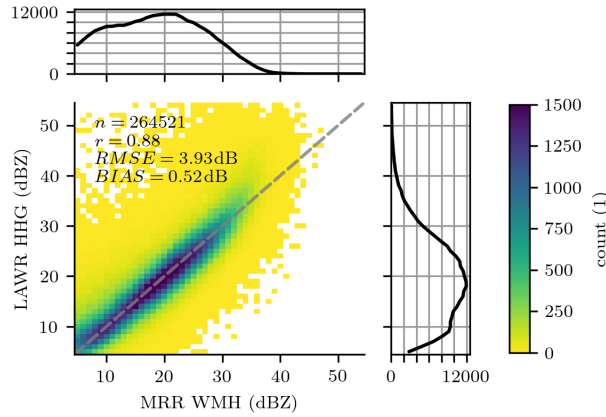


Figure A.5: 2d distribution of radar reflectivities estimated from LAWR and MRR WMH based on drop size distributions at common volumes and a temporal resolution of 30 s restricted to dBZ between 4.5dBZ and 59.5dBZ. The measurements are compared for the reanalysed data set covering the years 2013 to 2021.

The LAWR rainfall rate R (level 2 data set) is retrieved from the attenuation-corrected radar reflectivity using the Marshall-Palmer Z - R relation (Sect. A.3.6). The LAWR rainfall rate is on average 0.42 mm h^{-1} lower than the reference (Fig. A.6). The RMSE equals to 4.69 mm h^{-1} . The Pearson correlation coefficient for the logarithmic rainfall rate dBR is $r = 0.74$. Since the reflectivities of LAWR and the MRRs are in good agreement, the comparison of the rainfall rates mainly investigates the performance of the Marshall-Palmer Z - R relation. The average underestimation of rainfall rates is in line with Kirsch et al. (2019), who shows that the Marshall-Palmer Z - R relation underestimates rainfall accumulation derived from drop size distributions by between 6.3% and 17.4%. The error increases in cases of strong convective precipitation because raindrop size distributions start to deviate from Marshall-Palmer distributions for these cases (Schleiss et al., 2020).

Although, the rainfall rate estimates can deviate for individual time steps, LAWR measurements reproduce the frequency distribution of rainfall rates as observed by the two MRRs very well (Fig. A.7). In particular, the LAWR is able to identify rainy time intervals. The overestimation of low rainfall rates $R < 0.2 \text{ mm h}^{-1}$ is probably an issue of the MRR's attenuation correction. The decrease at the lower tail of the frequency distribution of MRR rainfall rate is only observable at high measurement levels (Fig. A.8), where the uncertainty of the attenuation correction increases. At near-ground measurement levels, the rainfall rate frequency distributions of MRR and LAWR are equal at low rainfall rates of $R < 1 \text{ mm h}^{-1}$ and high rainfall rates of $R > 10 \text{ mm h}^{-1}$. In hydrological applications, accurate rainfall estimates are of interest at ground level (Thorndahl et al., 2017). The vertical variability of rainfall

properties, e.g. due to evaporation or wind drift, may limit the application of the provided LAWR rainfall rates at ground level (Villarini and Krajewski, 2010). The evaluation of LAWR rainfall rate at beam height with the MRR WMH measurement at 105 m shows differences in the frequency distribution between 2 mm h^{-1} and 10 mm h^{-1} as a possible result of vertical rainfall variability (Fig. A.8). Nevertheless, the LAWR measurements yield reliable rainfall rate estimates at beam height and sub-minute temporal scale.

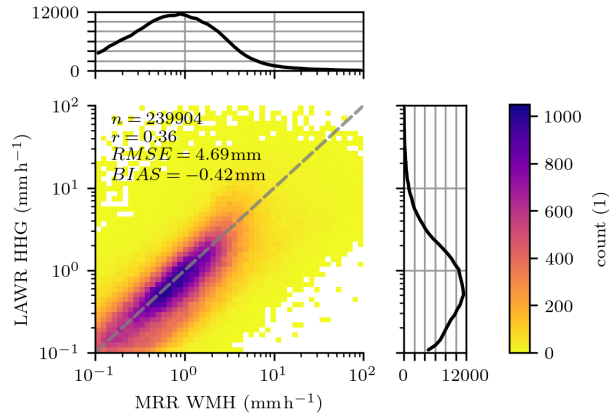


Figure A.6: 2d distribution of rainfall rates estimated from LAWR using a standard Z - R -relation and MRR WMH based on drop size distributions at a temporal resolution of 30 s and for R is between 0.1 mm h^{-1} and 100 mm h^{-1} .

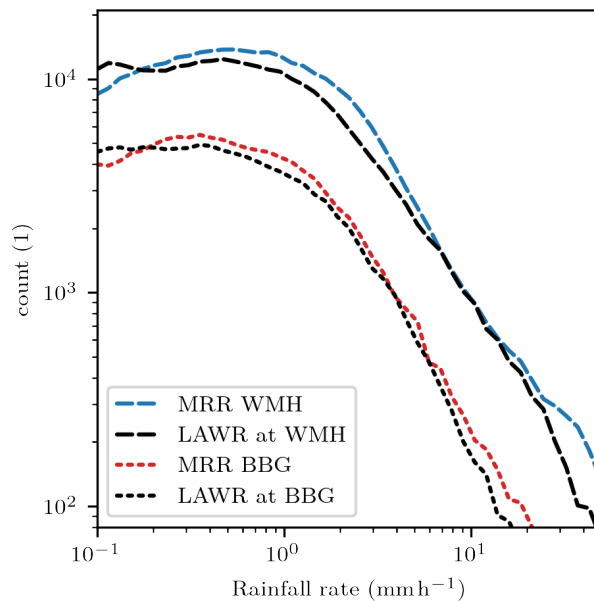


Figure A.7: Frequency distribution of rainfall rates estimated from LAWR using a Z - R -relation and MRR WMH and MRR BBG based on drop size distributions averaged at beam height at a temporal resolution of 30 s.

Qualitatively, the LAWR measurements provide continuous spatio-temporal rainfall patterns. The LAWR resolved a characteristic circular hook echo in the 30 s average rainfall rate, demonstrating a rotating rainfall circulation around a tornado

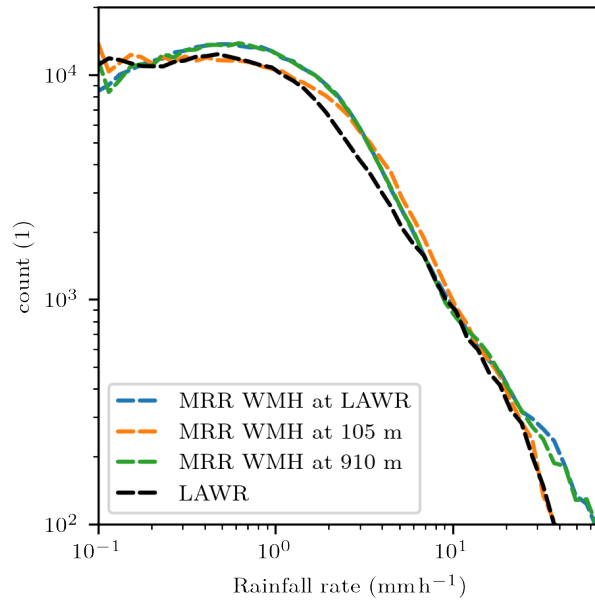


Figure A.8: Frequency distribution of rainfall rates estimated from LAWR using a Z - R relation and MRR WMH based on drop size distributions at a temporal resolution of 30 s at different height levels and averaged at beam height.

(Fig. A.9), as discussed by Hoffmann et al. (2018). The provided LAWR rainfall rate R (level 2 data set) shows less remaining clutter compared to the processed rainfall rate by Hoffmann et al. (2018). Differences between the rainfall rates occur due to differences in processing steps, e.g. clutter removal, attenuation correction, and the applied Z - R relationship. However, the qualitative statements remain the same. The hook echo is clearly visible for 8 min, in 16 measurement time steps, accordingly. The German nationwide C-band radars, measuring with 5 min temporal and 250 m range resolutions, show the general rainfall pattern, but the hook echo is only at one measurement time step. As a consequence, this event demonstrates that the LAWR, with its refined spatio-temporal resolution compared to coarser resolved C-band radars, is capable of resolving rainfall patterns with a short duration and relevant gradients at hectometre spatial scales.

The fine-scale structures in rainfall patterns are smoothed by temporal accumulation; nevertheless, spatial differences are still visible in the three-month rainfall accumulation (Fig. A.10). The rainfall pattern is mainly driven by convective summer rainfall events. The rainfall accumulations reveal long-term measurement errors, inter alia remaining clutter close to the radar and three spikes. First, range gates close to the radar are still affected by clutter after the application of correction algorithms, resulting in a small circle of high rainfall accumulations. Approximately 500 m around the radar location, the first 8 of 333 range gates show the overestimated total precipitation. Second, three spikes are characterized by an underestimation of total precipitation affecting multiple azimuth angles over the whole range. Two spikes in the north-east of the radar are a result of metal poles installed at a few metres distance to the radar on the rooftop, reaching into the radar beam. A third spike is in the south of the radar as a result of Hamburg's television tower, which is located in 550 m distant from the radar. The spikes affect the azimuth angles

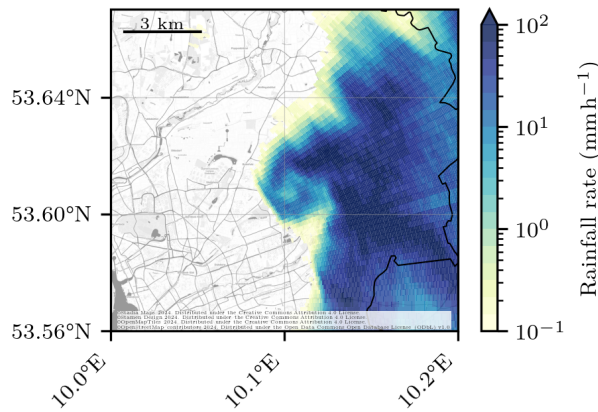


Figure A.9: Rainfall pattern during a tornado event on 07.06.2016 at 16:20:30 UTC. The rainfall rate is shown for a north-eastern section of the measurement domain in Hamburg. An animation of this event is provided in the Supplement.

roughly from 19° to 30° , 32° to 42° , and 166° to 171° . Note that measurements within these azimuth sectors, comprising 25 of 360 azimuth angles, need to be corrected for beam blockage or rejected for studies using this radar rainfall estimate. Without these errors, the 3-month total precipitation is in general not affected by clutter, noise, or attenuation (Fig. A.10). The total precipitation was on average 168.0 mm and the median is 165.1 mm within the measurement domain in summer 2019. The 3-month rainfall accumulations are spatially variable in Hamburg, with a minimum of 111.6 mm and a maximum of 271.3 mm. Note that the rainfall patterns at ground can deviate in comparison to the measured rainfall pattern at beam height because of vertical rainfall variability (Villarini and Krajewski, 2010). Four rain gauges measured 194.8 mm (north), 127.6 mm (east), 134.0 mm (south), and 172.9 mm (west) during the 3 months (Fig. A.10). The absolute biases between the radar rainfall accumulations and rain gauge measurements range from 1.9 mm to 20.1 mm. In general, the rain gauge observations are in agreement with the estimated radar rainfall accumulations during this measurement period. Consequently, the LAWR provides reliable rainfall estimates with accumulation times from 30 s to multiple months.

All in all, the reanalysed multi-year LAWR measurements give insight into the spatio-temporal structure of rainfall at 30 s temporal scale and hectometre spatial scale in an urban area. The LAWR and MRRs are continuously in good agreement. The reanalysed radar reflectivities and rainfall rates can be used for meteorological and hydrological studies, considering the following limitations:

- The LAWR data set is constrained to the liquid phase.
- The attenuation correction can be unstable; thus, radar reflectivities can be overestimated. In rare cases, radar reflectivities are not corrected for a numerically unstable attenuation correction.
- Differences between the LAWR measurements at beam height and ground observations are a result of vertical variability of rainfall due to wind advection and evaporation of rainfall. Variations between measurement devices arise due to differences in measurement principle and volume mismatches.

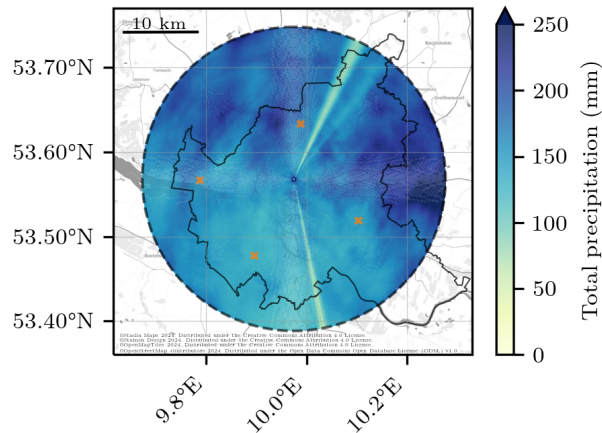


Figure A.10: Three-month total precipitation measured by the LAWR during June, July, and August 2019. The radar estimates at four rain gauge locations (orange crosses) are 174.7 mm (north), 146.7 mm (east), 132.1 mm (south), and 157.1 mm (west).

- Remaining clutter and noise may overestimate single measurements. The first range gates can be superimposed by clutter.
- The LAWR is affected by beam blockage in three directions, resulting in three spikes in range within the measurements.

A.5 CODE AND DATA AVAILABILITY

The pylawr python package (Burgemeister et al., 2023) provides useful tools to load, process, and plot the LAWR data and was used to process the provided data sets. The LAWR HHG data set of rainfall rates (level 2) and radar reflectivities (level 1) is available at WDCC: https://doi.org/10.26050/WDCC/LAWR_UHH_HHG_v2 (Burgemeister et al., 2024b). Further LAWR HHG observational data sets at different processing levels and MRR observations are available upon request. We strongly encourage anyone using the data set to be in contact with the authors.

A.6 CONCLUSIONS

Firstly, this study describes quality-tested radar reflectivities and rainfall rate estimates with 30 s temporal and hectometre spatial resolutions covering the years 2013 to 2021, which are provided as an open-access data set (Burgemeister et al., 2024b). Secondly, this study proves the multi-year performance of a local-area X-band weather radar (LAWR) despite the lack of polarization and Doppler information. The LAWR is deployed in combination with a vertically pointing micro rain radar (MRR) and rain gauge in the urban area of Hamburg, Germany, since 2013. The synergy of observations yield reliable LAWR measurements, confirmed by a second MRR.

Several sources of radar-based errors were adjusted gradually, affecting the precipitation estimate, e.g. noise, alignment, non-meteorological echoes, radar calibration, and attenuation. The manually adjusted LAWR alignment was accurately determined, using the solar signal appearing in radar reflectivities during sunrise and

sunset, facilitating comparisons with other measurement devices. The deployment of MRRs yields drop size distributions at LAWR beam height. The LAWR reflectivities are calibrated using MRR reflectivities at intersecting volumes. The subsequent calibration of the LAWR is mandatory because of strongly biased measurement periods due to maintenance, shown by the MRR observations. After calibration, the attenuation correction method, the modified Kraemer (MK) approach, is applied. The MRR drop size distributions facilitate the adjustment of parameters based on the relationship between the radar reflectivity and specific attenuation to apply the MK approach at X-band frequencies. This study presents the adjusted parameters and indicates that the MK approach is a reliable attenuation correction method for single-polarized X-band radars, shown with a long-term data set as suggested by Jacobi and Heistermann (2016). The LAWR rainfall rates were estimated from attenuation-corrected reflectivities using the Marshall-Palmer Z - R relationship. The MRR rainfall rates, estimated from drop size distributions, show an on average underestimation of the LAWR rainfall rates estimated. Nevertheless, the retrieved, multi-year LAWR radar reflectivities and rainfall rates are in good agreement with MRR measurements.

Several issues may limit the performance of the LAWR measurements. This study focuses on the liquid phase; hence, solid or mixed-phase precipitation, which is for instance dominant during the winter months, introduces errors within the provided data set, e.g. overestimated radar reflectivities due to the melting layer (Villarini and Krajewski, 2010). Remaining clutter and noise may remain within the reanalysed measurements. Rare unstable attenuation corrections overestimate the LAWR radar reflectivity. Affected radar reflectivities are labelled within the data set. Furthermore, LAWR measurements at beam height can differ from ground observations as a result of vertical rainfall variability due to wind drift and evaporation of rainfall, limiting the application of LAWR rainfall rates at ground level. The largest errors in rainfall rate estimates at individual time steps arise from inherent uncertainties of the Z - R relation, but they do not cause systematic deviation. The frequency distribution of rainfall rates is very well reproduced. Variations between measurement devices arise due to differences in measurement principles and volume mismatches. The assessment of the LAWR alignment identified measurement periods with beam elevation angles up to 6.1° . A high beam elevation angle leads to, inter alia, partial overshooting of MRR measurement volumes, which is a problem of measurement design. The measurement design can be optimized by using lower LAWR beam elevation angles, e.g. 3.5° , or a coarser MRR range resolution, e.g. 50 m. In future, the issue of overshooting will be avoided, by using lower beam elevation angles, adding the benefit of measurements at lower altitudes. Measurements at lower beam elevation angles than 3° are not recommended, because the LAWR beam elevation setting is a compromise between measurement altitude and the occurrence of clutter signals. Note that MRR measurements also need quality control (Reinoso-Rondinel and Schleiss, 2021).

This multi-year urban radar rainfall data set is groundwork for further meteorological and hydrological research and is actively used in different meteorological studies (e.g. Ferner et al., 2022; Kirsch et al., 2022; Schmitt et al., 2023). Prospective research may investigate conditional and event-based errors in the multi-year LAWR measurements to quantify limitations of the LAWR. By including comparisons from the LAWR to additional independent sensors, the added value of

the spatio-temporal information from low-cost, local-area X-band radars can be investigated. For hydrological research, LAWR rainfall rates should be evaluated with measurements at ground. Future urban precipitation studies will be improved by the extension of networked observations with a second X-band weather radar site and additional micro rain radars in Hamburg, measuring since the beginning of 2021.

ACKNOWLEDGEMENTS

Funded by the Deutsche Forschungsgemeinschaft (DFG, German Research Foundation) under Germany's Excellence Strategy – EXC 2037 'CLICCS - Climate, Climatic Change, and Society' – Project Number: 390683824, contribution to the Center for Earth System Research and Sustainability (CEN) of Universität Hamburg. Data from two rain gauges were provided by the German Weather Service (DWD). The X-band radar data was archived at the DKRZ.

ADDED VALUE OF SPATIO-TEMPORAL RESOLUTION FOR WEATHER RADAR OBSERVATIONS AT URBAN SCALES

The work in this appendix is in preparation for publication as:

F. Burgemeister, M. Clemens, and F. Ament (2024a). "Added value of spatio-temporal resolution for weather radar observations at urban scales." In: *preparation for the submission to the Journal of Hydrometeorology*

AUTHOR CONTRIBUTIONS

FB conceptualized the study with advice by FA and MC. FB planned and processed the measurement data, planned and performed the formal analysis, wrote and revised the draft. All authors reviewed the draft.

Added value of spatio-temporal resolution for weather radar observations at urban scales

Finn Burgemeister¹, Marco Clemens¹, Felix Ament¹

¹Meteorological Institute, Center for Earth System Research and Sustainability (CEN), Universität Hamburg

ABSTRACT

Knowledge of short-duration, sub-kilometer-scale rainfall variability is needed for several meteorological and hydrological applications, particularly in urban environments due to their sensitivity to water-related issues. Variability at these scales is a blind spot for both operational rain gauge networks and operational radar networks. Reanalysed rainfall rates from a single-polarized X-band weather radar are available at high temporal (30 s) and range (60 m) resolutions within a scan radius of 20 km covering the urban area of Hamburg, Germany. This study compares the reanalysed radar data from this local area weather radar (LAWR) with observations from two micro rain radars (MRRs), an operational C-band radar, combined networks of 33 rain gauges, and the radar-rainfall climatology RADKLIM.

What is the added value of a LAWR compared to operational C-band radar systems? In fact, the smaller radar volumes result in a closer agreement in terms of radar reflectivity with local radar observations by MRRs. However, this advantage does not translate in a better match to precipitation accumulations recorded by rain gauge, as differences in the Z-R relation and sample volume sizes between radar and rain gauge dominate the uncertainty for both the LAWR and operational radar systems. But the LAWR is clearly superior in describing spatial structure. Interestingly, operational radar observations overestimate spatial variability. This effect is caused by their intermittent scan strategy, taking just a snapshot every five minutes. We identify the benefits of the X-band radar's scan strategy results to all measurements taken every 2.5 s. The refined spatio-temporal resolution and scan strategy is also beneficial for capturing rainfall peaks. Finally, we demonstrate that the LAWR can monitor steeper spatial gradients. In summary, the LAWR is not able to provide better local rainfall estimates on the sampling scale of rain gauges, but still we can prove an added value to characterize the local rainfall intensity and spatio-temporal rainfall patterns.

B.1 INTRODUCTION

Capturing the true rainfall variability at sub-kilometre and sub-hourly scales with measurements remains a challenge, but rainfall information at these scales is required for several meteorological and hydrological applications, especially in urban areas that are highly sensitive to water-related issues (Cristiano et al., 2017; Sokol et al., 2021; Thorndahl et al., 2017). Operational rain gauge networks provide reliable local rainfall measurements, but are unable to represent spatial rainfall variability at the urban scale due to limited network densities (Ochoa-Rodriguez et al., 2019). Conventional weather radar systems are able to provide radar rainfall measurements over large domains of a hundred kilometres, but are limited to temporal resolutions of several minutes and spatial resolutions of a few hundred metres. Radar-based rainfall reanalyses based on conventional radars are available for Germany with a 5 min temporal resolution and 1 km spatial resolution (Winterrath et al., 2018a), and for Europe with an hourly temporal resolution and 2 km spatial resolution (Overeem et al., 2023). Gap-filling X-band radars are able to refine rainfall estimates in areas of special interest, like urban areas (e.g. Berenguer et al., 2012; Burgemeister et al., 2024c; Lo Conti et al., 2015; Maesaka et al., 2011; van de Beek et al., 2010; Wang and Chandrasekar, 2010; Yoon et al., 2017).

The spatial scale of rainfall is smaller than the inter distance of most operational rain gauge networks, indicated with radar observations up to hourly scales (Lengfeld et al., 2019; Marra and Morin, 2018a). However, there is an unmeasured rainfall variability in radar observations at sub-kilometre spatial scale (Gires et al., 2014; Peleg et al., 2018). Bárdossy and Anwar (2023) concluded that disregarding spatial rainfall variability causes problems that cannot be solved by any model or finer resolution temporal data. Therefore, in urban hydrology is a demand for high quality radar rainfall data with at least a temporal resolution of 1 min and spatial resolution of 100 m for small urban catchment sizes (Berne and Krajewski, 2013; Einfalt et al., 2004; Gires et al., 2013; Ochoa-Rodriguez et al., 2015; Thorndahl et al., 2017). Some studies call for the highest possible spatio-temporal resolution of rainfall measurements (e.g. Alves de Souza et al., 2018; Cao et al., 2023; Costabile et al., 2023). A higher temporal resolution would also reduce temporal sampling errors (Fabry et al., 1994; Shucksmith et al., 2011). Conventional radars perform a volumetric scan, resulting in an intermittent scanning strategy. Jordan et al. (2000) found errors of 30 to 40 % for 5- and 10-minute accumulations of large-scale stratiform precipitation, which increased to 50 to 60 % for small-scale convective precipitation based on 5-minute measurements averaged over 1 km. Advection correction procedures can reduce temporal sampling errors in rainfall accumulations (e.g. Jasper-Tönnies and Jessen, 2014; Nielsen et al., 2014; Seo and Krajewski, 2015). However, there are applications where advection correction could not solve temporal sampling errors. For instance, for the study of the initial phase of convective precipitation, a scan performed every 5 min is too coarse (Kim et al., 2019).

Research X-band radars monitor rainfall at temporal resolutions down to 16 s (van de Beek et al., 2010) and radial resolutions down to 3 m (Mishra et al., 2016), but most of them operate at or below 100 m spatial and 1 m temporal resolutions (e.g. Allegretti et al., 2012; Burgemeister et al., 2024c; Hosseini et al., 2020; Lengfeld et al., 2014; Schleiss et al., 2020; van de Beek et al., 2010; Ventura and Russchenberg,

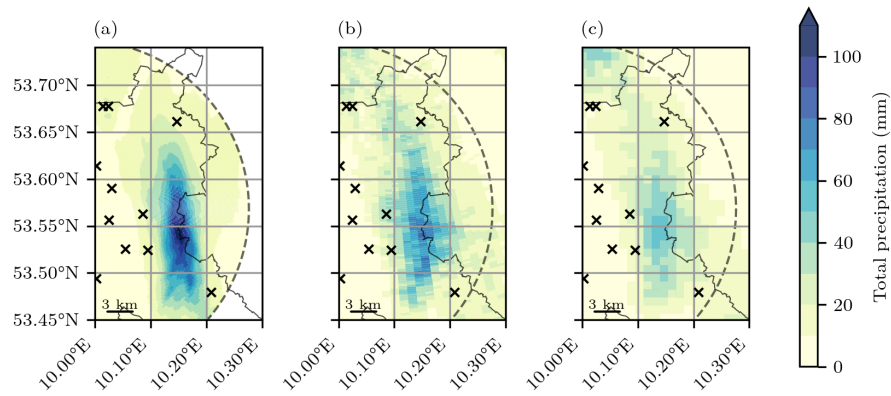


Figure B.1: Total precipitation observed by (a) a local area weather radar (LAWR), (b) a C-band radar, and (c) the radar-rainfall climatology RADKLIM on a day with a flooding event (10.05.2018). The black crosses mark the locations of available rain gauges with 1 min temporal resolution. The maximal total precipitation is (a)

2009; Wang and Chandrasekar, 2010; Yoon et al., 2017). Although most of the latest X-band radars have dual-polarimetric capabilities (e.g. Anagnostou et al., 2018; Cao et al., 2023; Hosseini et al., 2023; Neely III et al., 2021; Pejcic et al., 2022; Schleiss et al., 2020), where dual-polarimetric quantities improve rainfall estimates, even low-cost, single-polarized X-band radars provide valuable information on the spatio-temporal variability of precipitation (Allegretti et al., 2012; Lo Conti et al., 2015; Marra and Morin, 2018a; van de Beek et al., 2010). Nevertheless, single-polarimetric X-band radars require post-processing and the deployment of independent additional sensors (Thorndahl et al., 2017; Villarini and Krajewski, 2010).

Recently reanalysed radar rainfall estimates from a single-polarized X-band weather radar are available at hectometre and sub-minute scales within 20 km scan radius for the urban area of Hamburg, Germany, for multiple years (Burgemeister et al., 2024c). The local area weather radar (LAWR) operates at one elevation angle with a high temporal (30 s), range (60 m), and azimuthal sampling (1°) resolutions (Lengfeld et al., 2014), refining coarser observations of the German nationwide C-band radars at 250 m spatial and 5 min temporal resolution. Previous studies show that the LAWR provides detailed information on the structure of precipitation (Burgemeister et al., 2024c; Hoffmann et al., 2018; Lengfeld et al., 2018, 2016, 2014). For instance, Hoffmann et al. (2018) show that the LAWR is able to capture the circular pattern around a tornado in several measurements, in contrast to other rainfall observations, because of its higher resolutions in space and time.

Several rainfall events revealed strong differences in the spatial variability of rainfall observed by different measurement devices (Fig. B.1). This work aims to explore the added value of spatio-temporal resolution for weather radar observations at sub-hourly and sub-kilometre scales by addressing three research questions:

- Is the local rainfall rate of the LAWR superior to other rainfall estimates?
- Is the LAWR better in capturing spatial rainfall variability?
- Are there gradients within the LAWR not obtained by other measurement devices?

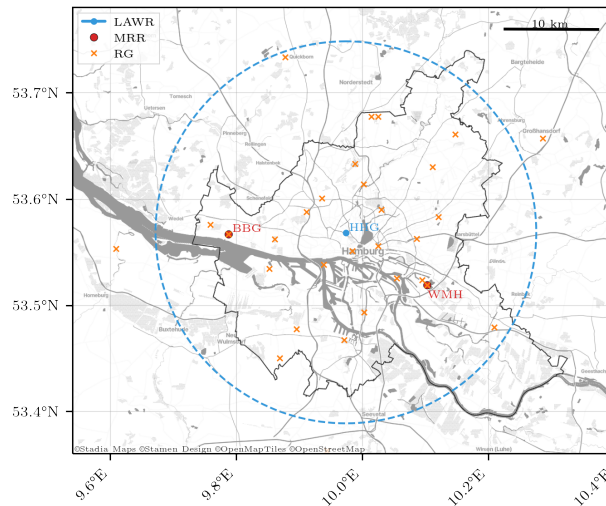


Figure B.2: Precipitation observations in Hamburg. The location of the local area weather radar (LAWR) / X-band radar (WRX) on the rooftop of the building "Geomatikum" in Hamburg (HHG) is indicated with a blue point. The blue dashed line shows the coverage with the 20 km scan radius. The locations of two micro rain radars (MRRs, red points) are by name Blankenese Bauersberg (BBG) and Wettermast Hamburg (WMH). Locations of rain gauges are indicated by orange crosses.

In this paper, we describe the unique availability of rainfall data sets combining the LAWR, two micro rain radars (MRRs), a C-band radar, combined networks of 33 rain gauges, and the radar-rainfall climatology RADKLIM (Sect. B.2). We evaluate the reliability of the radar reflectivity (Sect. B.3.1) and rainfall measurements (Sect. B.3.2) from the LAWR and C-band radar in comparison to the MRRs and rain gauges. We investigate the spatial rainfall structure at sub-hourly and sub-kilometre scales for the LAWR, the C-band radar, the rain gauge network, and RADKLIM (Sect. B.3.3). We revisit the effect of spatio-temporal resolution on the measurements of rainfall peaks (Sect. B.3.4). Additionally, we elaborate the sub-kilometre spatial rainfall variability with radar reflectivity gradients to give insights in the performance of measurements at the microscale (Sect. B.3.5). The different aspects of these analyses allow the research questions to be answered (Sect. B.4).

B.2 RAINFALL OBSERVATIONS

The study area around Hamburg, Germany (Fig. B.2) is disproportionately, densely covered by rainfall observations: a local area X-band radar (Sect. B.2.1), the nationwide C-band radar network (Sect. B.2.2), two micro rain radars (MRRs, Sect. B.2.3), and networks of rain gauges (Sect. B.2.4). This study focuses on a five-month period from 1 May to 30 September 2019 to constrain measurements to the liquid phase. Nevertheless, all rainfall observations are available for multiple years, facilitating the validation of results. This section will give an overview about in-situ and remote rainfall observations and introduces the used data sets briefly.

B.2.1 X-band radar (LAWR)

The University of Hamburg operates a single-polarized X-band weather radar in the city centre of Hamburg, Germany (Fig. B.2), to investigate rainfall variability at hectometre spatial and sub-minute temporal scales (Burgemeister et al., 2024c; Lengfeld et al., 2014). This local area weather radar (LAWR) is a modified ship navigation radar of type GEM scanner SU70-25E operating at a frequency of 9.41 GHz. The LAWR provides horizontally radar reflectivity measurements at one fixed elevation angle (5.4°) with 30 s temporal, 60 m range, and 1° azimuthal sampling resolution within a scan radius of 20 km. The radar reflectivity represents an 30 s average of approximately 67 pulses per 1° collected during 12 sweeps. The measurements were corrected for several sources of errors, e.g. noise, alignment, non-meteorological echoes, radar calibration, and attenuation, and quality checked (Burgemeister et al., 2024c).

The LAWR radar rainfall rates R (Burgemeister et al., 2024b) are estimated from radar reflectivities Z by applying a power-law Z - R relationship

$$Z = a R^b, \quad (\text{B.1})$$

where a and b are empirical parameters. The values of these parameters depend on the drop size distribution, which varies geographically, with rainfall intensity, and time (e.g. Berne and Krajewski, 2013; Doviak et al., 1993; Villarini et al., 2008). The rain retrieval can be improved with the parameters of the Z - R relationship. However, this study aims to investigate the effect of spatio-temporal resolution and scan strategy on the rainfall distribution, therefore one fixed Z - R relationship is applied to both radars. The parameters of this study are $a = 200$ and $b = 1.6$ as proposed by Marshall et al. (1955), representing average rainfall conditions in this climate (Burgemeister et al., 2024c; Holleman, 2006; Kirsch et al., 2019).

B.2.2 C-band radar and RADKLIM

The German weather service (DWDs) operates a nation-wide network of C-band weather radars. All C-band radars have dual-polarization and Doppler capabilities. For details on the C-band radar technical setup, data quality, and calibration, refer to (Frech et al., 2017). The DWD's scan strategy includes an orography-following precipitation scan for hydrological applications and volume scans at 9 elevation angles every five minutes (Frech et al., 2023). This study uses the precipitation scan from the nearest C-band radar to Hamburg, located near Boostedt about 50 km north of Hamburg. The Boosted C-band radar's precipitation scan provides radar reflectivity measurements within a 150 km radius, covering the entire study area. The scan operates at a constant elevation angle of 0.8° , with a 5 min temporal, 250 m range, and 1° sampling resolution. The measurements represent an 80 ms average of approximate 50 pulses per 1° azimuth collected during 1 sweep within the 5 min measurement interval. Radar reflectivities were corrected for attenuation using the method of Jacobi and Heistermann (2016), implemented by Heistermann et al. (2013). The rainfall rates were derived from attenuation-corrected horizontal reflectivities using the same power-law relationship between these two quantities (Z - R relationship) as for the LAWR (Sect. B.2.1). Polarimetric rain retrievals, based

on the specific attenuation and specific differential phase, would perform better than single radar reflectivity methodologies (e.g. Ryzhkov et al., 2022). Consequently, for the C-band radar, the rain retrieval can be improved based on polarimetric measurements. However, the focus is on the general performance of both radars and not on the variability of the Z - R relationship.

A further radar-rainfall data set used in this study, is the radar-based climatology RADKLIM (Winterrath et al., 2018a) provided by the DWD. The observations of the C-band radar network were adjusted with rain gauge measurement, corrected for errors, and quality-checked. For details on the climatology, refer to Winterrath et al. (2017). This study uses ground-based rainfall rates, the YW product (Winterrath et al., 2018a), with a 5 min temporal and a 1 km² spatial resolution.

B.2.3 *Micro rain radar (MRR)*

The MRR is a vertically pointing frequency-modulated-continuous wave (FM-CW) Doppler radar manufactured by METEK Meteorologische Messtechnik GmbH (Peters et al., 2002). The MRR retrieves drop size distributions (DSDs) from measured Doppler spectra using the terminal fall velocity given by Atlas et al. (1973). Rainfall rates and radar reflectivities are calculated from DSDs (Doviak et al., 1993). Noise and attenuation corrections are performed by the manufacturer's software (Metek, 2015). The DSD retrieval assumes stagnant air. Vertical wind and turbulence effects are discussed in Peters et al. (2005) and are neglected in this study. The transmit frequency is at 24.23 GHz (K-band). The MRR measures DSD profiles for 31 range gates, with a range resolution of 35 m and a temporal resolution of 10 s. The measurements represent an 8 s-average within its 10 s measurement interval. The rainfall rates and radar reflectivities were adjusted with a rain gauge at the same location (Burgemeister et al., 2024c). Additionally, the adjacent rain gauges monitor the MRR's performance.

The MRRs are deployed at two measurement sites in the study area (Fig. B.2). The MRR Wettermast Hamburg (WMH) is located at the scientific measuring site of the Meteorological Institute of the Universität Hamburg in the south-eastern part of the city. The MRR Blankenese Bauersberg (BBG) is deployed at a waterworks of the municipal water and wastewater utility Hamburg Wasser in the west of Hamburg. The MRRs and LAWR are 10.1 km (WMH) and 12.3 km (BBG) apart. The distances between the MRRs and the C-band radar Boostedt are 54.02 km (WMH) and 51.48 km (BBG), respectively.

B.2.4 *Rain gauges*

This study uses 33 rain gauges (Fig. B.2) from different rain gauge networks that were available during the study period. The University of Hamburg operates a network of weather stations throughout Hamburg, covering eight tipping bucket rain gauges (Campbell Young 52203) and two weighing rain gauges (OTT Pluvio). The two weighing rain gauges and two tipping bucket rain gauges are located close to the MRRs. Hamburg Wasser, the municipal water and wastewater utility, provided measurements of 18 weighing rain gauges (OTT Pluvio). The DWD operates five weighing rain gauges (Lambrecht rain[e]H3) in and around Hamburg.

The combined rain gauge network has a maximal pair distance of 46 km and median pair distance of 15 km. Although this rain gauge network is denser than widely-used rain gauge networks, only 7 rain gauge pairs have a distance below 1 km, capturing the rainfall variability at a sub-kilometre scale. Note that two DWD rain gauges and one Hamburg Wasser rain gauge are outside the LAWR scan radius (Fig. B.2). All rain gauges were checked for the data quality by investigating the cumulative rainfall accumulation and the probability of detecting with different rainfall thresholds.

B.3 RESULTS AND DISCUSSION

The LAWR offers the highest area-wide spatio-temporal resolution of measurements compared to the network of available rain gauges, the nearest operational C-band radar, and the radar-rainfall-climatology RADKLIM. However, the spatio-temporal resolution does not need to translate to measurements close to the truth. In order to ascertain the added value of the LAWR, we undertake a comparative analysis of the LAWR measurements with those of comparable measurement devices. Firstly, we verify the radar reflectivity (Sect. B.3.1) and rainfall distributions (Sect. B.3.2). Secondly, we investigate the measured spatio-temporal rainfall variability with the spatial correlation structure (Sect. B.3.3). Thirdly, we investigate features of radar measurement patterns in relation to the spatio-temporal resolution: measurement peaks (Sect. B.3.4) and spatial gradients (Sect. B.3.5).

B.3.1 Radar reflectivity distributions

The LAWR and C-band radar both measure radar reflectivity, but differ in spatio-temporal resolution and scan strategy (Sect. B.2). The LAWR radar reflectivity has a radial resolution of 60 m and represents a true 30 s average of its measurement interval. In contrast, the C-band radar reflectivity has a radial resolution of 250 m and measures 80 ms per azimuth of its represented 5 min measurement interval. The aim is to assess how well the LAWR and C-band radar represent the respective measurement intervals. Firstly, the MRR serves as reference, since the MRR profile covers the LAWR and C-band radar beam height partially and the MRR has a higher temporal resolution compared to the LAWR and C-band radar. Both MRRs are used as a reference combined. Secondly, the LAWR and C-band radar reflectivity distributions are compared spatially.

Micro rain radar as reference

The MRRs radar reflectivity factor profiles are averaged within the radar beam heights using a Gaussian weighting function, with its maximum at the beam centre (Burgemeister et al., 2024c). The two lowest MRR rain gates were excluded due to inapplicable assumptions in radar signal processing for those gates (Peters et al., 2005). The two highest MRR rain gates were excluded due to errors attributed to noise and aliasing effects. The LAWR and C-band radar beams overlap with the MRR at different heights and extents. The LAWR has a mean beam height of 1058 m and 1273 m at the MRR sites, with a beam width of 489 m and 598 m. Accordingly, the LAWR measurements are compared to an average of six and four MRR range

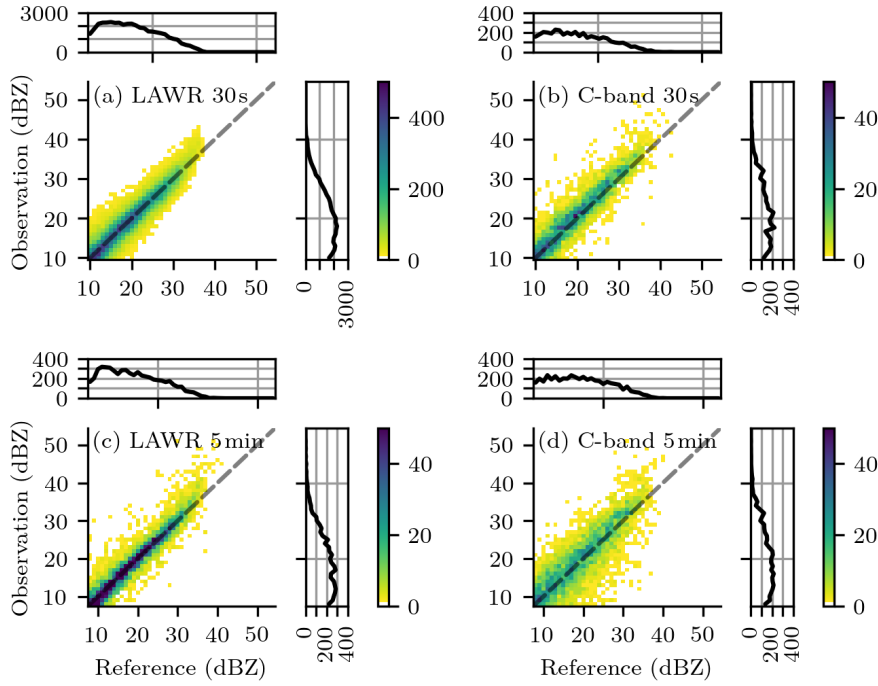


Figure B.3: 2d distribution of radar reflectivities measured by the LAWR and the C-band radar versus two MRRs as reference. The measurements are compared at common heights for the period May to September 2019. The MRR radar reflectivities were averaged to (a, b) 30 s and (c, d) 5 min. The LAWR radar reflectivities are shown at (a) 30 s temporal resolution and were averaged to (c) 5 min. The C-band radar reflectivities are the (b, d) instantaneous measurements from the 5 min measurement interval.

gates. The C-band radar has a mean beam height of 1052 m and 1001 m at the two MRR sites. The beam width is 848 m and 808 m. Due to the large beam width, measurements of 12 and 15 MRR range gates are averaged and compared to the C-band radar observations.

Prior to the comparison of radar reflectivities, the sensitivity of the MRR measurements is investigated, because electronic and thermal noise affects the MRR profile. The detectability of the MRR radar reflectivity is calculated with the 99 % quantile covering 17 clear-sky days following Kneifel et al. (2011) (not shown). Clear-sky days were found based on ceilometer data located near the MRR WMH. Radar reflectivities above the 99 % quantile are assumed to be free of noise. For 30 s averages of radar reflectivity, the MRR WMH detectability decreases from the third range gate with -4.03 dBZ (MRR BBG: -2.73 dBZ) up to 5.89 dBZ (MRR BBG: 9.15 dBZ) at range gate 29. In the case of 5 min averages of radar reflectivity, the MRR WMH detectability is -6.49 dBZ (MRR BBG: -5.27 dBZ) for the third range gate and 3.04 dBZ (MRR BBG: 7.48 dBZ) at range gate 28. We analyze only radar reflectivities that exceed 9.5 dBZ at 30 s averages and 7.5 dBZ at 5 min averages, respectively.

At a 30 s temporal resolution, both the LAWR and C-band radar reflectivities perform equally well (Fig. B.3). Both radar reflectivities show a similar bias and root-mean-square error (RMSE) (Table B.1). The LAWR and C-band radar reflectivities are highly correlated with the MRR measurements, respectively.

Table B.1: Validation metrics of radar reflectivity distributions comparing the LAWR and C-band radar with the MRRs, respectively, showing the Pearson correlation coefficient estimator (r), the mean bias, the root-mean-square error (RMSE), and the sample size (n).

	30 s		5 min	
	(a) LAWR	(b) C-band	(c) LAWR	(d) C-band
n	42899	4056	5651	4577
r	0.89	0.92	0.94	0.84
bias (dB)	0.33	1.10	0.28	0.65
RMSE (dB)	3.40	3.12	2.58	4.40

At a temporal resolution of 5 min, the LAWR radar reflectivity measurements are superior to those of the C-band radar. Although, the LAWR bias is nearly unchanged, the RMSE decrease by 0.82 dB (Table B.1). The correlation coefficient increases to 0.94. On the contrary, the C-band radar reflectivity RMSE increases by 1.28 dB and the correlation decreases to 0.84 but the bias decreases slightly. This is expected because the LAWR radar reflectivity is a continuous 5 min observation, whereas the C-band radar reflectivity is, as 80 ms average, a more instantaneous observational sample.

Spatial analysis

LAWR and C-Band radar data need to be interpolated on the same Cartesian grid for a spatial analysis, since the grid properties differ. For the regridding between the polar and Cartesian grid a nearest neighbor algorithm is applied. We use the native resolution of the C-Band radar and interpolate the C-Band radar on a $250 \text{ m} \times 250 \text{ m}$ Cartesian grid. The LAWR radar reflectivity is interpolated on the same Cartesian grid. We analyse the agreement between LAWR and C-band radar for reflectivities above 9.5 dBZ spatially (Fig. B.4), similar to the comparison to the MRRs at 30 s temporal resolution. The C-band radar reflectivity scan every 5 min is compared to the temporal closest 30 s LAWR radar reflectivity.

The LAWR underestimates the C-band radar reflectivity on average with 0.49 dB (Fig. B.4a). The bias is spatially variable between -2.90 dB and 1.26 dB . The bias's spatial variability is a consequence of both rainfall conditions and radar performance, as there are notable differences between periods (not shown). While the radars are observing the same rainfall conditions, there can be discrepancies in radar performance due to factors such as attenuation, sensitivity and maintenance. Radar artefacts, such as a dependence on the radius of the scores, are not visible, emphasising the data quality of the radar measurements. The LAWR and C-band radar reflectivity are highly correlated with 0.86. The correlation coefficient estimate varies spatially between 0.39 and 0.93 (Fig. B.4b). The RMSE equals to 3.97 dB and varies spatially between 2.60 dBZ and 6.09 dBZ (Fig. B.4c). The lowest match between the radar reflectivities, represented by decreased correlations and increased RMSE values, is at radar range gates affected by remaining clutter of both radars, respectively. The clutter values are mainly shown in the C-band radar reflectivity distribution as spikes (Fig. B.5). Additional to clutter values, spatial spikes appear

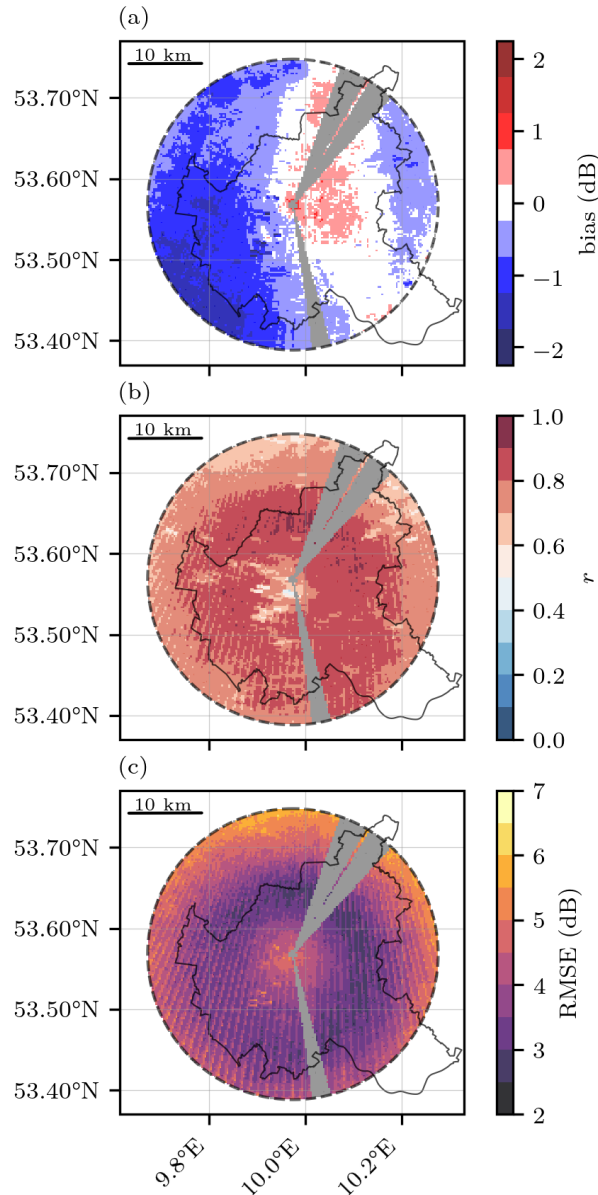


Figure B.4: Spatial evaluation of the radar reflectivity, comparing LAWR and C-band radar measurements, showing the additive bias (a), the correlation coefficient estimator (r) and the root-mean-square error (RMSE). The large spikes are known (due to the TV tower and masts on the rooftop).

in patterns of the correlation coefficient (Fig. B.4b) and RMSE (Fig. B.4c) in the direction of the C-band radar location. These spikes are between two azimuths of the C-band radar and are a result of the nearest neighbor interpolation, because the $250 \text{ m} \times 250 \text{ m}$ Cartesian grid is at this distance poorly sampled by the C-band radar observations (e.g. Brook et al., 2022). However, the best match between the radar reflectivities, represented by increased correlations and decreased RMSE values, is within a torus around the LAWR location (Fig. B.4b-c), where the LAWR and C-band radar measuring height and sampling volume sizes are at closest.

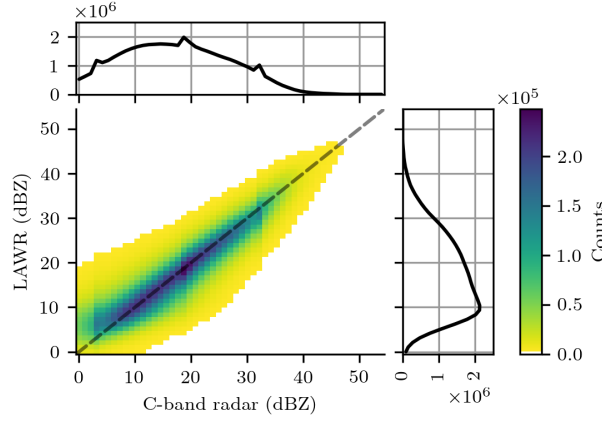


Figure B.5: Spatial evaluation of the radar reflectivity, comparing the X-band radar to the C-band radar.

B.3.2 Rainfall distributions

Rainfall rates R are retrieved from LAWR and C-band radar reflectivities Z , and from MRR drop size distributions, while rain gauges measure rainfall directly. Firstly, we compare the LAWR and C-band rainfall rates with the MRR observations as reference, which shows discrepancies between the used and actual Z - R relation. Secondly, we compare LAWR and C-band rainfall accumulations with rain gauges as a reference, which differ due to the Z - R relation variability, vertical rainfall variability and differences in sampling volume sizes.

To measure the agreement between different rainfall measurements, we calculate statistical standard metrics: the additive and multiplicative bias, the correlation coefficient, and the root-mean-square error (RMSE), to describe the ability of the radar to observe the correct rainfall amount. Following (Germann et al., 2006), we calculate additional statistical metrics, to describe the ability of the radar to distinguish between rainfall and no rainfall: the critical success index

$$\text{CSI} = \frac{H}{H + F + M}, \quad (\text{B.2})$$

the false alarm ratio

$$\text{FAR} = \frac{F}{H + F}, \quad (\text{B.3})$$

and the probability of detection

$$\text{POD} = \frac{H}{H + M}. \quad (\text{B.4})$$

H is the number of hits, when the tested radar and the reference both indicate rainfall. M is the number of misses, when only the reference indicates rainfall. F is the number of false alarms, when only the tested radar indicates rainfall. The metrics were calculated with a rainfall threshold of 0.1 mm h^{-1} for rainfall rates and 0.1 mm for rainfall accumulations. The metrics used in this study have been used in several other measurement performance studies (e.g. Germann et al., 2006; Habibi et al., 2021; Peleg et al., 2013). A perfect agreement between the radar rainfall

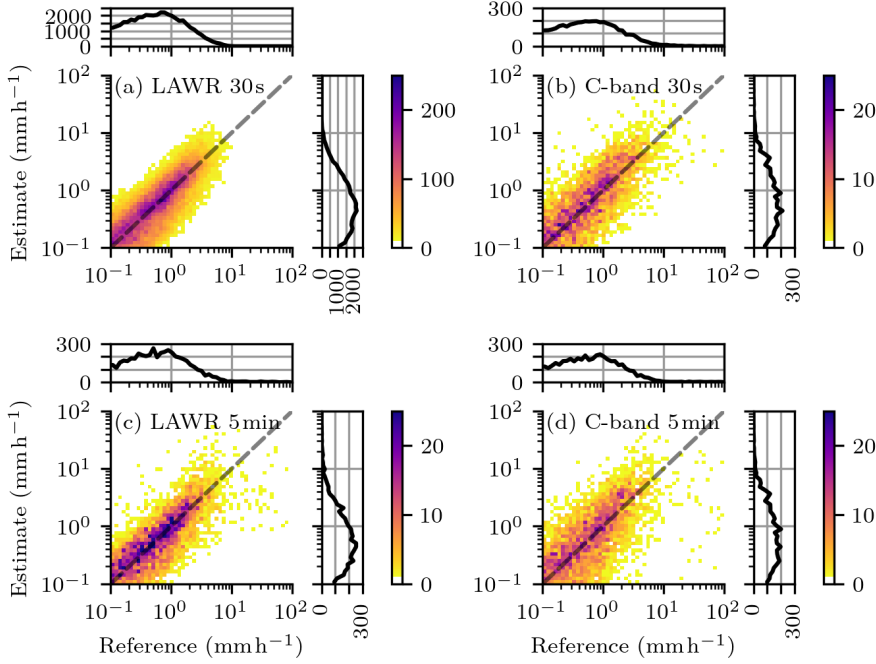


Figure B.6: Joint distribution of radar rainfall rates estimated from LAWR and C-band radar observations versus two MRRs as reference. The measurements are compared at overlapping heights for the period May to September 2019. The MRR rainfall rates were averaged to (a, b) 30 s and (c, d) 5 min. The LAWR rainfall rates are shown at (a) 30 s temporal resolution and were averaged to (c) 5 min. The C-band rainfall rates are the (b, d) instantaneous measurements from the 5 min measurement interval.

distributions and the reference would result in an additive bias, RMSE, and FAR of zero and a relative bias, correlation coefficient, CSI, and POD of one. The standard metrics are also calculated for the logarithmic rainfall rate dBR to balance the impact of rainfall rates across intensity scales.

Micro rain radar as a reference

Similar to Section B.3.1, the LAWR and C-band radar rainfall rates are compared to the MRR measurements as reference for the two represented temporal scales: 30 s and 5 min (Fig. B.6 and Table B.2). The LAWR and C-band radar rainfall rates are unbiased in linear and logarithmic space for both temporal scales (Table B.2). At 30 s temporal resolution, the RMSE is equal for the C-band radar (3.46 dB) and the LAWR (3.44 dB). The RMSE of the logarithmic rainfall rates is higher than the RMSE of the radar reflectivities due to the climatological Z-R-relation (Eq. B.1). The C-band radar has the lowest RMSE with 2.94 mm h^{-1} at 30 s resolution. However, at 5 min resolution, the LAWR has a lower RMSE with 3.51 mm h^{-1} than the C-band radar with 4.69 mm h^{-1} . The Pearson correlation coefficient estimated for the logarithmic rainfall rates (0.67 to 0.77, Table B.2) show decreased values compared to the radar reflectivities (0.84 to 0.94, Sect. B.3.1) due to the climatological Z-R-relation (Eq. B.1). In summary, the statistical standard metrics indicate that the LAWR and C-band radar measure the rainfall amount at 30 s temporal resolution equally well. The

Table B.2: Evaluation metrics of rainfall rate distributions comparing the LAWR and C-band radar with the MRRs, respectively. n is the number of observations above 0.1 mm h^{-1} for both rainfall rates. The standard statistical metrics are the bias, the relative bias mbias, the correlation coefficient estimator (r), the root-mean-square error (RMSE). The bias, r , and RMSE are also computed for the logarithmic rainfall rate dBR. Based on hits H , misses M , false alarms F , and correct negatives N , the critical success index (CSI), the false alarm ratio (FAR), and the probability of detection (POD) is calculated.

	30 s		5 min	
	(a) LAWR	(b) C-band	(c) LAWR	(d) C-band
n	45242	4183	4848	4224
bias / mm h^{-1}	0.10	0.19	-0.04	0.00
mbias	1.08	1.15	0.97	1.00
r (R)	0.32	0.41	0.34	0.26
RMSE / mm h^{-1}	3.46	2.94	3.61	4.69
bias / dB	-0.01	0.51	-0.05	0.33
r (dBR)	0.74	0.75	0.77	0.67
RMSE / dB	3.44	3.46	3.15	3.97
H	45294 (5.1 %)	4191 (5.3 %)	4851 (5.5 %)	4231 (5.4 %)
M	3781 (0.4 %)	265 (0.3 %)	494 (0.6 %)	627 (0.8 %)
F	11286 (1.3 %)	1134 (1.4 %)	673 (0.7 %)	1094 (1.4 %)
N	820880 (93.2 %)	73442 (93.0 %)	82110 (93.2 %)	73080 (92.4 %)
CSI	0.75	0.75	0.81	0.71
FAR	0.20	0.21	0.12	0.21
POD	0.92	0.94	0.91	0.87

5 min average of the LAWR rainfall rate outperforms the one C-band radar rainfall rate representing the 5 min temporal scale.

The CSI, POD, and FAR scores, which refer to rainfall intermittency, describe the alternation between rainy and dry periods. For the LAWR and C-band radar at 30 s temporal resolution (Table B.2), these scores are equal, indicating that both radars can represent the occurrence distribution of rainfall for a 30 s average equally well. For 5 min averages of the LAWR rainfall rates, the CSI increases from 0.75 to 0.81 because the FAR decreases from 0.23 to 0.13. Although the CSI and FAR improve for longer temporal averages, which follows Peleg et al. (2013) for the comparison of radar and rain gauge rainfall at different temporal scales, the POD remains equal. For the 5 min measurement period of the C-band radar rainfall rate, the CSI decreases slightly from 0.75 to 0.71, as well as the POD from 0.94 to 0.87. The CSI, FAR and POD impairs for the 5 min C-band radar rainfall rate compared to the 30 s because of the single 50 ms measurement within the measurement period.

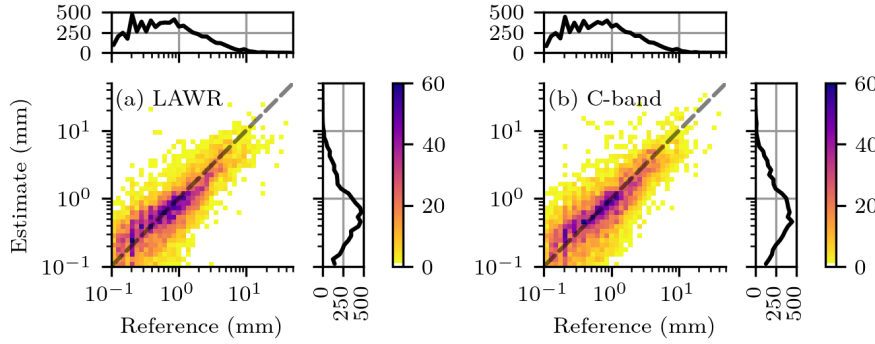


Figure B.7: Hourly rainfall accumulations estimated from (a) LAWR and (b) C-band radar measurements versus observed rainfall from rain gauges as reference.

Rain gauge as a reference

The network of 33 rain gauges (Sect. B.2.4) provides accurate point rainfall information at a 1 min temporal resolution. Wang et al. (2023b) noted that at small scales, measurement uncertainties and spatial-temporal sampling differences between radar and gauge observations prevail. For a more representative analysis, 15 min, 30 min, 1 h and 1 d accumulations of the LAWR and C-band radar rainfall are compared to the rain gauge rainfall (Table B.3 and Fig. B.7). This analysis gives insight in the consistency and limitations of the radar and rain gauge measurements.

Hourly rainfall accumulations estimated from LAWR and C-band radar measurements are equally in agreement with observed rainfall from rain gauges as reference (Fig. B.7). The LAWR measurements underestimate rainfall accumulations from rain gauges (Table B.3). The absolute additive bias (bias) of the LAWR rainfall accumulations increase with duration, from -0.11 mm for a 15 min duration to -0.40 mm for a daily duration. Consequently, the multiplicative bias (mbias) improves for longer accumulation durations up to 0.94. The RMSE increases for longer durations due to increasing values of rainfall accumulations. The LAWR rainfall accumulations are moderately correlated (0.68, 15 min) up to highly correlated (0.85, daily) with the rain gauge measurements. The absolute bias of logarithmic rainfall accumulations decrease from 15 min to hourly durations but increase for daily accumulations. In logarithmic space, the RMSE is almost constant. The CSI and POD of the LAWR rainfall accumulation increase with duration. In the case of the C-band radar, the rainfall accumulations are found to be almost entirely unbiased in comparison to the rain gauges (Table B.3). This may be attributed to a superior calibration of the radar system. The mbias is between 0.94 for 15 min and 30 min durations and 0.98 for a daily duration. The RMSE, correlation coefficient estimate, and CSI of the C-band radar and LAWR are nearly the same for the different durations. Only the FAR and POD of the C-band radar rainfall accumulations (e.g. for daily durations, FAR= 1.22 and POD= 0.95) are higher than the LAWR estimates (FAR= 1.22 and POD= 0.95). Consequently, the improved POD is compensated by the FAR. The statistical metrics indicate that the LAWR and the C-band radar capture the rain gauge point rainfall observations equally well.

Table B.3: Evaluation metrics of rainfall accumulation distributions, comparing the LAWR and C-band radar with rain gauges as reference. The used statistical metrics were introduced in Table B.2.

	LAWR			
	15 min	30 min	1 h	1 d
n	12568	9503	7261	2113
bias / mm	-0.11	-0.13	-0.17	-0.40
mbias	0.83	0.85	0.86	0.91
r	0.65	0.69	0.73	0.83
RMSE / mm	0.80	1.05	1.35	3.16
bias / dB	-0.51	-0.29	-0.08	0.40
RMSE / dB	2.76	2.81	2.92	2.81
H	12568 (1.5 %)	9503 (2.3 %)	7261 (3.5 %)	2113 (24.4 %)
M	4641 (0.6 %)	2762 (0.7 %)	1663 (0.8 %)	274 (3.2 %)
F	17340 (2.1 %)	13426 (3.2 %)	10339 (4.9 %)	2259 (26.1 %)
N	802610 (95.9 %)	392860 (93.9 %)	189984 (90.8 %)	4018 (46.4 %)
CSI	0.36	0.37	0.37	0.45
FAR	0.58	0.59	0.59	0.52
POD	0.73	0.77	0.81	0.89
	C-band			
	15 min	30 min	1 h	1 d
n	12844	9619	7199	1815
bias / mm	-0.06	-0.08	-0.10	-0.21
mbias	0.90	0.91	0.92	0.95
r	0.65	0.70	0.73	0.84
RMSE / mm	0.85	1.07	1.35	3.17
bias / dB	-0.29	-0.16	0.01	0.43
RMSE / dB	2.79	2.90	3.03	2.82
H	12844 (1.6 %)	9619 (2.4 %)	7199 (3.6 %)	1815 (25.9 %)
M	3547 (0.4 %)	1992 (0.5 %)	1145 (0.6 %)	89 (1.3 %)
F	18764 (2.4 %)	14593 (3.7 %)	11196 (5.8 %)	2207 (31.4 %)
N	753965 (95.5 %)	367696 (93.3 %)	176780 (90.0 %)	2909 (41.4 %)
CSI	0.37	0.37	0.37	0.44
FAR	0.59	0.60	0.61	0.55
POD	0.78	0.83	0.86	0.95

B.3.3 Spatial correlations

The spatial rainfall structure is determined for the different rainfall data sets using the spatial correlation (Fig. B.8). The Pearson's product-moment correlation is used

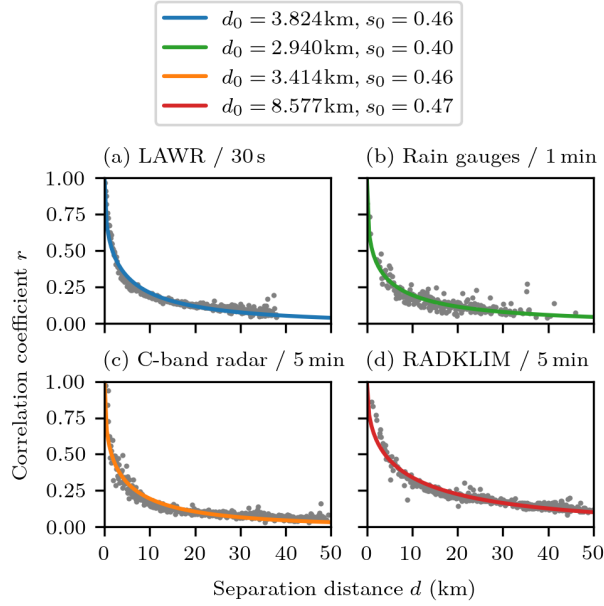


Figure B.8: Examples of the spatial correlation of the rainfall data sets for the months May to September 2019: (a) LAW R at 30 s, (b) rain gauge network at 1 min, (c) C-band radar at 5 min, and (d) RADKLIM at 5 min time scale.

to estimate the spatial correlation, as commonly done in many studies (e.g. Ciach and Krajewski, 2006; De Vos et al., 2017; Krajewski et al., 2003; Leth et al., 2021; Peleg et al., 2013; Tokay et al., 2014; Villarini et al., 2008). The correlograms were calculated based on pairs of rain gauges and pairs of a randomly drawn sample of 100 grid points using a bin size of 100 m and different timescales, ranging from 1 min to daily rainfall accumulations. The correlation decays as the separation distance between two locations increases due to spatio-temporal rainfall variability (Fig. B.8). The spatial correlation can be parameterised with an isotropic, three-parameter exponential function:

$$r(d) = r_0 \exp \left[- \left(\frac{d}{d_0} \right)^{s_0} \right] \quad (\text{B.5})$$

where d is the separation distance between two locations, r_0 is the nugget parameter, d_0 is the correlation distance and e-folding distance, and s_0 is the shape parameter (e.g. Ciach and Krajewski, 2006; Foelsche et al., 2019; Habib et al., 2001; Krajewski et al., 2003; Peleg et al., 2013; Villarini et al., 2008).

The nugget parameter represents the zero-distance correlation and thus describes the uncertainty of measurements at the same location. In this study, the analysis of the rainfall data sets yield a nugget parameter of one. Therefore, we focus on the two remaining parameters and use only a two-parameter exponential function without the nugget parameter, as done by other studies (Leth et al., 2021; Mascaro, 2017; Thomassen et al., 2022).

The correlation distance d_0 , describing the decay of the spatial correlation, and the shape parameter s_0 , characterising the shape of the exponential function, differ for the different rainfall data sets at their observational time scales. The rain gauge measurements (Fig. B.8b) observe the highest spatial rainfall variability with $d_0 = 2.940 \text{ m}$ and the radar-rainfall climatology RADKLIM (Fig. B.8d) shows

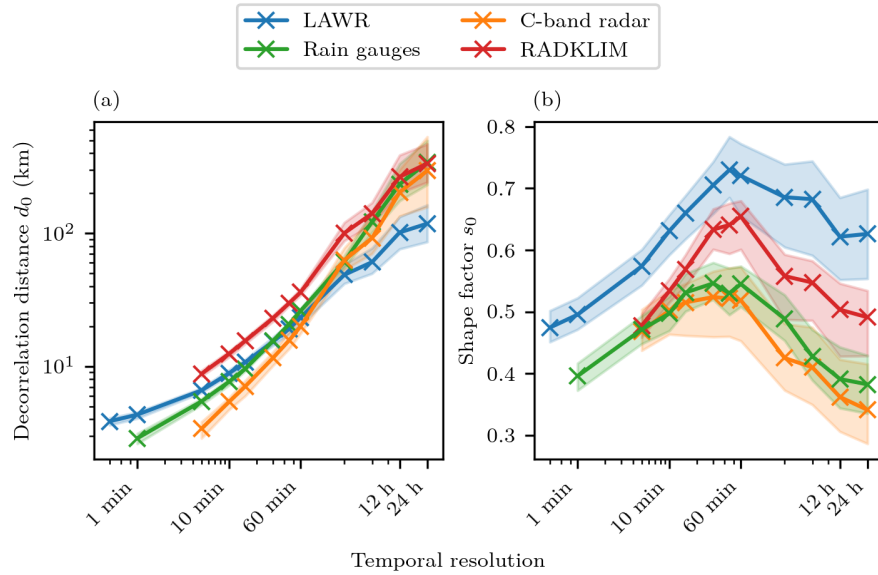


Figure B.9: Correlation distance (a) and shape factor (b) for different timescales (30 s, 1 min, 5 min, 15 min, 30 min, 45 min, 1 h, 3 h, 6 h, 12 h, and 24 h; crosses) for the months May to September 2019. The colors indicate the rainfall data sets: X-band radar (blue), rain gauges (green), C-band radar (orange), RADKLIM (red). The solid lines mark the median and the shaded area is the 5- to 95-percentile range of a bootstrap sample.

the lowest spatial variability with $d_0 = 8.577$ m. The estimated C-band radar (Fig. B.8c) and LAWR (Fig. B.8a) spatial rainfall variability is in between those with $d_0 = 3.414$ m and $d_0 = 3.824$ m. The shape parameters are between 0.40 and 0.46.

The correlation distance increases with timescale, from a few kilometers for rainfall accumulation of a few minutes to several hundred kilometers for daily rainfall accumulations (Fig. B.9a). The rainfall data sets capture a different rainfall variability, where the LAWR correlation distance is between 3.84 km and 117.37 km, the rain gauge correlation distance is between 2.89 km and 325.48 km, the C-band radar correlation distance is between 3.44 km and 267.97 km, and the RADKLIM correlation distance is between 8.79 km and 301.43 km. The uncertainty of the correlation distance is analysed by calculating the correlograms for different samples of the same rainfall data sets. For the rain gauge network, we apply bootstrapping using the same sample size. For the gridded rainfall data sets, we create 100 randomly drawn samples of 100 grid points. The 5- to 95-percentile range of correlation distances, as measure of uncertainty, increases with timescale (Fig. B.9a). The 5- to 95-percentile range, in relation to the median, tends to be narrow and constant for timescales up to an hour, in contrast to longer timescales (not shown). The correlation length, which exceeds the maximal separation distance within the measurement domain for all data sets for these timescales, can explain the increasing uncertainty for timescales longer than an hour.

The shape parameter is between 0.34 and 0.73 (Fig. B.9a). It increases with timescale up to an hour and decreases for longer durations. The rainfall data sets spatial correlation shows a faster exponential decay at shorter separation distances and a slower exponential decay at longer separation distances because the shape parameter is smaller than one (e.g. Tokay et al., 2014). The 5- to 95-percentile range

of shape parameters, as measure of uncertainty, increases with timescale (Fig. B.9b). For timescales up to an hour, the 5- to 95-percentile range in relation to the median, tends to be narrow and constant. This is in contrast to longer timescales (not shown), except for the C-band radar measurements, where the shape parameter's uncertainty increases continuously.

The spatial rainfall structure of the LAWR and rain gauge measurements match best for sub-hourly timescales, since differences of the correlation distances are between 278 m and 1.58 km (Fig. B.9a). However, at 1 min timescale, the rainfall variability is characterised by correlation distances of the LAWR of 4.35 km and the rain gauge network of 2.88 km. The relatively high deviation of the correlation distances at 1 min timescale compared to other sub-hourly timescales can be explained by the different measurement principles. At an hourly timescale the LAWR correlation distance is with 23.15 km slightly lower than the rain gauge correlation distance with 26.01 km, which is within the uncertainty range. For longer timescales, the LAWR correlation distance increasingly underestimates the correlation distance compared to the other rainfall data sets. Increasing differences with increasing correlation distances can be explained with the LAWR scan radius of 20 km. The scan radius limits the maximal separation distance to 40 km, hence for correlation distances larger than the maximal separation distance, rainfall variability is not fully captured within the measurement domain. The other rainfall data sets contain measurement points with slightly larger separation distances, up to 55 km. Contrary to the LAWR, the C-band radar underestimates correlation distances for timescales up to an hour. The 5 min C-band radar measurements have a correlation distance of 3.44 km, which is lower than the 5 min rain gauge correlation distance of 5.48 km. This underestimation contradicts the assumption that a decreased spatio-temporal resolution comes along with a decrease in correlation distances, but is a reason of the C-band radar scan strategy. The C-band radar scans 50 ms per azimuth and needs 30 s for the measurement scan, therefore the C-band radar measures at an expected timescale of 5 min, a mixture of spatial variabilities below a timescale of 30 s. For the 3 h timescale, the correlation distances of the C-band radar and rain gauges match best. Note that the C-band radar correlation distances have the highest uncertainty (Fig. B.9). The RADKLIM rainfall underestimates the spatial rainfall variability compared to the other observations up to the 3 h timescale. This underestimation comes along with the lowest spatial resolution compared to the other rainfall data sets. Kreklow et al. (2020) and Pöschmann et al. (2021) outline the underestimation of high intensity rainfall due to spatial averaging. Peleg et al. (2018) shows that extreme rainfall intensities within a radar pixel are on average at least 10 % larger than values estimated from weather radars. However, for longer timescales, the correlation distances of RADKLIM and the rain gauges match best. This can be explained by the rain gauge adjustment of RADKLIM (Winterrath et al., 2017). Although, the rain gauge network for RADKLIM adjustment is less dense than the one used in this study within the study's measurement domain.

Finally, it should be noted, that estimating Pearson's product-moment correlation from skewed and long-tailed distributions can result in biased and uncertain correlation estimates (Habib et al., 2001). Habib et al. (2001) proposed a scheme to reduce the uncertainty of correlation estimates by applying a logarithmic transformation to the non-zero rainfall values, which is applicable for mixed lognormal rainfall distributions. We decided not to apply the scheme by Habib et al. (2001), or the

logarithmic transforms by Jaffrain and Berne (2012) and by Foelsche et al. (2019) for various reasons. Firstly, Leth et al. (2021) follows the reasoning of Ciach and Krajewski (2006) for rainfall in central Oklahoma and Villarini et al. (2008) for rainfall in southwest England, expecting the probability density function of rainfall rates to have a lighter tail than the mixed lognormal distribution. Therefore, they do not apply the logarithmic transformation for rainfall in the Netherlands, which has similar rainfall conditions like Hamburg. Secondly, our results on spatial rainfall variability can be directly compared to previous studies (e.g. Ciach and Krajewski, 2006; De Vos et al., 2017; Krajewski et al., 2003; Leth et al., 2021; Peleg et al., 2013; Tokay et al., 2014; Villarini et al., 2008). Thirdly, we expect that the estimation of correlations is (un-)biased equally for the different rainfall data sets, since the measurements sample from the same intrinsic rainfall distribution. Fourthly, the rainfall distributions measured at short timescales show truncated distributions at lower tails due to the sensitivity of the different measurement devices. A logarithmic transformation would give the affected lower tail of the rainfall distribution more weighting and therefore hamper the comparison of the correlation distances of the different rainfall data sets. Fifthly, since we focus on the months May to September 2019, our focus lies in convective rainfall and hence in the spatial variability of higher rainfall rates.

In conclusion, the spatial variability based on the spatial correlation has been investigated for four different observational rainfall data sets within the same measurement domain at sub-hourly to daily timescales. Spatial rainfall variability, i.a. correlation distance, has been estimated from an isotropic, two-parameter exponential function. The uncertainty has been estimated using bootstrapping. The spatial rainfall structure captured by LAWR and rain gauge measurements is found to be similar for sub-hourly timescales. For longer timescales, the 20 km scan radius of the LAWR is limiting the performance of the radar in capturing the spatial rainfall structure. The C-band radar is overestimating spatial rainfall variability at sub-hourly timescales, due to its intermittent scan strategy every five minutes. The radar-rainfall climatology RADKLIM is found to underestimate spatial rainfall variability due to its coarser spatial resolution. The most accurate measurements of rainfall patterns at sub-hourly timescales are those made by a dense network of rain gauges or a radar with high spatio-temporal resolution and a continuous scan strategy.

B.3.4 *Peak attenuation*

The link between spatio-temporal rainfall variability and flood response is complex (Zhou et al., 2021). One driver for the hydrological response are rainfall peaks (e.g. Bruni et al., 2015; Cao et al., 2023). Wang et al. (2023a) conclude that the accuracy of rainfall estimates significantly impact modelled peak flows in cases of heavy rainfall. Bárdossy and Anwar (2023) highlight that interpolation and low rainfall data density can lead to peak flow underestimation in rainfall-runoff modelling. Rain gauge networks sample less likely from the upper tail of the rainfall distribution due to the limited spatial coverage. Whereas, weather radars fill the gap of spatial coverage, nonetheless they represent volume samples and averages. The differences in spatio-temporal resolution and scan strategy affect the spatio-

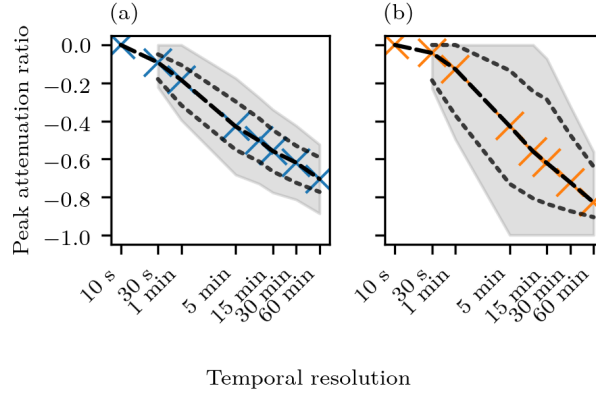


Figure B.10: Peak attenuation ratio (Eq. B.6) associated with the rainfall rate at different temporal resolutions based on MRR measurements available at 10 s temporal resolution. Variables were averaged (a) or the first sample of the interval was used (b). The crosses show the median, the dotted lines show the inner quartile range, and the grey area is the range of the whiskers.

temporal variability of the observed rainfall distributions. Therefore, the effect of spatio-temporal coarsening on rainfall peaks is investigated. Following Cristiano et al. (2018, 2019), we calculate the peak attenuation ratio $P(R)$ for rainfall,

$$P(R) = -\frac{R_{\max,\text{ref}} - R_{\max,\Delta s\Delta t}}{R_{\max,\text{ref}}}, \quad (\text{B.6})$$

where $R_{\max,\text{ref}}$ is the peak rainfall rate at the highest spatio-temporal resolution and $R_{\max,\Delta s\Delta t}$ is the peak rainfall rate at radial resolution Δs and temporal resolution Δt . The peak attenuation ratio quantifies the rainfall peak underestimation as a consequence of spatio-temporal coarsening.

Firstly, the importance of the temporal resolution and scan strategy on the measured rainfall peaks is investigated. The effects of temporal coarsening on the peak attenuation ratio can be analysed with MRR measurements available at 10 s temporal resolution (Fig. B.10). This study distinguishes between temporal coarsening methods, considering averages or instantaneous samples. For instance, a radar system like the LAWR, which provides continuous measurements, represents temporal coarsening as averages (Fig. B.10a), whereas a radar system with an intermittent scan strategy, such as the C-band radar, represents temporal coarsening as an instantaneous sample (Fig. B.10b). Therefore, averages of the radar reflectivity factors or first samples of radar reflectivity within the timescales are used. The corresponding rainfall rates are derived using a standard Z-R relationship ($Z = 200 R^{1.6}$). The peak attenuation ratio (Eq. B.6) is calculated for the coarsened rainfall rates at timescales between 30 s and 60 min with the 10 s rainfall rates as the reference, when the 10 s reference rainfall rate is above 0.1 mm h^{-1} (Fig. B.10). The results demonstrate that temporal coarsening has a strong impact on rainfall peaks. Rainfall peaks are reduced by 9 % in median for 30 s averages and up to 70 % in median for hourly averages in comparison to the 10 s rainfall rates (Fig. B.10a). When only the first 10 s measurement is used to represent the measuring period, rainfall peaks are reduced by 4 % in median for the 30 s timescale and up to 83 % in median for the hourly timescale compared to the 10 s rainfall rates (Fig. B.10b). For

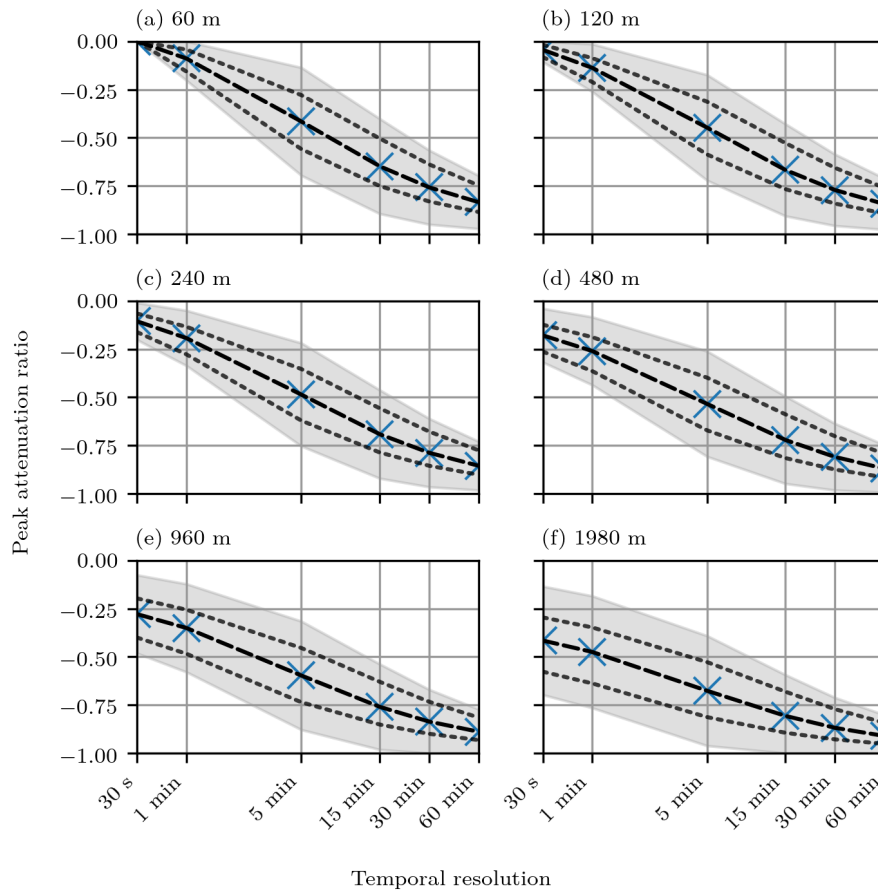


Figure B.11: Peak attenuation ratio (Eq. B.6) associated with the rainfall rate at different temporal resolutions based on LAWR measurements available at 60 m range and 30 s temporal resolution. Rainfall rates were coarsened for spatial scales (a) 60 m, (b) 120 m, (c) 240 m, (d) 480 m, (e) 960 m, (f) 1980 m and for temporal scales from 30 s to 60 min.

the 5 min timescale, both scan strategies underestimate the rainfall peaks, with a peak attenuation ratio of -0.43 . However, the temporal sampling exhibits greater variability compared to the temporal average, as shown by the quantiles of the peak attenuation ratio in Figure B.10. For timescales greater than 5 min, the temporal averaging outperforms temporal sampling in terms of capturing the rainfall peak in the median. For every timescale, the use of temporal sampling for coarsening can result in the total loss of the rainfall peak by missing it, whereas the temporal averaging preserves some amount of the rainfall peak.

Secondly, we investigate the importance of spatio-temporal resolution combined on measured rainfall peaks. Therefore, the impact of spatio-temporal coarsening on the peak attenuation ratio can be evaluated with the LAWR measurements available at 60 m range and 30 s temporal resolution (Fig. B.11). For the spatio-temporal coarsening, the radar reflectivity factors Z are averaged and converted to rainfall rates R using a standard Z - R relationship ($Z = 200 R^{1.6}$) to avoid additional effects due to the non-linear Z - R relationship. In order to avoid additional effects due to interpolation schemes, the radar reflectivity factors are averaged on the native polar radar grid. The computations are limited to the ranges around 4 km due

to computational efficiency. The peak attenuation ratio (Eq. B.6) is calculated for the coarsened rainfall rates at spatial scales between 60 m (Fig. B.11a) and 1980 m (Fig. B.11f) and timescales between 30 s and 60 min with the rainfall rates at 60 m and 30 s as reference, when the reference rainfall rate is above 0.1 mm h^{-1} . The results indicate that spatio-temporal coarsening has a strong impact on rainfall peaks (Fig. B.11). Rainfall peaks are reduced up to 91 % in median at 1980 m and 60 min spatio-temporal resolution compared to the reference resolution of 60 m and 30 s. For a temporal resolution of 30 s, spatial averaging reduces the peak attenuation ratio from -0.04 at a spatial resolution of 120 m (Fig. B.11b) down to -0.41 at a spatial resolution of 1980 m (Fig. B.11b). For a spatial resolution of 60 m, temporal averaging results in a reduction of the peak attenuation ratio from -0.09 at a temporal resolution of 1 min down to -0.83 at a temporal resolution of 60 min (Fig. B.11a). Consequently, temporal averaging exerts a greater impact on rainfall peaks than spatial averaging, which is consistent with previous studies (Cristiano et al., 2018, 2019).

The results highlight the importance of spatio-temporal resolution and scan strategy in accurately measuring rainfall peaks. The LAWR is able to capture rainfall peaks better than the C-band radar due to the used scan strategy (Fig. B.10) and spatio-temporal resolution (Fig. B.11). Note that the simple arithmetic averaging or sampling of the radar rainfall only approximates the lower spatio-temporal resolutions due to post-processing steps applied to the radar reflectivity factor.

B.3.5 Gradients

Since differences in spatio-temporal resolution and scan strategy affect peaks (Sect. B.3.4) and spatial structure (Sect. B.3.3) of the measured rainfall distribution, this study investigates observations of sub-kilometre spatial radar rainfall variability more closely. To work out the continuity and new structures of radar rainfall variability at the microscale, gradients of radar reflectivity are calculated. Differences of radar reflectivity gradients of the LAWR derived at higher (60 m) radial resolution compared to the C-band radar at 250 m radial resolution are discussed. Furthermore, the effect of spatial averaging on radar reflectivity gradients is analysed.

The radar reflectivity gradients are derived from radial difference of the radar reflectivity on the native polar radar grid at highest spatio-temporal resolution, which is for the LAWR 60 m and 30 s and for the C-band radar 250 m and 50 ms. Because we focus on the radial direction, the C-band radar gradients are truly representative at this high temporal resolution. The differences of scan strategies and spatio-temporal resolutions are considered and discussed alongside the results. The computation on the native polar grid in radial direction results in a fast computation, uses regular distances over the range, and avoids additional effects due to grid interpolation schemes. The gradients are calculated for radar reflectivities exceeding a threshold of 10 dBZ, which is equivalent to a low intensity rainfall rate. The gradients are computed for a second threshold of 40 dBZ, to prove the results at radar reflectivities equivalent to high intensity rainfall rates. Gradients for LAWR radar reflectivities were only computed for values with a stable attenuation correction and directly measured, thus not influenced by interpolation schemes

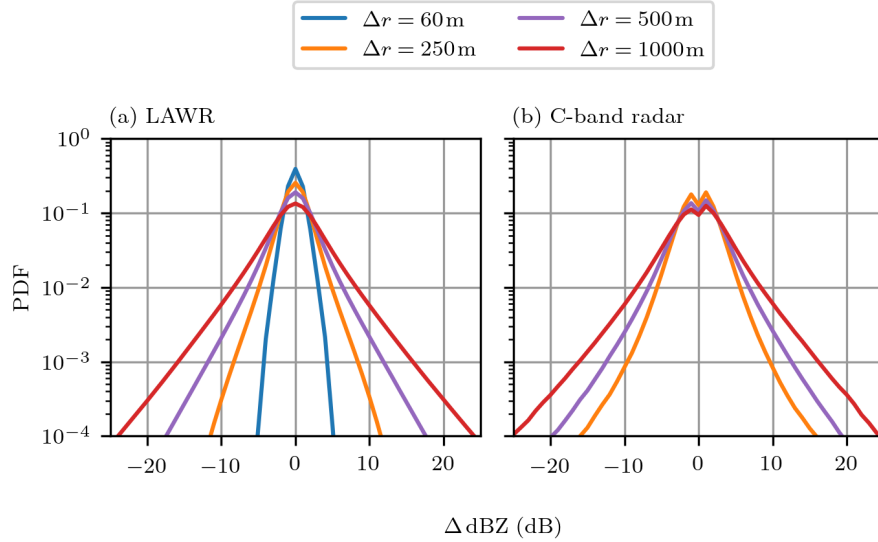


Figure B.12: PDF of (a) LAWR and (b) C-band radar reflectivity differences in radial direction using lag differences Δr of 60 m, 250 m, 500 m, and 1000 m. The gradients were calculated for radar reflectivities greater than a threshold of 10 dBZ. Statistics of the distributions are shown in Table B.4.

Table B.4: Distribution moments of (a) LAWR and (b) C-band radar reflectivity differences in radial direction using lag differences Δr of 60 m, 250 m, 500 m, and 1000 m.

Δr	LAWR				C-band		
	60 m	240 m	480 m	1020 m	250 m	500 m	1000 m
mean (dB)	-0.00	-0.01	-0.02	-0.05	-0.01	-0.01	-0.01
variance (dB ²)	1.16	3.94	8.81	18.84	5.94	10.43	19.08
skewness	0.00	0.02	0.03	0.02	-0.02	-0.02	-0.04
kurtosis	4.17	5.88	7.16	6.90	13.31	8.07	7.45

or an unstable clutter correction. The radial differences of radar reflectivities were calculated for radial lag distance up to 1 km and shown for selected lag distances (Fig. B.12 and Table B.4). Gradients are calculated from the radial radar reflectivity differences (Fig. B.13). The terms of the difference distribution and gradient distribution are used synonymously in this section, as most statements apply to both distributions.

The statistical moments, i.e. mean, variance, skewness, and kurtosis, of the radar reflectivity gradient distributions describe the gradients on average (Table B.4): the gradient distributions are unbiased for both radars and all lag distances, represented by the mean of the distributions. The variance of the gradient distributions increases with lag distance as a result of spatial variability. The variance is used by many studies to describe the spatial radar rainfall variability (e.g. Berne et al., 2004; Emmanuel et al., 2012; Germann and Joss, 2001; Ochoa-Rodriguez et al., 2015). Higher statistical moments, like the skewness and kurtosis, of the radar reflectivity gradients are not commonly discussed in other studies, but may give insights in errors and extremes. The distributions are not skewed. Since the gradient

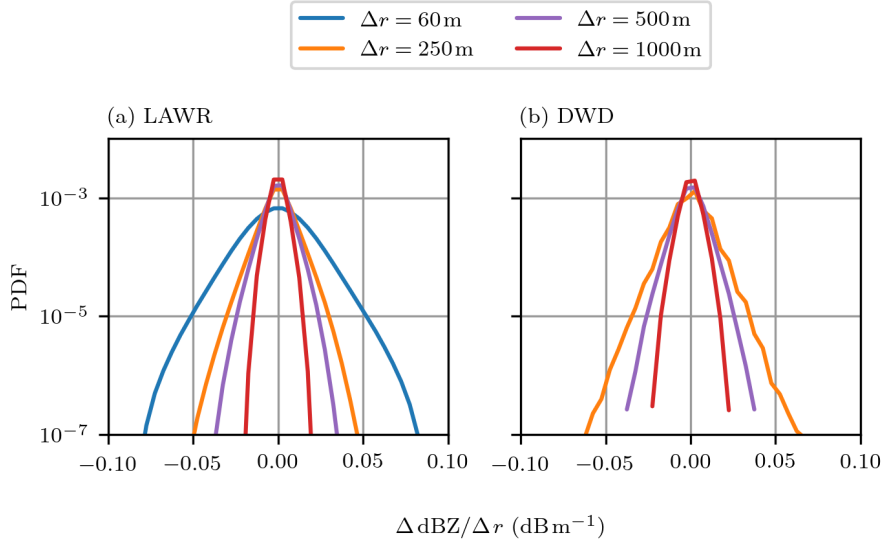


Figure B.13: PDF of (a) LAWR and (b) C-band radar reflectivity gradients in radial direction using lag differences Δr of 60 m, 250 m, 500 m, and 1000 m. The gradients were calculated for radar reflectivities greater than a threshold of 40 dBZ.

distributions are unbiased and unskewed, the radar reflectivities were on average successfully corrected for attenuation. The gradients are not normally distributed, as shown with a kurtosis unequal three. The gradient distributions have more outliers, i.a. stronger deviations from the mean, compared to a normal distribution, because the kurtosis is greater than three.

There are notable differences between the LAWR and C-band radar reflectivity gradients. The LAWR gradients are continuously distributed with a peak at 0 dB (Figures B.12a and B.13a). The C-band radar reflectivity difference distribution exhibits a decreased count for the centre bin between -0.5 dB and 0.5 dB (Fig. B.12b), for which we have no logical explanation and this issue has to be investigated in further studies. The decreased peak is not visible for gradients (Fig. B.13b) independently of the radar reflectivity threshold due to the bin size (not shown). Nevertheless, the diminished peak is not affecting the kurtosis, since the kurtosis is mainly influenced by the distribution tails (Westfall, 2014). The kurtosis is observed to be similar for lag distances greater than or equal to 500 m for both LAWR and C-band radar reflectivities. For shorter lag distances, there are significant differences in the kurtosis of the LAWR and C-band radar reflectivity differences. The LAWR gradient distribution is at closest to a normal distribution for lag distances of 60 m and 240 m, whereas the kurtosis of the C-band radar reflectivity difference distribution for a lag distance of 250 m is at maximum (Table B.4). The kurtosis of the C-band radar reflectivity difference distribution for a lag distance of 250 m is strongly affected by outliers in the vicinity of ± 30 dB, which might be clutter signals (Sect. B.3.1). Without these outliers, the kurtosis is 9.1, which is still higher than the LAWR kurtosis. Radar reflectivity differences derived from radar reflectivities above the 40 dBZ threshold have the same kurtosis for both radars (Fig. B.13), which is around 3.9 and 4.9 (not shown). The lower kurtosis is due to the smaller possible differences caused by the clipping of the lower radar reflectivity threshold. The kurtosis indicate that the C-band radar measures more radar reflectivity gradients

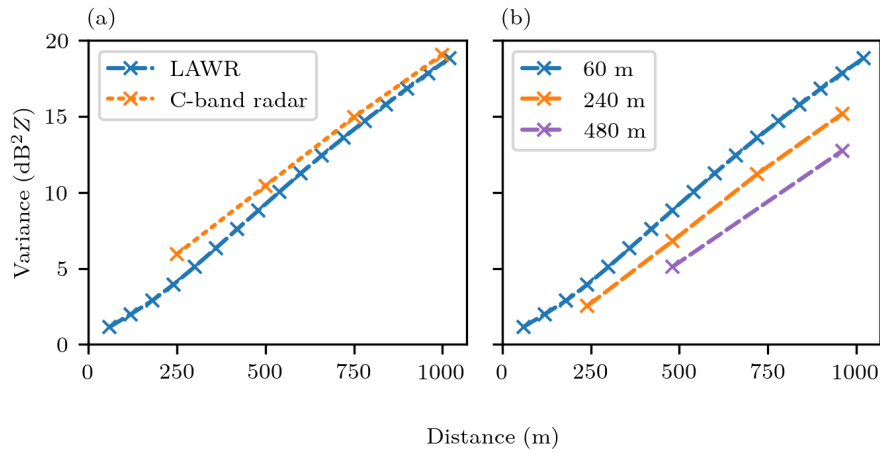


Figure B.14: Radial variogram of radar reflectivities above 10 dBZ for the months May to September 2019. (a) LAWR radar reflectivities of 60 m radial resolution (blue) are compared with C-band radar reflectivities of 250 m radial resolution (orange). (b) LAWR radar reflectivities of 60 m radial resolution (blue) are compared with spatial averages of 240 m (orange) and 480 m (purple) radial resolution.

at the distribution tails than the LAWR, despite the coarser spatial resolution. The higher radar reflectivity gradients of the C-band radar may be a result of outliers. However, this kurtosis effect cannot be seen at high rainfall intensities.

The higher spatial variability of the C-band radar measurements compared to the LAWR measurements was already discussed in Section B.3.3 and is also represented by the variance of the radar reflectivity difference distributions at different lag distances (Fig. B.14 and Table B.4). At a 250 m lag distance, the LAWR variance is reduced by 34 % in comparison to the C-band radar variance (Fig. B.14a). The variance reduction is less than 7 % for a 1 km lag distance. At zero lag distance, the variance is defined as nugget variance and expected to be zero (Cressie, 1993). However, the variogram of the radar reflectivities indicates a higher nugget variance than zero (Fig. B.14a). The non-zero nugget variance is a discontinuity caused by microscale variability and measurement errors (Germann and Joss, 2001), which well explains that the C-band radar measurements with a 250 m radial resolution seem to have a higher discontinuity than the LAWR observations with a 60 m resolution. As expected, the LAWR is capable to measure microscale rainfall variability better than the C-band radar due to its higher spatial resolution. The general results remain unchanged for radar reflectivities at higher intensities, tested with a radar reflectivity threshold of 40 dBZ (not shown).

Furthermore, the LAWR is capable of measuring steeper radar reflectivity gradients than the C-band radar (Fig. B.15). The variance of radar reflectivity gradients decreases with increasing lag distances. Consequently, the radar reflectivity gradients differ from a white noise field, because the variance is not constant. At a 250 m lag distance, the LAWR and C-band radar are directly comparable. The C-band radar measures steeper gradients than the LAWR, due to differences in scan strategy and hence temporal resolutions, despite the C-band radar having a coarser spatial resolution than the LAWR. However, the LAWR radar reflectivity gradients exhibit higher variance at 60 m and 120 m lag distances than the C-band radar reflectivity

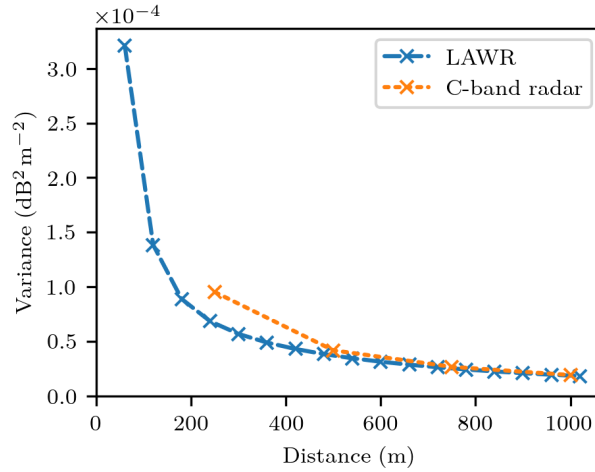


Figure B.15: Variance of radar reflectivity gradients for LAWR and C-band radar reflectivities above 10 dBZ for the months May to September 2019.

gradients at 250 m lag distance. The variance of C-band radar reflectivity gradients with the native 250 m radial resolution is reduced by 30 % compared to LAWR with native 60 m radial resolution.

A lower spatial resolution results in a reduction of the measured spatial variability, as expressed by a lower variance of gradients (Fig. B.14a). The LAWR radar reflectivity factor was averaged on the native polar grid for 240 m and 480 m radial resolutions to simulate conventional radar resolutions. The radar reflectivity gradients remain unbiased, unskewed, and the kurtosis is unchanged (not shown). The variance of radar reflectivity gradients for a lag distance of 240 m is reduced by 35 % at a radial resolution of 240 m compared to the native radial resolution of 60 m. A comparable reduction in variance was observed in the comparison of the C-band radar at a radial resolution of 250 m to the LAWR at a radial resolution of 60 m, as discussed with Figure B.15. The variance reduction is less than 15 % at lag distances of 980 m. For a radial resolution of 480 m the variance of radar reflectivity gradients is reduced by 42 % at a lag distance of 480 m compared to the radial resolution of 60 m. At a 1 km lag distance, the variance reduction is about 29 %. The spatial averages of LAWR radar reflectivities demonstrate the importance of spatial resolution to capture the spatial variability of rainfall.

In conclusion, the statistical moments of radar reflectivity gradients have been discussed. The bias and skewness can show effects of attenuation. The kurtosis is sensitive to the tails of the gradient distribution and is mostly affected by measurement errors. The variance of the radar reflectivity gradients highlights that a radar with higher spatio-temporal resolution is capable of measuring steeper gradients and captures microscale rainfall variability more accurately than conventional radars at coarser resolutions.

B.4 CONCLUSIONS

This study presents a throughout discussion of the added value of a refined spatio-temporal resolution for weather radar observations at sub-hourly temporal and

sub-kilometre spatial scales, which are relevant scales for meteorological and hydrological applications in urban environments. The recently available reanalysed radar-rainfall estimates of a single-polarized X-band weather radar measuring at hectometre spatial and 30 s temporal scales (Burgemeister et al., 2024c) facilitate this refined study on rainfall variability. The high-resolution measurements of this local area weather radar (LAWR) were compared with measurements of one operational C-band radar of the nationwide radar network, operating at 250 m radial resolution and scanning every five minutes. The radar reflectivities and rainfall estimates were checked with two micro rain radars operating at a 10 s temporal resolution. As ground-based reference, 33 rain gauges from different institutions were combined and quality-checked to set up a dense rain gauge network operating at 1 min temporal scale. The radar-based precipitation climatology RADKLIM, available at 1 km spatial and 5 min temporal scales, gave insights in rainfall variability of a radar-rainfall reanalysis calibrated with rain gauges and interpolated on a regular grid. This study focused on a five-month period from 1 May to 30 September 2019. The unique availability of different rainfall data sets facilitates analysis answering the research questions on the added value of spatio-temporal resolution for weather radar observations.

- *Is the local rainfall rate of the LAWR superior to other rainfall estimates?*

The local rainfall observations are represented by MRRs and rain gauges. The LAWR and C-band radar differ in spatio-temporal resolution and scan strategy. The LAWR radar reflectivity has a radial resolution of 60 m and represents a true 30 s average of its measurement interval. In contrast, the C-band radar reflectivity has a radial resolution of 250 m and measures 80 ms per azimuth of its represented 5 min measurement interval. The MRR observations show that both the LAWR and C-band radar reflectivities and rainfall rates perform equally well at 30 s temporal resolution. For 5 min time scales, the LAWR measurements outperform observations of the C-band radar due to the continuous scan strategy and temporal resolution. This better performance does not translate in a better match to rainfall accumulations recorded by rain gauges, as differences in the Z-R relation and sample volume sizes between radar and rain gauge dominate the uncertainty for both the LAWR and C-band radar.

A high spatio-temporal resolution and continuous scan strategy results in more accurate measurements of rainfall peaks, which is known to be one driver for the hydrological response (e.g. Bruni et al., 2015; Cao et al., 2023). The LAWR is capable to capture rainfall peaks better than the C-band radar due to the used scan strategy and spatio-temporal resolution. This study confirms findings from Cristiano et al. (2018, 2019) that temporal averaging exerts a greater impact on rainfall peaks than spatial averaging.

- *Is the LAWR better in capturing spatial rainfall variability?*

Despite the differences in spatio-temporal resolution and scan strategy, the LAWR and C-band radar can be compared spatially well, as the measurements are highly correlated, where the measuring heights and sampling volumes are at closest. The most accurate measurements of spatial rainfall variability at sub-hourly timescales are those made by a dense network of rain gauges or

a radar with high spatio-temporal resolution and a continuous scan strategy, like the LAWR. For longer timescales, the 20 km scan radius of the LAWR is limiting the performance of the radar in capturing the spatial rainfall structure, which can be circumvented with a network of radars (Lengfeld et al., 2014). The C-band radar is overestimating spatial rainfall variability at sub-hourly timescales, due to its intermittent scan strategy every five minutes. The C-band radar measurements represent a mixture of spatial variabilities below a timescale of 30 s. The radar-rainfall climatology RADKLIM is found to underestimate spatial rainfall variability at sub-hourly scales caused by its coarser spatial resolution and interpolation.

- *Are there gradients within the LAWR not obtained by other measurement devices?*

The variance of the C-band radar reflectivity gradients at 250 m spatial resolution is reduced by 30 % compared to the LAWR radar reflectivity gradients at 60 m spatial resolution. The higher variance of the LAWR radar reflectivity gradients is no additional noise, since the nugget variance of radar reflectivity differences approximates zero. The variance of the radar reflectivity gradients highlights that a radar, like the LAWR, with higher spatio-temporal resolution is capable of measuring steeper gradients and captures microscale rainfall variability more accurately than conventional radars.

A LAWR operating at hectometre spatial and 30 s temporal resolution fills a gap in rainfall observations capturing variability at short-duration, sub-kilometre scales. The effect of a spatio-temporal refinement of C-band radar measurements, like advection interpolation (e.g. Jasper-Tönnies and Jessen, 2014; Nielsen et al., 2014; Seo and Krajewski, 2015; Wang et al., 2015), on spatio-temporal variability can be addressed in a further study, but goes along with additional computational costs. The LAWR observation do not need such downscaling and will still outperform the C-band radar in capturing spatio-temporal features, like rainfall peaks and steep gradients, since the initial measurements fails to capture these features. RADKLIM is too coarse to contain spatial rainfall variability at sub-hourly scales. The free available reanalysed LAWR measurements can be used in further studies on spatio-temporal rainfall variability, as different rainfall data sets proofed its general performance. Statistics obtained from these measurements can parametrize spatio-temporal rainfall generators (e.g. Andersen et al., 2024; Green et al., 2024a) for urban hydrological applications. The spatial limitation of the LAWR can be tackled in future urban rainfall studies by networked observations with a second LAWR in Hamburg, measuring since the beginning of 2021.

ACKNOWLEDGEMENTS

The project was funded by the Deutsche Forschungsgemeinschaft (DFG, German Research Foundation) under Germany's Excellence Strategy – EXC 2037 'CLICCS - Climate, Climatic Change, and Society' – Project Number: 390683824, contribution to the Center for Earth System Research and Sustainability (CEN) of Universität Hamburg. The authors thank Hamburg Wasser and Andreas Kuchenbecker for providing data of their rain gauge network. The authors thank the German Weather Service (DWD) for providing data of one C-band radar on request and rain gauge

data and the radar-based precipitation climatology RADKLIM freely. The authors thank the German Climate Computing Center (DKRZ) for archiving our data sets.

BIBLIOGRAPHY

- Allegretti, M., S. Bertoldo, A. Prato, C. Lucianaz, O. Rorato, R. Notarpietro, and M. Gabella (2012). "X-Band Mini Radar for Observing and Monitoring Rainfall Events." en. In: *Atmospheric and Climate Sciences* 2.3. Number: 3 Publisher: Scientific Research Publishing, pp. 290–297. DOI: [10.4236/acs.2012.23026](https://doi.org/10.4236/acs.2012.23026).
- Alves de Souza, B., I. da Silva Rocha Paz, A. Ichiba, B. Willinger, A. Gires, J. C. C. Amorim, M. de Miranda Reis, B. Tisserand, I. Tchiguirinskaia, and D. Schertzer (2018). "Multi-hydro hydrological modelling of a complex peri-urban catchment with storage basins comparing C-band and X-band radar rainfall data." In: *Hydrological sciences journal* 63.11, pp. 1619–1635.
- Anagnostou, M. N., E. I. Nikolopoulos, J. Kalogiros, E. N. Anagnostou, F. Marra, E. Mair, G. Bertoldi, U. Tappeiner, and M. Borga (2018). "Advancing precipitation estimation and streamflow simulations in complex terrain with X-band dual-polarization radar observations." In: *Remote Sensing* 10.8, p. 1258.
- Andersen, C. B., D. B. Wright, and S. Thorndahl (2024). "CON-SST-RAIN: Continuous Stochastic Space-Time Rainfall generation based on Markov chains and transposition of weather radar data." In: *Journal of Hydrology*, p. 131385.
- Atlas, D., R. C. Srivastava, and R. S. Sekhon (1973). "Doppler radar characteristics of precipitation at vertical incidence." In: *Reviews of Geophysics* 11.1, pp. 1–35. DOI: <https://doi.org/10.1029/RG011i001p00001>.
- Bárdossy, A. and F. Anwar (2023). "Why do our rainfall–runoff models keep underestimating the peak flows?" In: *Hydrology and Earth System Sciences* 27.10, pp. 1987–2000.
- Berenguer, M., S. Park, D. Sempere-Torres, J. Didszun, M. Pool, and M. Pfeifer (2012). "RAINSCANNER@Barcelona: an experiment to assess the hydrological value of a portable X-band radar." In: *Conference Proceedings of the Seventh European Conference on Radar in Meteorology and Hydrology (ERAD)*.
- Berne, A. and W. Krajewski (2013). "Radar for hydrology: Unfulfilled promise or unrecognized potential?" en. In: *Advances in Water Resources* 51, pp. 357–366. DOI: [10.1016/j.adwatres.2012.05.005](https://doi.org/10.1016/j.adwatres.2012.05.005).
- Berne, A. and R. Uijlenhoet (2006). "Quantitative analysis of X-band weather radar attenuation correction accuracy." en. In: *Natural Hazards and Earth System Sciences* 6.3, pp. 419–425. DOI: [10.5194/nhess-6-419-2006](https://doi.org/10.5194/nhess-6-419-2006).
- Berne, A., G. Delrieu, J.-D. Creutin, and C. Obled (2004). "Temporal and spatial resolution of rainfall measurements required for urban hydrology." In: *Journal of Hydrology* 299.3-4, pp. 166–179.
- Brandes, E. A., G. Zhang, and J. Vivekanandan (2002). "Experiments in rainfall estimation with a polarimetric radar in a subtropical environment." In: *Journal of Applied Meteorology* 41.6, pp. 674–685.
- Brast, M. and P. Markmann (2020). "Detecting the melting layer with a micro rain radar using a neural network approach." In: *Atmospheric Measurement Techniques* 13.12, pp. 6645–6656.
- Brook, J. P., A. Protat, J. S. Soderholm, R. A. Warren, and H. McGowan (2022). "A Variational Interpolation Method for Gridding Weather Radar Data." EN.

- In: *Journal of Atmospheric and Oceanic Technology* 39.11. Publisher: American Meteorological Society Section: Journal of Atmospheric and Oceanic Technology, pp. 1633–1654. DOI: [10.1175/JTECH-D-22-0015.1](https://doi.org/10.1175/JTECH-D-22-0015.1).
- Bruni, G., R. Reinoso, N. C. van de Giesen, F. H. L. R. Clemens, and J. A. E. ten Veldhuis (2015). “On the sensitivity of urban hydrodynamic modelling to rainfall spatial and temporal resolution.” In: *Hydrology and Earth System Sciences* 19.2, pp. 691–709. DOI: [10.5194/hess-19-691-2015](https://doi.org/10.5194/hess-19-691-2015).
- Burgemeister, F., M. Clemens, and F. Ament (2022a). *Multi-year X-band weather radar observations in Hamburg (LAWR HHG) (Version 1)*. World Data Center for Climate (WDCC) at DKRZ [data set]. DOI: [10.26050/WDCC/LAWR_UHH_HHG](https://doi.org/10.26050/WDCC/LAWR_UHH_HHG).
- (2022b). *Rainfall rates estimated from X-Band radar observations during FESSTVaL 2021*. Universität Hamburg [data set]. DOI: [10.25592/uhhfdm.10090](https://doi.org/10.25592/uhhfdm.10090).
- (2024a). “Added value of spatio-temporal resolution for weather radar observations at urban scales.” In: *preparation for the submission to the Journal of Hydrometeorology*.
- (2024b). *Multi-year X-band weather radar observations in Hamburg (LAWR HHG) (Version 2)*. World Data Center for Climate (WDCC) at DKRZ [data set]. DOI: [10.26050/WDCC/LAWR_UHH_HHG_v2](https://doi.org/10.26050/WDCC/LAWR_UHH_HHG_v2).
- (2024c). “Reanalysis of multi-year high-resolution X-band weather radar observations in Hamburg.” In: *Earth System Science Data* 16.5, pp. 2317–2332. DOI: [10.5194/essd-16-2317-2024](https://doi.org/10.5194/essd-16-2317-2024).
- Burgemeister, F., T. Finn, M. Schaper, and Y. Büchau (2023). *pylawr: A Python Package For Processing Local Area Weather Radars*. Zenodo [code]. Version v0.4.0. DOI: [10.5281/zenodo.8182628](https://doi.org/10.5281/zenodo.8182628).
- Cao, X., Y. Qi, and G. Ni (2023). “X-band polarimetric radar QPE for urban hydrology: The increased contribution of high-resolution rainfall capturing.” en. In: *Journal of Hydrology* 617, p. 128905. DOI: [10.1016/j.jhydrol.2022.128905](https://doi.org/10.1016/j.jhydrol.2022.128905).
- Ciach, G. J. and W. F. Krajewski (2006). “Analysis and modeling of spatial correlation structure in small-scale rainfall in Central Oklahoma.” In: *Advances in water resources* 29.10, pp. 1450–1463.
- Costabile, P., C. Costanzo, J. Kalogiros, and V. Bellos (2023). “Toward street-level nowcasting of flash floods impacts based on HPC hydrodynamic modeling at the watershed scale and high-resolution weather radar data.” In: *Water Resources Research* 59.10, e2023WR034599.
- Cressie, N. (1993). *Statistics for spatial data*. John Wiley & Sons. DOI: [10.1002/9781119115151](https://doi.org/10.1002/9781119115151).
- Cristiano, E., M.-C. ten Veldhuis, S. Gaitan, S. Ochoa Rodriguez, and N. van de Giesen (2018). “Critical scales to explain urban hydrological response: an application in Cranbrook, London.” en. In: *Hydrology and Earth System Sciences* 22.4, pp. 2425–2447. DOI: [10.5194/hess-22-2425-2018](https://doi.org/10.5194/hess-22-2425-2018).
- Cristiano, E., M.-c. ten Veldhuis, and N. Van De Giesen (2017). “Spatial and temporal variability of rainfall and their effects on hydrological response in urban areas—a review.” In: *Hydrology and Earth System Sciences* 21.7, pp. 3859–3878.
- Cristiano, E., M.-c. ten Veldhuis, D. B. Wright, J. A. Smith, and N. van de Giesen (2019). “The Influence of Rainfall and Catchment Critical Scales on Urban Hydrological Response Sensitivity.” en. In: *Water Resources Research* 55.4. _eprint: <https://onlinelibrary.wiley.com/doi/pdf/10.1029/2018WR024143>, pp. 3375–3390. DOI: [10.1029/2018WR024143](https://doi.org/10.1029/2018WR024143).

- De Vos, L., H. Leijnse, A. Overeem, and R. Uijlenhoet (2017). "The potential of urban rainfall monitoring with crowdsourced automatic weather stations in Amsterdam." In: *Hydrology and Earth System Sciences* 21.2, pp. 765–777.
- Delrieu, G., L. Hucke, and J. D. Creutin (1999). "Attenuation in rain for X-and C-band weather radar systems: Sensitivity with respect to the drop size distribution." In: *Journal of Applied Meteorology* 38.1, pp. 57–68.
- Delrieu, G., A. K. Khanal, F. Cazenave, and B. Boudevillain (2022). "Sensitivity analysis of attenuation in convective rainfall at X-band frequency using the mountain reference technique." English. In: *Atmospheric Measurement Techniques* 15.11. Publisher: Copernicus GmbH, pp. 3297–3314. DOI: [10.5194/amt-15-3297-2022](https://doi.org/10.5194/amt-15-3297-2022).
- Diederich, M., A. Ryzhkov, C. Simmer, P. Zhang, and S. Trömel (2015). "Use of Specific Attenuation for Rainfall Measurement at X-Band Radar Wavelengths. Part I: Radar Calibration and Partial Beam Blockage Estimation." EN. In: *Journal of Hydrometeorology* 16.2. Publisher: American Meteorological Society Section: Journal of Hydrometeorology, pp. 487–502. DOI: [10.1175/JHM-D-14-0066.1](https://doi.org/10.1175/JHM-D-14-0066.1).
- Doviak, R. J. et al. (1993). *Doppler radar and weather observations*. Courier Corporation.
- Einfalt, T., K. Arnbjerg-Nielsen, C. Golz, N.-E. Jensen, M. Quirmbach, G. Vaes, and B. Vieux (2004). "Towards a roadmap for use of radar rainfall data in urban drainage." In: *Journal of Hydrology* 299.3-4, pp. 186–202.
- Emmanuel, I., H. Andrieu, E. Leblois, and B. Flahaut (2012). "Temporal and spatial variability of rainfall at the urban hydrological scale." In: *Journal of hydrology* 430, pp. 162–172.
- Fabry, F., A. Bellon, M. R. Duncan, and G. L. Austin (1994). "High resolution rainfall measurements by radar for very small basins: the sampling problem reexamined." In: *Journal of Hydrology* 161.1-4, pp. 415–428.
- Ferner, K. S., M. Boettcher, and K. H. Schlünzen (2022). "Modelling the heterogeneity of rain in an urban neighbourhood with an obstacle-resolving model." In: *Meteorologische Zeitschrift*. DOI: [10.1127/metz/2022/1149](https://doi.org/10.1127/metz/2022/1149).
- Foelsche, U. et al. (2019). "Assessment of spatial uncertainty of heavy rainfall at catchment scale using a dense gauge network." In: *Hydrology and Earth System Sciences* 23.7, pp. 2863–2875.
- Frech, M., C. Hald, M. Schaper, B. Lange, and B. Rohrdantz (2023). "Assessing and mitigating the radar-radar interference in the German C-band weather radar network." In: *Atmospheric Measurement Techniques* 16.2, pp. 295–309. DOI: [10.5194/amt-16-295-2023](https://doi.org/10.5194/amt-16-295-2023).
- Frech, M., M. Hagen, and T. Mammen (2017). "Monitoring the absolute calibration of a polarimetric weather radar." In: *Journal of Atmospheric and Oceanic Technology* 34.3, pp. 599–615.
- Germann, U., M. Berenguer, D. Sempere-Torres, and M. Zappa (2009). "REAL—Ensemble radar precipitation estimation for hydrology in a mountainous region." In: *Quarterly Journal of the Royal Meteorological Society: A journal of the atmospheric sciences, applied meteorology and physical oceanography* 135.639, pp. 445–456.
- Germann, U., G. Galli, M. Boscacci, and M. Bolliger (2006). "Radar precipitation measurement in a mountainous region." In: *Quarterly Journal of the Royal Meteorological Society: A journal of the atmospheric sciences, applied meteorology and physical oceanography* 132.618, pp. 1669–1692.

- Germann, U. and J. Joss (2001). "Variograms of radar reflectivity to describe the spatial continuity of Alpine precipitation." In: *Journal of Applied Meteorology and Climatology* 40.6, pp. 1042–1059.
- Gires, A., I. Tchiguirinskaia, D. Schertzer, and S. Lovejoy (2013). "Multifractal analysis of a semi-distributed urban hydrological model." en. In: *Urban Water Journal* 10.3, pp. 195–208. DOI: [10.1080/1573062X.2012.716447](https://doi.org/10.1080/1573062X.2012.716447).
- Gires, A., I. Tchiguirinskaia, D. Schertzer, A. Schellart, A. Berne, and S. Lovejoy (2014). "Influence of small scale rainfall variability on standard comparison tools between radar and rain gauge data." In: *Atmospheric Research* 138, pp. 125–138.
- Green, A. C., C. Kilsby, and A. Bárdossy (2024a). "A framework for space–time modelling of rainfall events for hydrological applications of weather radar." In: *Journal of Hydrology* 630, p. 130630.
- Green, A. C., C. Kilsby, and A. Bárdossy (2024b). "Assessing rainfall radar errors with an inverse stochastic modelling framework." In: *Available at SSRN* 4478761.
- Grimmond, S., V. Bouchet, L. T. Molina, A. Baklanov, J. Tan, K. H. Schlünzen, G. Mills, B. Golding, V. Masson, C. Ren, et al. (2020). "Integrated urban hydrometeorological, climate and environmental services: Concept, methodology and key messages." In: *Urban Climate* 33, p. 100623.
- Habib, E., W. F. Krajewski, and G. J. Ciach (2001). "Estimation of rainfall interstation correlation." In: *Journal of Hydrometeorology* 2.6, pp. 621–629.
- Habibi, H., R. Awal, A. Fares, and M. Temimi (2021). "Performance of multi-radar multi-sensor (mrms) product in monitoring precipitation under extreme events in Harris county, Texas." In: *Journal of Hydrology* 598, p. 126385.
- Heistermann, M., S. Jacobi, and T. Pfaff (2013). "Technical Note: An open source library for processing weather radar data (wradlib)." In: *Hydrology and Earth System Sciences* 17.2, pp. 863–871. DOI: [10.5194/hess-17-863-2013](https://doi.org/10.5194/hess-17-863-2013).
- Hitschfeld, W. and J. Bordan (1954). "Errors inherent in the radar measurement of rainfall at attenuating wavelengths." In: *Journal of Meteorology* 11.1, pp. 58–67.
- Hoffmann, P., C. Merker, K. Lengfeld, and F. Ament (2018). "The Hamburg Tornado (7 June 2016) from the perspective of low-cost high-resolution radar data and weather forecast model." In: *Atmospheric Research* 211, pp. 1–11.
- Hohenegger, C. et al. (2023). "FESSTVaL: The Field Experiment on Submesoscale Spatio-Temporal Variability in Lindenberg." In: *Bulletin of the American Meteorological Society* 104.10, E1875–E1892. DOI: [10.1175/BAMS-D-21-0330.1](https://doi.org/10.1175/BAMS-D-21-0330.1).
- Holleman, I. (2006). *Bias adjustment of radar-based 3-hour precipitation accumulations*. Tech. rep. KNMI.
- Hosseini, S. H., H. Hashemi, R. Berndtsson, N. South, H. Aspegren, R. Larsson, J. Olsson, A. Persson, and L. Olsson (2020). "Evaluation of a new X-band weather radar for operational use in south Sweden." In: *Water Science and Technology* 81.8, pp. 1623–1635.
- Hosseini, S. H., H. Hashemi, R. Larsson, and R. Berndtsson (2023). "Merging dual-polarization X-band radar network intelligence for improved microscale observation of summer rainfall in south Sweden." en. In: *Journal of Hydrology* 617, p. 129090. DOI: [10.1016/j.jhydrol.2023.129090](https://doi.org/10.1016/j.jhydrol.2023.129090).
- Hubbert, J. C., M. Dixon, and S. M. Ellis (2009). "Weather Radar Ground Clutter. Part II: Real-Time Identification and Filtering." EN. In: *Journal of Atmospheric and Oceanic Technology* 26.7. Publisher: American Meteorological Society Section:

- Journal of Atmospheric and Oceanic Technology, pp. 1181–1197. DOI: [10.1175/2009JTECHA1160.1](https://doi.org/10.1175/2009JTECHA1160.1).
- Huuskonen, A. and I. Holleman (2007). “Determining weather radar antenna pointing using signals detected from the sun at low antenna elevations.” In: *Journal of Atmospheric and Oceanic Technology* 24.3, pp. 476–483. DOI: [10.1175/JTECH1978.1](https://doi.org/10.1175/JTECH1978.1).
- Imhoff, R., C. Brauer, K.-J. van Heeringen, H. Leijnse, A. Overeem, A. Weerts, and R. Uijlenhoet (2021). “A climatological benchmark for operational radar rainfall bias reduction.” en. In: *Hydrology and Earth System Sciences* 25.7, pp. 4061–4080. DOI: [10.5194/hess-25-4061-2021](https://doi.org/10.5194/hess-25-4061-2021).
- Jacobi, S. and M. Heistermann (2016). “Benchmarking attenuation correction procedures for six years of single-polarized C-band weather radar observations in South-West Germany.” In: *Geomatics, Natural Hazards and Risk* 7.6, pp. 1785–1799. DOI: [10.1080/19475705.2016.1155080](https://doi.org/10.1080/19475705.2016.1155080).
- Jaffrain, J. and A. Berne (2012). “Quantification of the small-scale spatial structure of the raindrop size distribution from a network of disdrometers.” In: *Journal of Applied Meteorology and Climatology* 51.5, pp. 941–953.
- Jasper-Tönnies, A. and M. Jessen (2014). “Improved radar QPE with temporal interpolation using an advection scheme.” In: *Proc. ERAD, Garmisch*, pp. 1–5.
- Jensen, N. and L. Pedersen (2005). “Spatial variability of rainfall: Variations within a single radar pixel.” In: *Atmospheric Research* 77.1-4, pp. 269–277.
- Jordan, P., A. Seed, and G. Austin (2000). “Sampling errors in radar estimates of rainfall.” en. In: *Journal of Geophysical Research* 105.D2, pp. 2247–2257. DOI: [10.1029/1999JD900130](https://doi.org/10.1029/1999JD900130).
- Kim, Y., M. Maki, D.-I. Lee, J.-H. Jeong, and C.-H. You (2019). “Three-dimensional analysis of the initial stage of convective precipitation using an operational X-band polarimetric radar network.” In: *Atmospheric Research* 225, pp. 45–57. DOI: <https://doi.org/10.1016/j.atmosres.2019.03.015>.
- Kirsch, B., M. Clemens, and F. Ament (2019). “Stratiform and Convective Radar Reflectivity–Rain Rate Relationships and Their Potential to Improve Radar Rainfall Estimates.” EN. In: *Journal of Applied Meteorology and Climatology* 58.10. Publisher: American Meteorological Society Section: Journal of Applied Meteorology and Climatology, pp. 2259–2271. DOI: [10.1175/JAMC-D-19-0077.1](https://doi.org/10.1175/JAMC-D-19-0077.1).
- Kirsch, B., C. Hohenegger, and F. Ament (2024). “Morphology and growth of convective cold pools observed by a dense station network in Germany.” In: *Quarterly Journal of the Royal Meteorological Society* 150.759, pp. 857–876.
- Kirsch, B., C. Hohenegger, D. Klocke, R. Senke, M. Offermann, and F. Ament (2022). “Sub-mesoscale observations of convective cold pools with a dense station network in Hamburg, Germany.” English. In: *Earth System Science Data* 14.8. Publisher: Copernicus GmbH, pp. 3531–3548. DOI: [10.5194/essd-14-3531-2022](https://doi.org/10.5194/essd-14-3531-2022).
- Kneifel, S., M. Maahn, G. Peters, and C. Simmer (2011). “Observation of snowfall with a low-power FM-CW K-band radar (Micro Rain Radar).” In: *Meteorology and Atmospheric Physics* 113, pp. 75–87.
- Krajewski, W. F., G. J. Ciach, and E. Habib (2003). “An analysis of small-scale rainfall variability in different climatic regimes.” In: *Hydrological sciences journal* 48.2, pp. 151–162.
- Krajewski, W. F. and K. P. Georgakakos (1985). “Synthesis of radar rainfall data.” In: *Water Resources Research* 21.5, pp. 764–768.

- Krämer, S. and H. Verworn (2008). "Improved C-band radar data processing for real time control of urban drainage systems." In: *Proceedings of the 11th International Conference on Urban Drainage*. Vol. 31. IWA Publ. London, pp. 1–10.
- Kreklow, J., B. Tetzlaff, B. Burkhard, and G. Kuhnt (2020). "Radar-Based Precipitation Climatology in Germany—Developments, Uncertainties and Potentials." In: *Atmosphere* 11.2. DOI: [10.3390/atmos11020217](https://doi.org/10.3390/atmos11020217).
- Lammert, A., V. Grützun, and E. Stamnas (2018). *The SAMD Product Standard (Standardized Atmospheric Measurement Data)*. DOI: [10.5281/zenodo.1741364](https://doi.org/10.5281/zenodo.1741364).
- Leinonen, J. (2014). "High-level interface to T-matrix scattering calculations: architecture, capabilities and limitations." In: *Optics express* 22.2, pp. 1655–1660. DOI: [10.1364/OE.22.001655](https://doi.org/10.1364/OE.22.001655).
- Lengfeld, K., M. Berenguer, and D. S. Torres (2018). "Intercomparison of attenuation correction algorithms for single-polarized X-band radars." In: *Atmospheric Research* 201, pp. 116–132.
- Lengfeld, K., M. Clemens, C. Merker, H. Münster, and F. Ament (2016). "A simple method for attenuation correction in local X-band radar measurements using C-band radar data." In: *Journal of Atmospheric and Oceanic Technology* 33.11, pp. 2315–2329.
- Lengfeld, K., M. Clemens, H. Münster, and F. Ament (2014). "Performance of high-resolution X-band weather radar networks—the PATTERN example." In: *Atmospheric Measurement Techniques* 7, pp. 4151–4166. DOI: [10.5194/amt-7-4151-2014](https://doi.org/10.5194/amt-7-4151-2014).
- Lengfeld, K., T. Winterrath, T. Junghänel, M. Hafer, and A. Becker (2019). "Characteristic spatial extent of hourly and daily precipitation events in Germany derived from 16 years of radar data." en. In: *Meteorologische Zeitschrift* 28.5, pp. 363–378. DOI: [10.1127/metz/2019/0964](https://doi.org/10.1127/metz/2019/0964).
- Leth, T. C. v., H. Leijnse, A. Overeem, and R. Uijlenhoet (2021). "Rainfall Spatiotemporal Correlation and Intermittency Structure from Micro- γ to Meso- β Scale in the Netherlands." EN. In: *Journal of Hydrometeorology* 22.8. Publisher: American Meteorological Society Section: Journal of Hydrometeorology, pp. 2227–2240. DOI: [10.1175/JHM-D-20-0311.1](https://doi.org/10.1175/JHM-D-20-0311.1).
- Liebe, H. J., G. A. Hufford, and T. Manabe (1991). "A model for the complex permittivity of water at frequencies below 1 THz." In: *International Journal of Infrared and Millimeter Waves* 12.7, pp. 659–675.
- Lim, S., V. Chandrasekar, P. Lee, and A. Jayasumana (2011). "Real-time implementation of a network-based attenuation correction in the CASA IP1 testbed." In: *Journal of atmospheric and oceanic technology* 28.2, pp. 197–209.
- Lo Conti, F., A. Francipane, D. Pumo, and L. V. Noto (2015). "Exploring single polarization X-band weather radar potentials for local meteorological and hydrological applications." en. In: *Journal of Hydrology* 531, pp. 508–522. DOI: [10.1016/j.jhydrol.2015.10.071](https://doi.org/10.1016/j.jhydrol.2015.10.071).
- Maesaka, T., M. Maki, and K. Iwanami (2011). "Operational Rainfall Estimation by X-band MP Radar Network in MLIT, Japan." en. In: *In Proceedings of the 35th Conference on Radar Meteorology, Pittsburgh, PA, USA, 26–30 September 2011*, p. 8.
- Maier, R., G. Krebs, M. Pichler, D. Muschalla, and G. Gruber (2020). "Spatial rainfall variability in urban environments—High-density precipitation measurements on a city-scale." In: *Water* 12.4, p. 1157.

- Marra, F. and E. Morin (2018a). "Autocorrelation structure of convective rainfall in semiarid-arid climate derived from high-resolution X-Band radar estimates." en. In: *Atmospheric Research* 200, pp. 126–138. DOI: [10.1016/j.atmosres.2017.09.020](https://doi.org/10.1016/j.atmosres.2017.09.020).
- (2018b). "Autocorrelation structure of convective rainfall in semiarid-arid climate derived from high-resolution X-Band radar estimates." In: *Atmospheric Research* 200, pp. 126–138.
- Marshall, J., W. Hitschfeld, and K. Gunn (1955). "Advances in radar weather." In: *Advances in geophysics*. Vol. 2. Elsevier, pp. 1–56.
- Mascaro, G. (2017). "Multiscale Spatial and Temporal Statistical Properties of Rainfall in Central Arizona." In: *Journal of Hydrometeorology* 18.1, pp. 227–245. DOI: [10.1175/JHM-D-16-0167.1](https://doi.org/10.1175/JHM-D-16-0167.1).
- Metek (2015). *MRR Physical Basics*. Tech. rep. Metek Meteorologische Messtechnik GmbH.
- Mishra, K. V., W. F. Krajewski, R. Goska, D. Ceynar, B.-C. Seo, A. Kruger, J. J. Niemeier, M. B. Galvez, M. Thurai, V. N. Bringi, L. Tolstoy, P. A. Kucera, W. A. Petersen, J. Grazioli, and A. L. Pazmany (2016). "Deployment and Performance Analyses of High-Resolution Iowa XPOL Radar System during the NASA IFloodS Campaign." EN. In: *Journal of Hydrometeorology* 17.2. Publisher: American Meteorological Society Section: Journal of Hydrometeorology, pp. 455–479. DOI: [10.1175/JHM-D-15-0029.1](https://doi.org/10.1175/JHM-D-15-0029.1).
- Neely III, R. R., L. Parry, D. Dufton, L. Bennett, and C. Collier (2021). "Radar Applications in Northern Scotland (RAiNS)." In: *Journal of Hydrometeorology* 22.2, pp. 483–498.
- Nielsen, J. E., S. Thorndahl, and M. R. Rasmussen (2014). "A numerical method to generate high temporal resolution precipitation time series by combining weather radar measurements with a nowcast model." In: *Atmospheric research* 138, pp. 1–12.
- Ochoa-Rodriguez, S., L.-P. Wang, P. Willems, and C. Onof (2019). "A review of radar-rain gauge data merging methods and their potential for urban hydrological applications." In: *Water Resources Research* 55.8, pp. 6356–6391.
- Ochoa-Rodriguez, S. et al. (2015). "Impact of spatial and temporal resolution of rainfall inputs on urban hydrodynamic modelling outputs: A multi-catchment investigation." en. In: *Journal of Hydrology*. Hydrologic Applications of Weather Radar 531, pp. 389–407. DOI: [10.1016/j.jhydro.2015.05.035](https://doi.org/10.1016/j.jhydro.2015.05.035).
- Overeem, A., H. de Vries, H. Al Sakka, R. Uijlenhoet, and H. Leijnse (2021). "Rainfall-induced attenuation correction for two operational dual-polarization C-band radars in the Netherlands." In: *Journal of Atmospheric and Oceanic Technology* 38.6, pp. 1125–1142. DOI: [10.1175/JTECH-D-20-0113.1](https://doi.org/10.1175/JTECH-D-20-0113.1).
- Overeem, A., E. van den Besselaar, G. van der Schrier, J. F. Meirink, E. van der Plas, and H. Leijnse (2023). "EURADCLIM: the European climatological high-resolution gauge-adjusted radar precipitation dataset." English. In: *Earth System Science Data* 15.3. Publisher: Copernicus GmbH, pp. 1441–1464. DOI: [10.5194/essd-15-1441-2023](https://doi.org/10.5194/essd-15-1441-2023).
- Pejčić, V., J. Soderholm, K. Mühlbauer, V. Louf, and S. Trömel (2022). "Five years calibrated observations from the University of Bonn X-band weather radar (BoX-Pol)." en. In: *Scientific Data* 9.1. Number: 1 Publisher: Nature Publishing Group, p. 551. DOI: [10.1038/s41597-022-01656-0](https://doi.org/10.1038/s41597-022-01656-0).

- Peleg, N., M. Ben-Asher, and E. Morin (2013). "Radar subpixel-scale rainfall variability and uncertainty: lessons learned from observations of a dense rain-gauge network." In: *Hydrology and Earth System Sciences* 17.6, pp. 2195–2208.
- Peleg, N., F. Marra, S. Fatichi, A. Paschalis, P. Molnar, and P. Burlando (2018). "Spatial variability of extreme rainfall at radar subpixel scale." In: *Journal of Hydrology* 556, pp. 922–933.
- Peters, G., B. Fischer, and T. Andersson (2002). "Rain observations with a vertically looking Micro Rain Radar (MRR)." In: *Boreal environment research* 7.4, pp. 353–362.
- Peters, G., B. Fischer, H. Münster, M. Clemens, and A. Wagner (2005). "Profiles of raindrop size distributions as retrieved by microrain radars." In: *Journal of applied meteorology* 44.12, pp. 1930–1949.
- Pöschmann, J. M., D. Kim, R. Kronenberg, and C. Bernhofer (2021). "An analysis of temporal scaling behaviour of extreme rainfall in Germany based on radar precipitation QPE data." In: *Natural Hazards and Earth System Sciences* 21.4, pp. 1195–1207. DOI: [10.5194/nhess-21-1195-2021](https://doi.org/10.5194/nhess-21-1195-2021).
- Reda, I. and A. Andreas (2008). *Solar Position Algorithm for Solar Radiation Applications (Revised)*. Tech. rep. National Renewable Energy Lab. (NREL), Golden, CO (United States). DOI: [10.2172/15003974](https://doi.org/10.2172/15003974).
- Reinoso-Rondinel, R. and M. Schleiss (2021). "Quantitative Evaluation of Polarimetric Estimates from Scanning Weather Radars Using a Vertically Pointing Micro Rain Radar." EN. In: *Journal of Atmospheric and Oceanic Technology* 38.3. Publisher: American Meteorological Society Section: Journal of Atmospheric and Oceanic Technology, pp. 481–499. DOI: [10.1175/JTECH-D-20-0062.1](https://doi.org/10.1175/JTECH-D-20-0062.1).
- Rubel, F. and M. Hantel (1999). "Correction of daily rain gauge measurements in the Baltic Sea drainage basin." In: *Hydrology Research* 30.3, pp. 191–208.
- Ryzhkov, A., P. Zhang, P. Bukovčić, J. Zhang, and S. Cocks (2022). "Polarimetric radar quantitative precipitation estimation." In: *Remote Sensing* 14.7, p. 1695.
- Saltikoff, E., K. Friedrich, J. Soderholm, K. Lengfeld, B. Nelson, A. Becker, R. Hollmann, B. Urban, M. Heistermann, and C. Tassone (2019). "An overview of using weather radar for climatological studies: successes, challenges, and potential." In: *Bulletin of the American Meteorological Society* 100.9, pp. 1739–1752.
- Schleiss, M., J. Olsson, P. Berg, T. Niemi, T. Kokkonen, S. Thorndahl, R. Nielsen, J. Ellerbæk Nielsen, D. Bozhinova, and S. Pulkkinen (2020). "The accuracy of weather radar in heavy rain: a comparative study for Denmark, the Netherlands, Finland and Sweden." In: *Hydrology and Earth System Sciences* 24.6. Publisher: Copernicus GmbH, pp. 3157–3188. DOI: [10.5194/hess-24-3157-2020](https://doi.org/10.5194/hess-24-3157-2020).
- Schlünzen, K. H., P. Hoffmann, G. Rosenhagen, and W. Riecke (2010). "Long-term changes and regional differences in temperature and precipitation in the metropolitan area of Hamburg." In: *International journal of climatology* 30.8, pp. 1121–1136.
- Schmitt, A. U., F. Burgemeister, H. Dorff, T. Finn, A. Hansen, B. Kirsch, I. Lange, J. Radtke, and F. Ament (2023). "Assessing the weather conditions for urban cyclists by spatially dense measurements with an agent-based approach." In: *Meteorological Applications* 30.6, e2164. DOI: <https://doi.org/10.1002/met.2164>.
- Seo, B.-C. and W. F. Krajewski (2015). "Correcting temporal sampling error in radar-rainfall: Effect of advection parameters and rain storm characteristics on the correction accuracy." In: *Journal of Hydrology* 531, pp. 272–283.

- Shucksmith, P., L. Sutherland-Stacey, and G. Austin (2011). "The spatial and temporal sampling errors inherent in low resolution radar estimates of rainfall." In: *Meteorological Applications* 18.3, pp. 354–360.
- Sokol, Z., J. Szturc, J. Orellana-Alvear, J. Popova, A. Jurczyk, and R. Céleri (2021). "The role of weather radar in rainfall estimation and its application in meteorological and hydrological modelling—A review." In: *Remote Sensing* 13.3, p. 351.
- Stafford, B. et al. (2021). *Pysolar: staring directly at the sun since 2007 (pingswept/pysolar: 0.10)*. Zenodo [code]. Version 0.10. DOI: [10.5281/zenodo.5518129](https://doi.org/10.5281/zenodo.5518129).
- Terink, W., H. Leijnse, G. van den Eertwegh, and R. Uijlenhoet (2018). "Spatial resolutions in areal rainfall estimation and their impact on hydrological simulations of a lowland catchment." In: *Journal of Hydrology* 563, pp. 319–335.
- Thomassen, E. D., S. L. Thorndahl, C. B. Andersen, I. B. Gregersen, K. Arnbjerg-Nielsen, and H. J. D. Sørup (2022). "Comparing spatial metrics of extreme precipitation between data from rain gauges, weather radar and high-resolution climate model re-analyses." In: *Journal of Hydrology* 610, p. 127915.
- Thorndahl, S., T. Einfalt, P. Willems, J. E. Nielsen, M.-C. ten Veldhuis, K. Arnbjerg-Nielsen, M. R. Rasmussen, and P. Molnar (2017). "Weather radar rainfall data in urban hydrology." In: *Hydrology and Earth System Sciences* 21.3, pp. 1359–1380. DOI: [10.5194/hess-21-1359-2017](https://doi.org/10.5194/hess-21-1359-2017).
- Tokay, A., R. J. Roche, and P. G. Bashor (2014). "An experimental study of spatial variability of rainfall." In: *Journal of Hydrometeorology* 15.2, pp. 801–812.
- Van de Beek, C. Z., H. Leijnse, J. N. M. Stricker, R. Uijlenhoet, and H. W. J. Russchenberg (2010). "Performance of high-resolution X-band radar for rainfall measurement in The Netherlands." English. In: *Hydrology and Earth System Sciences* 14.2. Publisher: Copernicus GmbH, pp. 205–221. DOI: [10.5194/hess-14-205-2010](https://doi.org/10.5194/hess-14-205-2010).
- Ventura, J. F. i. and H. W. J. Russchenberg (2009). "Towards a better understanding of the impact of anthropogenic aerosols in the hydrological cycle: IDRA, IRCTR drizzle radar." In: *Physics and Chemistry of the Earth, Parts A/B/C* 34.1, pp. 88–92. DOI: <https://doi.org/10.1016/j.pce.2008.02.038>.
- Villarini, G. and W. F. Krajewski (2010). "Review of the Different Sources of Uncertainty in Single Polarization Radar-Based Estimates of Rainfall." en. In: *Surveys in Geophysics* 31.1, pp. 107–129. DOI: [10.1007/s10712-009-9079-x](https://doi.org/10.1007/s10712-009-9079-x).
- Villarini, G., P. V. Mandapaka, W. F. Krajewski, and R. J. Moore (2008). "Rainfall and sampling uncertainties: A rain gauge perspective." In: *Journal of Geophysical Research: Atmospheres* 113.D11.
- Villarini, G., B.-C. Seo, F. Serinaldi, and W. F. Krajewski (2014). "Spatial and temporal modeling of radar rainfall uncertainties." In: *Atmospheric research* 135, pp. 91–101.
- Wang, J., L. Zhuo, D. Han, Y. Liu, and M. A. Rico-Ramirez (2023a). "Hydrological model adaptability to rainfall inputs of varied quality." In: *Water Resources Research* 59.2, e2022WR032484.
- Wang, L.-P., S. Ochoa-Rodriguez, J. Van Assel, R. D. Pina, M. Pessemier, S. Kroll, P. Willems, and C. Onof (2015). "Enhancement of radar rainfall estimates for urban hydrology through optical flow temporal interpolation and Bayesian gauge-based adjustment." In: *Journal of Hydrology* 531, pp. 408–426.
- Wang, X., S. Shi, L. Zhu, Y. Nie, and G. Lai (2023b). "Traditional and Novel Methods of Rainfall Observation and Measurement: A Review." In: *Journal of Hydrometeorology* 24.12, pp. 2153–2176.

- Wang, Y. and V. Chandrasekar (2010). "Quantitative Precipitation Estimation in the CASA X-band Dual-Polarization Radar Network." EN. In: *Journal of Atmospheric and Oceanic Technology* 27.10. Publisher: American Meteorological Society Section: Journal of Atmospheric and Oceanic Technology, pp. 1665–1676. DOI: [10.1175/2010JTECHA1419.1](https://doi.org/10.1175/2010JTECHA1419.1).
- Waterman, P. (1965). "Matrix formulation of electromagnetic scattering." In: *Proceedings of the IEEE* 53.8, pp. 805–812.
- Wesson, S. and G. Pegram (2004). "Radar rainfall image repair techniques." In: *Hydrology and Earth System Sciences* 8.2, pp. 220–234. DOI: [10.5194/hess-8-220-2004](https://doi.org/10.5194/hess-8-220-2004).
- Westfall, P. H. (2014). "Kurtosis as peakedness, 1905–2014. RIP." In: *The American Statistician* 68.3, pp. 191–195.
- Winterrath, T., C. Brendel, M. Hafer, T. Junghänel, A. Klameth, K. Lengfeld, E. Walawender, E. Weigl, and A. Becker (2018a). *RADKLIM Version 2017.002: Re-processed quasi gauge-adjusted radar data, 5-minute precipitation sums (YW)*. DOI: [10.5676/DWD/RADKLIM_YW_V2017.002](https://doi.org/10.5676/DWD/RADKLIM_YW_V2017.002).
- Winterrath, T., C. Brendel, M. Hafer, T. Junghänel, A. Klameth, E. Walawender, E. Weigl, and A. Becker (2017). *Erstellung einer radargestützten Niederschlagsklimatologie*. Tech. rep. Deutscher Wetterdienst.
- Winterrath, T., T. Brendel, T. Junghänel, A. Klameth, K. Lengfeld, E. Walawender, E. Weigl, M. Hafer, and A. Becker (2018b). "An overview of the new radar-based precipitation climatology of the Deutscher Wetterdienst—data, methods, products." In: *Rainfall Monitoring, Modelling and Forecasting in Urban Environment. UrbanRain18: 11th International Workshop on Precipitation in Urban Areas. Conference Proceedings*. ETH Zurich, Institute of Environmental Engineering, pp. 132–137.
- Yoon, J., J. Joo, C. Yoo, S. Hwang, and S. Lim (2017). "On quality of radar rainfall with respect to temporal and spatial resolution for application to urban areas." In: *Meteorological Applications* 24.1, pp. 19–30.
- Zhou, Z., J. A. Smith, M. L. Baeck, D. B. Wright, B. K. Smith, and S. Liu (2021). "The impact of the spatiotemporal structure of rainfall on flood frequency over a small urban watershed: An approach coupling stochastic storm transposition and hydrologic modeling." In: *Hydrology and Earth System Sciences* 25.9, pp. 4701–4717.

ACKNOWLEDGMENTS

I would like to take this opportunity to thank everyone who has motivated and supported me over the past few years.

First and foremost, I would like to extend my deepest thanks to my supervisors Prof. Dr. Felix Ament and Dr. Marco Clemens for all the valuable scientific and non-scientific advices. They were always available for constructive discussions, even during the challenges of remote work, and showed great interest in clarifying any ambiguities. At the same time, they gave me the freedom to develop my own project. I have always been able to rely on their positivity and encouragement.

I would also like to thank Dr. Lutz Hirsch for his role as the chair of my advisory panel, and Dr. Berit Hachfeld from SICSS for her assistance with organizational matters.

My thanks extend to all my colleagues in the AMPM group. The regular stand-up meetings with Amelie, Bastian, Heike, Henning, Jule, and Tobias were a source of support and motivation, especially during the long periods of working from home. A special thanks to Tobias for a productive working environment and the great atmosphere in our shared office. The numerous (remote) coffee breaks were not only professionally valuable but also personally uplifting. I am grateful to Ingo for his assistance with measurement data, and to Michael and Patrick for their technical support with radar systems (at many times). I would also like to acknowledge my colleagues from the CliCCS C₁ project for many interesting meetings.

I am very thankful to Tobias, Daniel and Lara for their time and effort in reading earlier drafts of this dissertation, and for their thoughtful comments that greatly contributed to its improvement.

I thank the members of my doctoral committee for taking the time to review this dissertation.

Lastly, I wish to express my deepest gratitude to my friends and family for their unwavering support, understanding, and encouragement throughout this journey.

EIDESSTATTLICHE VERSICHERUNG

Eidesstattliche Versicherung

Declaration on Oath

Hiermit erkläre ich an Eides statt, dass ich die vorliegende Dissertationsschrift selbst verfasst und keine anderen als die angegebenen Quellen und Hilfsmittel benutzt habe. Sofern im Zuge der Erstellung der vorliegenden Dissertationsschrift generative Künstliche Intelligenz (gKI) basierte elektronische Hilfsmittel verwendet wurden, versichere ich, dass meine eigene Leistung im Vordergrund stand und dass eine vollständige Dokumentation aller verwendeten Hilfsmittel gemäß der Guten wissenschaftlichen Praxis vorliegt. Ich trage die Verantwortung für eventuell durch die gKI generierte fehlerhafte oder verzerrte Inhalte, fehlerhafte Referenzen, Verstöße gegen das Datenschutz- und Urheberrecht oder Plagiate.

I hereby declare and affirm that this doctoral dissertation is my own work and that I have not used any aids and sources other than those indicated. If electronic resources based on generative artificial intelligence (gAI) were used in the course of writing this dissertation, I confirm that my own work was the main and value-adding contribution and that complete documentation of all resources used is available in accordance with good scientific practice. I am responsible for any erroneous or distorted content, incorrect references, violations of data protection and copyright law or plagiarism that may have been generated by the gAI.

Hamburg, den 07. Oktober 2024

Hamburg, October 07, 2024

Finn Burgemeister